EVALUATION OF WEDM PERFORMANCE CHARACTERISTICS OF INCONEL 706 FOR TURBINE DISC PROFILE APPLICATION

Thesis

Submitted in partial fulfillment of the requirements for the degree of

DOCTOR OF PHILOSOPHY

by

PRIYARANJAN SHARMA

DEPARTMENT OF MECHANICAL ENGINEERING

NATIONAL INSTITUTE OF TECHNOLOGY KARNATAKA,

SURATHKAL, MANGALORE - 575025

JANUARY, 2017

D E C L A R A T I O N

I hereby declare that the Research Thesis entitled "**Evaluation of WEDM Performance Characteristics of Inconel 706 for Turbine Disc Profile Application**" which is being submitted to the **National Institute of Technology Karnataka, Surathkal** in partial fulfillment of the requirements for the award of the degree of **Doctor of Philosophy** in **Mechanical Engineering** is a *bonafide report of the research work carried out by me*. The material contained in this Research Thesis has not been submitted to any other Universities or Institutes for the award of any degree.

<div align="right">

PRIYARANJAN SHARMA

Register Number: **135065ME13F05**

Department of Mechanical Engineering

</div>

Place: NITK-Surathkal

Date:

C E R T I F I C A T E

This is to certify that the Research Thesis entitled "**Evaluation of WEDM Performance Characteristics of Inconel 706 for Turbine Disc Profile Application**" submitted by **Mr. Priyaranjan Sharma (Register Number: 135065ME13F05)** as the record of the research work carried out by him, *is accepted as the Research Thesis submission* in partial fulfillment of the requirements for the award of the degree of **Doctor of Philosophy.**

Research Guide(s)

Dr. D. Chakradhar   **Dr. Narendranath S.**

Assistant Professor   Professor

Department of Mechanical Engg.   Department of Mechanical Engg.

Chairman - DRPC

Date:

Dedicated to …

My beloved parents
and family members…
&
All of my Teachers and Colleagues
who taught and encouraged me
with positive thoughts…

ACKNOWLEDGEMENTS

My sincere thanks to my seniors and friends Dr. Raghvendra K, Dr. Arun Shettigar, Dr. Muralidhar A., Dr. Manjunath Patel, Dr. M. Manjaiah, Mr. Gangadhar N., Mr. G. Venkatesh, Mr. Hargovind Soni, Mr. Abhinaba Roy, Mr. Ashwin K, Mr. Bhaskar M, Mr. Gajanan Anne, Mr. Thippesh LR, Mr. Venkatesh TL, Mr. Girish, Mr. Rajesh M, Mr. Sreejith BK, Mr. Hemanth K, Mr. Nitin Gowda, Mr. Madhusudana, Mr. Jaideep Dutta and Mr. Gajanan Nayak for their constant help and support.

I would also like to share the happiest moment of my life with my respected parents. Their blessing, guidance and endeavour kept my moral high throughout the research work. I feel happy to express my sincere appreciation to all my family members, specially my sisters and brothers for their understanding, care, support and encouragement.

Finally, I want to express my sincere thanks to all those who helped me directly or indirectly at various stages of this research work. I THANK YOU ALL…………..!

(*Priyaranjan Sharma*)

ABSTRACT

Nickel-iron-based superalloys are categorized as an exceptional class of structural material. These superalloys contain both nickel and iron as base elements and characterized by the high phase stability of FCC austenitic matrix. These superalloys exhibit excellent mechanical properties such as high tensile strength, excellent creep, improved fatigue life, good surface stability, resistance to degradation in corrosive and oxidizing environments. Therefore, these superalloys are best suited for manufacturing of gas turbine components. The machining of these superalloys has become an active area of research due to their growing demands in aircraft and power generation turbines. These superalloys typically constitute around 40–50 % of the total weight of an aircraft engine and most extensively used in the combustor and turbine sections of the engine where elevated temperatures are maintained during operation. The turbine disc is amongst the most critical components in an aero engine which includes a number of complex slots to fix the turbine blades. The combined assembly of turbine disc and blade is located in a hot gas stream from which mechanical power is extracted to drive the compressor, gearbox and other accessories of aero engine.

Since Inconel 718 was being used in manufacturing of turbine disc in aircraft engines for more than 35 years, with the new arrival of advanced gas turbines with working firing temperature of 1260 °C, it became necessary to develop the advanced superalloy (i.e., Inconel 706) with improved fabricability along with high mechanical strength. Machining of this superalloy to a very close tolerance and producing a high surface finish is essential for achieving superior performance of turbine disc. Owing to high quality requirement of turbine disc such as complex profile slots along with high dimensional accuracy (within the range of ±5 μm) and also excellent surface finish (surface roughness less than 0.8 μm), conventional machining process seems to be ineffective for turbine disc slot production. The conventional machining of nickel-iron-based superalloys also exhibits poor machining performance due to high chemical affinity, strong work-hardening tendency.

To overcome these issues, non-conventional machining methods such as laser beam machining (LBM), electrochemical machining (ECM), abrasive water jet machining (AWJM), and electrical discharge machining (EDM) are effectively implemented for machining of these superalloys. However, there are certain issues with non-conventional machining processes such as micro-cracking, poor surface quality, low dimensional accuracy and significant recast layer formation in the LBM process; more chance of corrosion due to acidic electrolyte, comparatively low MRR and require special shaped electrode in the ECM process; impingement of abrasive particles into matrix, crack propagation and burr formation at the edge in the AWJM process; less recast layer formation compare to LBM and require special shaped electrode in EDM process.

To develop the gas turbine components, an efficient manufacturing process is required for aerospace and power generating industries. Wire electrical discharge machining (WEDM) is an advanced version of EDM capable of manufacturing components with intricate shapes and sharp edge profiles, which is difficult to be obtained by other machining process. Moreover, it eliminates the need of special shaped electrode and reduces the recast layer thickness (RLT) significantly with the use of low discharge pulse. Additionally, WEDM is more efficient than the EDM in terms of flexibility and offers low residual stresses on the machined component. In the past few years, WEDM allowed success in the production of gas turbine components which required complex shaped profiles with high precision. The high degree of dimensional accuracy and better surface quality of the machined components make WEDM valuable.

The main aim of this study is to evaluate the WEDM performance characteristics of Inconel 706 for turbine disc application. To achieve the feasibility in manufacturing of turbine disc profile slots, the current research work has been divided into four parts. In first part, one factor at a time approach was used to understand the effect of various control parameter such as pulse on time, pulse off time, servo voltage, wire feed, servo feed and flushing pressure on WEDM performance characteristics. In second part, the effect of wire materials and wire diameters on WEDM performance characteristics (i.e., cutting speed, surface roughness, surface topography, recast layer,

subsurface microhardness, microstructural and metallurgical changes) have been evaluated by considering the significant control parameters and different discharge mode. In third part, turbine disc profile slots were machined successfully on Inconel 706 superalloy as per the standard of gas turbine industries. Moreover, the various WEDM performance characteristics of profile slots such as cutting speed, surface roughness, subsurface microhardness, surface topography, recast surface, crystal structure, residual stresses, profile accuracy, microstructural and elemental changes have been evaluated. In fourth part, the modeling and optimization of WEDM performance characteristics have been carried out by considering optimum wire material as well as optimum wire diameter. The mathematical models for MRR and SR have been developed using response surface methodology (RSM) followed by backward elimination method. Then, teaching learning based optimization (TLBO) algorithm was used for individual as well as multi-objective optimization. Finally, Pareto optimal solutions have been obtained at different weightage which might be beneficial to gas turbine manufacturing industries.

The manufactured turbine disc profile slots have shown low level of tensile residual stresses (less than 850 MPa), average surface roughness less than 0.8 μm, profile accuracy within the range of ±5 μm, almost negligible recast layer, minimum hardness alteration, no micro cracks, and no thermal alterations while using hard brass wire of diameter 150 μm followed by appropriate trim cut strategy.

Keywords: Inconel 706; Wire electrical discharge machining; Turbine disc; Profile slots; Topography; Microstructure; Microhardness; Recast layer; Profile accuracy; Residual stresses; Teaching learning based optimization.

CONTENTS

LIST OF FIGURES

xi

LIST OF TABLES

LIST OF SYMBOLS AND ABBREVIATIONS

ABC   : Artificial Bee Colony

ANN   : Artificial Neural Networks

ANOVA   : Analysis of Variance

AWJM   : Abrasive Water Jet Machining

B–150   : Hard Brass Wire of Diameter 150 μm

B–200   : Hard Brass Wire of Diameter 200 μm

B–250   : Hard Brass Wire of Diameter 250 μm

CCD   : Central Composite Design

CMM   : Coordinate Measuring Machine

CNC   : Computer Numerical Control

D–250   : Diffused Wire of Diameter 250 μm

DE   : Differential Evolution

DOE   : Design of Experiment

DOF   : Degree of Freedom

ECM   : Electrochemical Machining

EDM   : Electrical Discharge Machining

EDS   : Energy Dispersive X-Ray Spectroscopy

E_e : Discharge Energy

GA   : Genetic Algorithm

Hv   : Vickers Hardness

I_e : Discharge Current

LBM   : Laser Beam Machining

MRR   : Material Removal Rate

MS   : Mean Square

OFAT   : One Factor At A Time

PSO   : Particle Swarm Optimization

R^2 : Determination Coefficient

Ra   : Average Surface Roughness

RLT	:	Recast Layer Thickness
RSM	:	Response Surface Methodology
Rz	:	Roughness Depth Mean
SEI	:	Secondary Electron Image
SEM	:	Scanning Electron Microscope
SR	:	Surface Roughness
SS	:	Sum of Squares
SV	:	Servo Voltage
t	:	Machining Time
T_F	:	Teaching Factor
t_i	:	Pulse Duration
TLBO	:	Teaching Learning Based Optimization
T_{off}	:	Pulse off Time
T_{on}	:	Pulse on Time
U_e	:	Discharge Voltage
w_1	:	Weightage for MRR
w_2	:	Weightage for SR
w_a	:	Weight of the Workpiece After Machining
w_b	:	Weight of the Workpiece Before Machining
WEDM	:	Wire Electrical Discharge Machining
WF	:	Wire Feed
XRD	:	X-ray Diffraction
Zn–200	:	Zinc Coated Wire of Diameter 200 µm
Zn–250	:	Zinc Coated Wire of Diameter 250 µm
ε	:	Experimental Error
ρ	:	Density of the Workpiece

CHAPTER 1

INTRODUCTION

In recent years, manufacturing technology goes on continuous improvement due to the development of materials with improved thermal, mechanical and chemical properties. High productivity and low manufacturing cost associated with excellent surface finish and high dimensional accuracy are always the main aim of the modern manufacturing industries. These industries are facing challenges from the components required in challenging environments (i.e., aircraft and industrial gas turbines, space vehicles, nuclear reactors, and chemical treatment plants). Gas turbine engines, which operate in a most degrading environment, impose the development of advanced materials. Superalloys are most suitable for such application because of their improved mechanical strength, creep resistance, better surface stability, corrosion and oxidation resistance at elevated temperature (Campbell, 2006).

1.1   BACKGROUND OF SUPERALLOYS

Materials which can be used at 0.6 times of their melting temperature, yet maintain their strength to withstand severe mechanical stresses and strains in corrosive environments are called superalloys (Sims et al., 1987). Generally, superalloys are classified into three categories according to their base element. They are nickel-based, cobalt-based and nickel-iron-based superalloys (Geddes et al., 2010). However, nickel-based superalloys are quite popular among the superalloys. This is because, these superalloys can be used typically at a higher proportion of their melting temperature and exhibits excellent creep, good surface stability, improved fatigue life, corrosion and oxidation resistance. Thus, these superalloys are extensively employed in marine equipment, nuclear plants, petrochemical refineries, gas turbine engines and rocket engine components (Reed, 2006). The contributions of alloying elements in nickel-based superalloys are shown in Figure 1.1. The addition of iron and cobalt deliver the long term stability to these alloys, whereas chromium contents provide

oxidation and corrosion resistance. Moreover, the addition of aluminium, titanium and niobium improves the mechanical strength of these alloys.
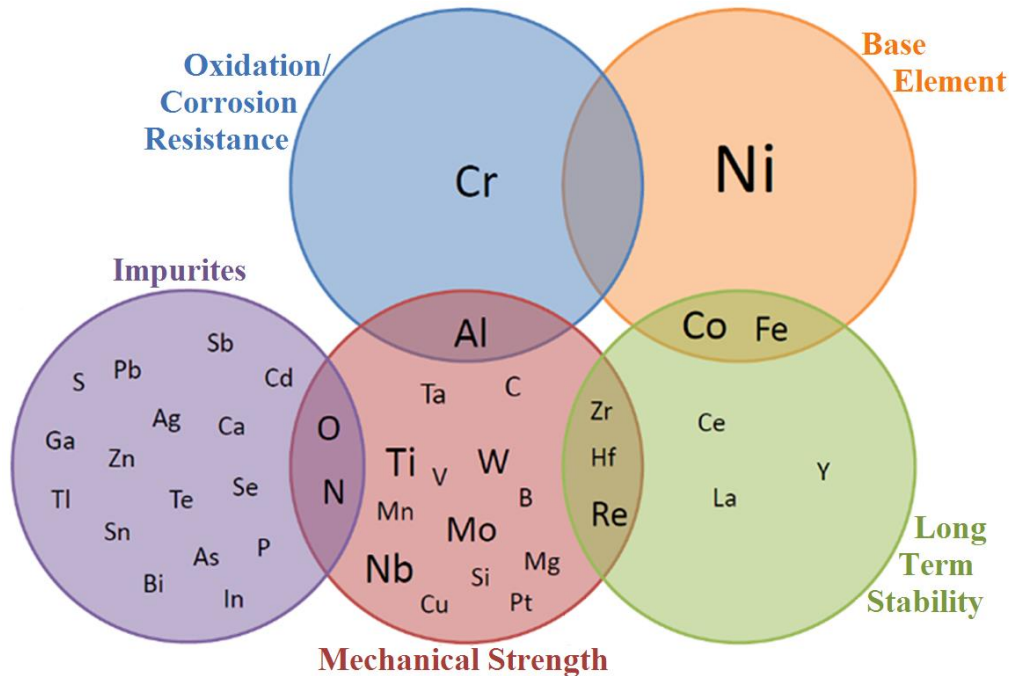
Figure 1.1 Contribution of alloying elements in nickel-based superalloys (Bedder and Baylis, 2013).

1.2 NICKEL-IRON-BASED SUPERALLOYS AND THEIR APPLICATIONS

The nickel-iron-based superalloys, which contain both nickel and iron as base elements, are a unique category of structural materials. The utilization of nickel-iron-based superalloys in aerospace, nuclear and defense industries cannot be ignored because of their exceptional properties such as high temperature strength, good toughness, corrosion and oxidation resistance at elevated temperatures. Therefore, their usage has vital importance in the building of high performance gas turbine engines (Zhang and Zhao, 2012).

In recent year, the machining of nickel-iron-based superalloys has become an interesting area of research due to their increasing demand in aircraft and power generation turbines, nuclear power and rocket engines. For an instant, these alloys typically contributes at least 40% of the total weight of jet engine and most widely used in the combustor and turbine sections of jet engine where a high amount of

temperature are produced during operation (Schafrik and Sprague, 2004). For the GE CF6 aircraft engine (Campbell, 2006), nickel-iron-based superalloys comprise about one half of the finished weight of the aircraft engine as shown in Figure 1.2.
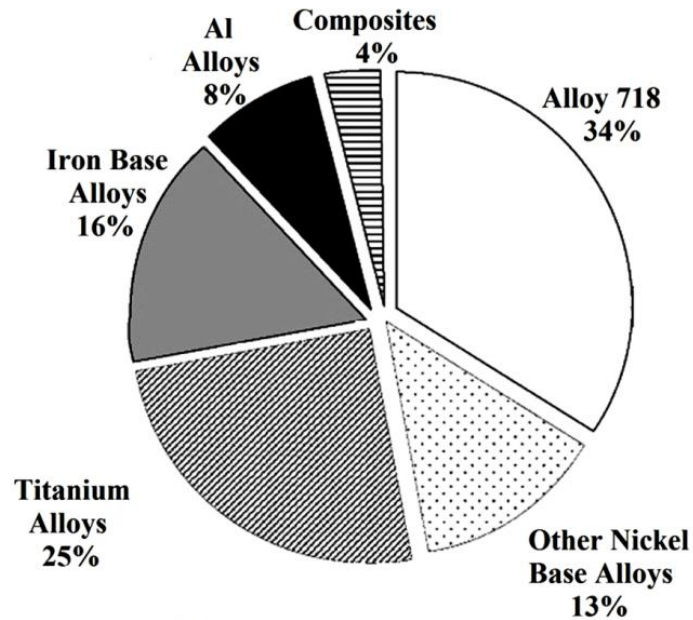
Figure 1.2 Materials distribution in GE CF6 aircraft engine (Campbell, 2006).

The nickel-based alloys are generally solid solution hardened for low temperature application and precipitation hardened for high temperature application. Nickel-iron-based alloys are precipitation hardened superalloys in which Nb is the main strengthening element. These alloys contain at least 39 wt. % nickel (Ni) + cobalt (Co) and up to 27 wt. % chromium (Cr). These alloys exhibit stable face centered cubic (FCC) structure (Campbell, 2006). The other essential precipitate in nickel-iron-based alloys are the secondary precipitate phase (γ'). If the aluminium/titanium content added to γ nickel matrix increases, a γ' (Ni_3 (Al, Ti)) phase forms (Pollock and Tin, 2006). Ni_3Al exhibits good heat and creep resistance properties. The nickel-iron-based alloys containing niobium are strengthened primarily by hard secondary phase of γ'' (Ni_3Nb) which improves the creep rupture properties of the alloy. These alloys also contain controlled amount of refractory elements for example tantalum (Ta), tungsten (W) and molybdenum (Mo) which improve the strength and oxidation properties of the alloy.

Most of the military and civilian aircrafts are operated by gas turbine engines. Figure 1.3 shows the different sections of gas turbine engine. Due to more advanced and sophisticated technology used in modern gas turbine engines, it is challenging for a material which is to be placed at the turbine inlet. This is because, it is subjected to extreme conditions such as very high temperature, great pressure, high rotational speed and vibration. The components of nickel-iron-based superalloys used in aircraft engines are blades and the discs in the high pressure compressor and turbine (Locq and Caron, 2011). These components include several outstanding properties such as high strength at elevated temperature, better surface stability, creep resistance at elevated temperature, oxidation, and corrosion resistance (Pollock and Tin, 2006).
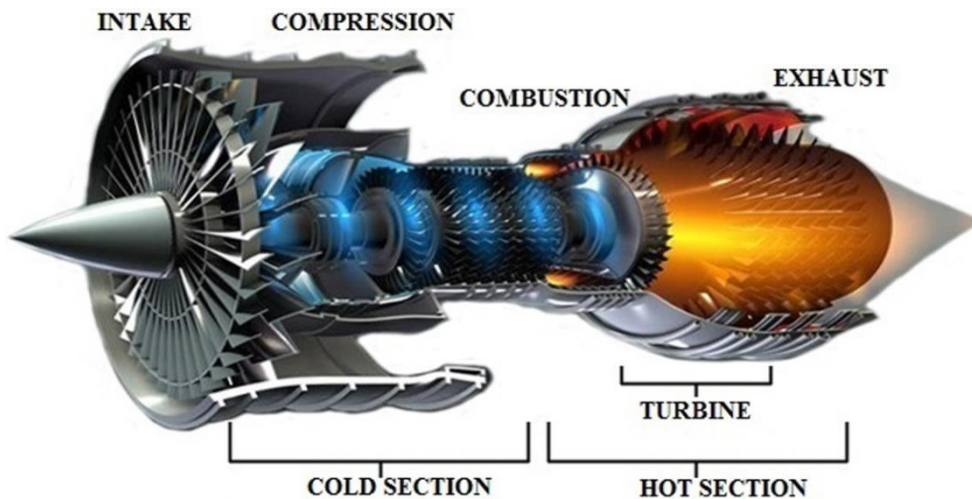
Figure 1.3 Different sections of gas turbine engine (Rolls Royce, 2015).

The turbine discs are amongst the most critical components in gas turbine engines (Reed, 2006). The main role of the turbine disc is to provide attachment for the turbine blades which is located in a hot gas stream, from which mechanical power is extracted. The combined assembly of turbine disc and turbine blades is then capable of transmitting the power to the fan and compressor sections through shafts. Inconel 718 is being used for manufacturing of turbine disc in aircraft engines since 35 years (Schilke, 2004). Due to the requirement of firing temperatures of 1260 °C in advanced gas turbine engines, it became essential to utilize a new nickel-iron-based superalloy (Inconel 706) for the rotors. This alloy exhibits a high yield strength at elevated temperature and best suited for such applications because of its good mechanical properties. The chemistry of Inconel 706 was derived from Inconel 718.

The alloy 706 was developed at the International Nickel Company (INCO) to achieve exceptional metallurgical properties such as improved machinability, low cost and improved fabricability compared to Inconel 718 (Schilke et al., 1994). The alloy contains niobium, titanium and aluminium and strengthened by a combination of both γ' and γ''. The characteristics of Inconel 706 are more or less similar to Inconel 718 except that this alloy has improved fabricability. Inconel 706 may be considered as nickel-based superalloy, but it include sufficient iron content and classified as nickel-iron-based superalloy (Geddes et al., 2010).

Table 1.1 Nickel-based superalloy developed for turbine disc application (Muktinutalapati, 2011).

Grade	Chemical composition	Base element
Inconel 718	50–55 Ni, 19 Cr, 18.5 Fe, 3 Mo, 0.9 Ti, 0.5 Al, 5.1 Cb, 0.03 C	Nickel and iron
Inconel 706	39–44 Ni, 16 Cr, 37 Fe, 1.8 Ti, 2.9 Cb, 0.03 C	Nickel and iron
IN 100	60 Ni, 10 Cr, 15 Co, 3 Mo, 4.7 Ti, 5.5 Al, 0.15 C, 0.015 B, 0.06 Zr, 1.0 V	Nickel
Rene 95	61 Ni, 14 Cr, 8 Co, 3.5 Mo, 3.5 W, 3.5 Nb, 2.5 Ti, 3.5 Al, 0.16 C, 0.01 B, 0.05 Zr	Nickel
LC Astroloy	56.5 Ni, 15 Cr, 15 Co, 5.25 Mo, 3.5 Ti, 4.4 Al, 0.06 C, 0.03 B, 0.06Zr	Nickel
MERL–76	54.4 Ni, 12.4 Cr, 18.6 Co, 3.3 Mo, 1.4 Nb, 4.3 Ti, 5.1 Al, 0.02 C, 0.03 B, 0.35 Hf, 0.06 Zr	Nickel
Rene88 DT	56.4 Ni, 16 Cr, 13 Co, 4 Mo, 4 W, 0.7 Nb, 3.7 Ti, 2.1 Al, 0.03 C, 0.015 B, 0.03 Zr	Nickel
Udimet 720	55 Ni, 18 Cr, 14.8 Co, 3 Mo, 1.25 W, 5 Ti, 2.5 Al, 0.035 C, 0.033 B, 0.03 Zr	Nickel
Udimet 720LI	57 Ni, 16 Cr, 15 Co, 3 Mo, 1.25 W, 5 Ti, 2.5 Al, 0.025 C, 0.018 B, 0.03 Zr	Nickel

Besides, Inconel 706 contains a lower proportion of alloying elements than Inconel 718 and delivers better stress rupture and tensile yield strength compared to the other superalloys. In addition, the alloy exhibits less prone to segregation. Therefore, it

could be forged in large diameter unlike Inconel 718. Consequently, Inconel 706 could be used to build large sized rotors for industrial gas turbines (Schafrik and Sprague, 2004). In aerospace field, Inconel 706 alloy is being used for turbine discs, diffuser cases, engine mounts, fasteners, compressor discs and shafts. The newly invented superalloy Inconel 706 has been developed in such a way that gas turbine industries never replace this material which combines excellent mechanical properties, easy fabricability and low cost. Therefore, current research work mainly emphasizes on the use of advanced nickel-iron-based superalloy i.e. Inconel 706 for gas turbine applications, particularly in turbine disc. Table 1.1 shows some of the nickel-based superalloys developed for turbine disc application.

1.3   MACHINING OF NICKEL-IRON-BASED SUPERALLOYS

Even though Nickel-iron-based superalloys are extensively used in aerospace and industrial gas turbines, machining of these superalloys is prime concern due to high quality requirement of gas turbine components. Usually, conventional machining of these nickel-iron-based superalloys offer poor machining performance, low dimensional accuracy and lower surface quality of the machined components. These problems are frequently observed due to their high work-hardening tendency, chemical affinity, abrasive nature and low thermal conductivity (Arunachalam and Mannan, 2000; Ezugwu et al., 2003). To overcome these issues, non-conventional machining methods such as laser beam machining (LBM), electrochemical machining (ECM), abrasive water jet machining (AWJM), and electrical discharge machining (EDM) are effectively implemented for machining of these superalloys. Unlike conventional machining, there is no plastic deformation and chip formation in non-conventional machining. These non-conventional processes require some form of energy like thermal, mechanical and chemical for machining.

Looking into severe economic conditions and increased demands for manufacturing of advanced materials for challenging application, wire electrical discharge machining (WEDM) is found to be superior to die-sinking EDM. This is because die-sinking EDM require special shape electrode to produce any complex profile which will increase the tooling cost. Further, it yields high inflexibility in case if the shape of the

6

component is more frequently changing and increase the production time of the components. However, WEDM is quite flexible in cutting any complex shape profile using computer numerical control (CNC) programming. Moreover, WEDM doesn't require any special shape electrode. In terms of surface integrity, EDM produces a significant recast layer on the machined surface which is highly detrimental to aircraft application. In case of WEDM, recast layer formation can be reduced significantly with the use of low discharge pulse. According to Aspinwall et al. (2008), almost negligible recast layer was observed during WEDM while using appropriate trim cut strategy and this strategy is most suited for manufacturing of aircraft components. Further, EDM induces comparatively high residual stresses on the machined components which reduce the fatigue life of aircraft components. While, WEDM offers relatively low residual stresses on machined components and provides comparatively better fatigue life. In the past few years, WEDM has got success in the production of complex gas turbine components with acceptable tolerance limit. An improved shape accuracy and better surface integrity of the machined parts make WEDM valuable (Xu, 2012). Nevertheless, there is only one limitation of WEDM as it can't be used for machining for non-conductive materials. A detailed description of WEDM process has been provided under following section:

1.3.1 Introduction of WEDM

Generally, WEDM is an electro-thermal controlled metal removal process in which material is removed from the workpiece by a series of rapid, repetitive and controlled electrical discharges between workpiece (positive electrode) and wire (negative electrode). The electrodes are separated by a dielectric fluid (De-ionized water) and subjected to a high potential difference. WEDM can cut any conductive material irrespective of their mechanical properties such as hardness, toughness, wear resistance and tensile strength. Through the usage of CNC programing and multi-axis movement, WEDM can produce intricate parts with outstanding precision. Currently, WEDM is being used in precision manufacturing of gas turbine components because it is flexible in cutting complex and intricate shapes with high dimensional accuracy.

1.3.2 Principle of WEDM mechanism

The principal of WEDM mechanism has been illustrated in Figure 1.4 in which wire is attached to the negative terminal of the pulse generator whereas workpiece is attached to the positive terminal of the pulse generator. Before WEDM operation, it should be ensured that both wire and workpiece are a good conductor of electricity. De-ionized water is commonly employed as a dielectric fluid in WEDM process. When an electrical potential difference is applied between workpiece and wire, then electrical field has been established between the gap of wire and workpiece. Depending upon the amount of potential difference applied, free electrons available on the wire are subjected to strong electro-static forces. If the bonding strength of the electrons is less than the strength of electric field, then these electrons are cold emitted from the wire and accelerated towards the workpiece material. During this process, there is a collision between the electrons and the molecules of dielectric fluid. As a result, ionization of dielectric fluid will take place depending upon the ionization energy of dielectric fluid and kinetic energy of the electrons. Due to collisions, number of electrons and ions are generated between workpiece and wire. This repeated process will increase the concentration of electrons and ions between the electrode gaps which is known as the plasma channel. This plasma channel has very low electrical resistance. Therefore, suddenly, a huge number of electrons are moving towards workpiece and ions towards the wire. This phenomena, called as avalanche motion of electrons and ions which is optically seen as electrical spark. Thus, the kinetic energy of the electrons and ions has been converted into the thermal energy of the spark.

When high speed electrons impact on the workpiece and ions on the wire. In this process, their kinetic energy is converted into the intense heat flux of about 10^{17} W/m^2 which leads to extreme rise in temperature around more than 10,000 °C (El-Hofy, 2005). Within a short period of time (0.1 to 2000 µs) workpiece temperature raised to more than their boiling temperature. Due to this extreme rise in temperature, workpiece material melts and vaporizes but not completely. When the applied potential difference is detached, then the plasma channel is no longer continued. As this plasma channel collapse, it produces high pressure waves which expel the molten

metal from the discharge channel and thus forming a crater on the cut surface. The unexpelled molten metal resolidify on the machined surface to form a recast layer.
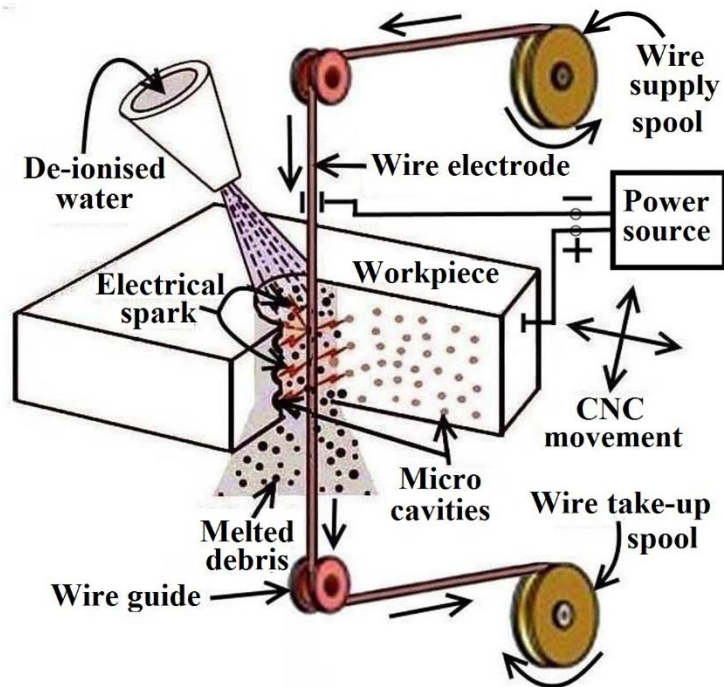
Figure 1.4 Mechanism of metal removal in WEDM process (Sharma et al., 2017).

Generally, WEDM involves complex mechanism of material removal. Therefore, its performance depends on the several factors such workpiece materials, wire materials, wire diameters, control parameters, dielectric flushing pressure and generator circuits while machining any conductive materials. In WEDM process, deionized water is the most commonly used dielectric fluid because it is easily available, cost effective and environmental friendly in nature.

1.3.3   Workpiece material

In the current study, Inconel 706 superalloy was selected as a workpiece material based on its application in advanced gas turbine engines. For WEDM operation, workpiece material should be electrically conductive (at least 0.1 µΩ/cm), non-combustible, no residual stresses, appropriate for holding and nonviolent reactivity with water. The alloy 706 is a good conductor and has been procured in the form of plate which is ideal for clamping. Moreover, the alloy is non-combustible in nature and having nonviolent chemical reactions with water.

1.3.4   Wire materials

The wire material is one of the most important factor as it helps to improve the WEDM performance. There are several wire properties which help to select the wire material for a specific application. These properties are tensile strength, conductivity, elongation, melting point, straightness and flushability. Brass wire is commonly employed as a WEDM tool. However, some high performance wires have also been developed to improve the productivity of WEDM process. These wires are coated wire, composite wire and diffused wire. In the current study, three different wire materials such as hard brass wire, zinc coated wire and diffused wire have been selected as these wires are commercially available and commonly employed in WEDM process.

1.3.4.1 Hard brass wire

Hard brass wire is an alloy of copper and zinc, which includes Cu – 40 % and Zn – 60 %. This wire offers low cost, high tensile strength, reasonable conductivity and improved flushability compared to copper wire. It is to be noted that the addition of a little quantity of zinc to copper significantly decreases the conductivity but improve the tensile strength and flushability. Practically, it is impossible to cold draw the wire with zinc content higher than 40 %, which leads to the evolution of coated wire.

1.3.4.2 Zinc coated wire

Zinc coated wire consists of additional zinc on the wire surface which delivers improved flushability compared to the hard brass wire. This wire contains zinc coating of 5 μm thickness which offers higher cutting speed compared to the hard brass wire.

1.3.4.3 Diffused wire

Diffused wire is developed by heat treating a zinc coated wire in a controlled high temperature environment. As a result of the diffusion process, the copper atoms diffuse into zinc and vice versa. Thus, it creates metallurgical bonding between zinc

coating and core material. As a result, diffusion process converts the zinc coating into high zinc content alloy.

1.3.5   Control parameters

The success of any manufacturing industry usually depends upon the appropriate selection of control parameters, since an inappropriate setting of control parameters may result in lower productivity and poor surface quality. In the current study, total eight control parameters are selected, including rough cut as well as trim cut mode. These control parameters have been defined below:

1.3.5.1 Pulse current

Pulse current is defined as the amount of current flow per cycle. In 'Electronica Eco-cut' WEDM, only two settings are available to change the pulse current. This WED machine can be operated either in power pulse mode having pulse current of 12 A or in a fine pulse mode having pulse current of 2 A. Generally, the power pulse mode is employed for the basic cutting operation, whereas fine pulse mode is used for removal of recast layer.

1.3.5.2 Pulse on time

Pulse on time is defined as the time duration of spark allowed per cycle. Pulse on time can be changed from 100 µs to 129 µs as per capability of 'Electronica Eco-cut' WED machine. In the current study, the working range of pulse on time has been estimated between 105 µs and 125 µs to avoid the gap short and wire breakage issues.

1.3.5.3 Pulse off time

Pulse off time is defined as the time interval between two successive sparks. In this WED machine, pulse off time can be changed from 15 µs to 63 µs. To allow continuous WEDM operation, the working range of pulse off time has been estimated between 18 µs to 54 µs.

1.3.5.4 Servo voltage

Servo voltage is defined as the voltage between the wire electrode and the workpiece. Mainly, servo voltage controls the spark gap which allows an operator to increase or decrease the cutting speed. Fundamentally, a low servo voltage tends to a low spark gap and vice versa. In this WED machine, servo voltage can be changed from 1 to 100 V as per the requirement. Based on trial experiment, it was observed that servo voltage lower than 20 V in power pulse mode leads to more frequent wire rupture whereas servo voltage higher than 60 V leads to a gap short issue. Therefore, the working range of servo voltage has been estimated between 20 V to 60 V.

1.3.5.5 Servo feed

Servo feed controls the speed of an advancing axis during WEDM operation. Generally, servo feed is the function of workpiece thickness. If workpiece thickness is higher, than the lower servo feed is desired and vice versa. With a proper servo feed, wire electrode can approach to the workpiece at a proper rate to give accurate control. In this WED machine, servo feed can be changed from 5 mm/min to 95 mm/min as per the requirement. In the current study, workpiece height is constant at 10 mm. Hence, it doesn't require to change the servo feed even after changing the servo feed, no significant change in WEDM performance has been detected.

1.3.5.6 Wire feed

Wire feed is defined as the speed at which fresh wire is served continuously for sparking. Wire feed is one of the most important control parameters which help to maintain the stability of WEDM process. Generally, a proper wire feed result in better machining stability, less wire rupture and slightly higher cutting speed. Thus, it is desirable to maintain the optimum cutting speed during WEDM operation. In this WED machine, wire feed can be changed from 1 m/min to 15 min as per the requirement. However, in the current study, wire feed has been selected between 3 mm/min to 12 mm/min to avoid the wire breakage.

1.3.5.7 Wire offset

Wire offset is generally employed in trim cut mode to offset the wire from the previous position. To obtain the accurate profile on the machined components, it is necessary to provide the extra margin within the nominal profile. As per the WEDM technology manual, 50 μm offset should be given in the actual profile while switching from rough cut mode to trim cut mode.

1.3.5.8 Flushing pressure

It is the pressure of dielectric fluid which helps to flush out the melted debris during WEDM operation. In WEDM, proper flushing pressure is required to achieve stable machining condition. In the current study, flushing pressure has been selected within the range of 1.37 bars to 2.55 bars as per capability of Electronica Eco-cut' WED machine. Generally, high flushing pressure is required in rough cut operation for effective removal of debris whereas low flushing pressure is desired in finishing operation to avoid the geometrical part errors.

1.3.6 Dielectric fluid

De-ionized water is mostly employed as a dielectric medium in the WEDM process because it allows the widening of the spark gap to minimize the short-circuiting between electrodes, resulting in higher cutting speed. Additionally, de-ionized water has a good cooling effect on wire compared to Kerosene. Moreover, it is non-flammable and non-toxic in nature. In WEDM, conductivity of dielectric fluid is one of the most important aspects as it decides the overcut. An ionization of de-ionized water leads to increase in conductivity during WEDM process. It is essential to maintain low conductivity of dielectric fluid. Therefore, in the dielectric distribution system of WEDM, an ion exchange resin is used which helps to maintain constant conductivity.

1.3.7 Application of WEDM

WEDM is most widely used in machining of conductive materials where high accuracy and tight tolerance is the prime concern. Currently, WEDM is being used by

aerospace, automobile, medical, tool and die making industries for manufacturing of precise and complex shaped components. These components are turbine blades, turbine disc slots, fuel injector nozzles, self-locking bone screw, extrusion tools and extrusion dies. However, current studies mainly emphasizes on the manufacturing of gas turbine components such as blade root and fir tree profile slots through advanced turbine disc alloy as shown in Figure 1.5.
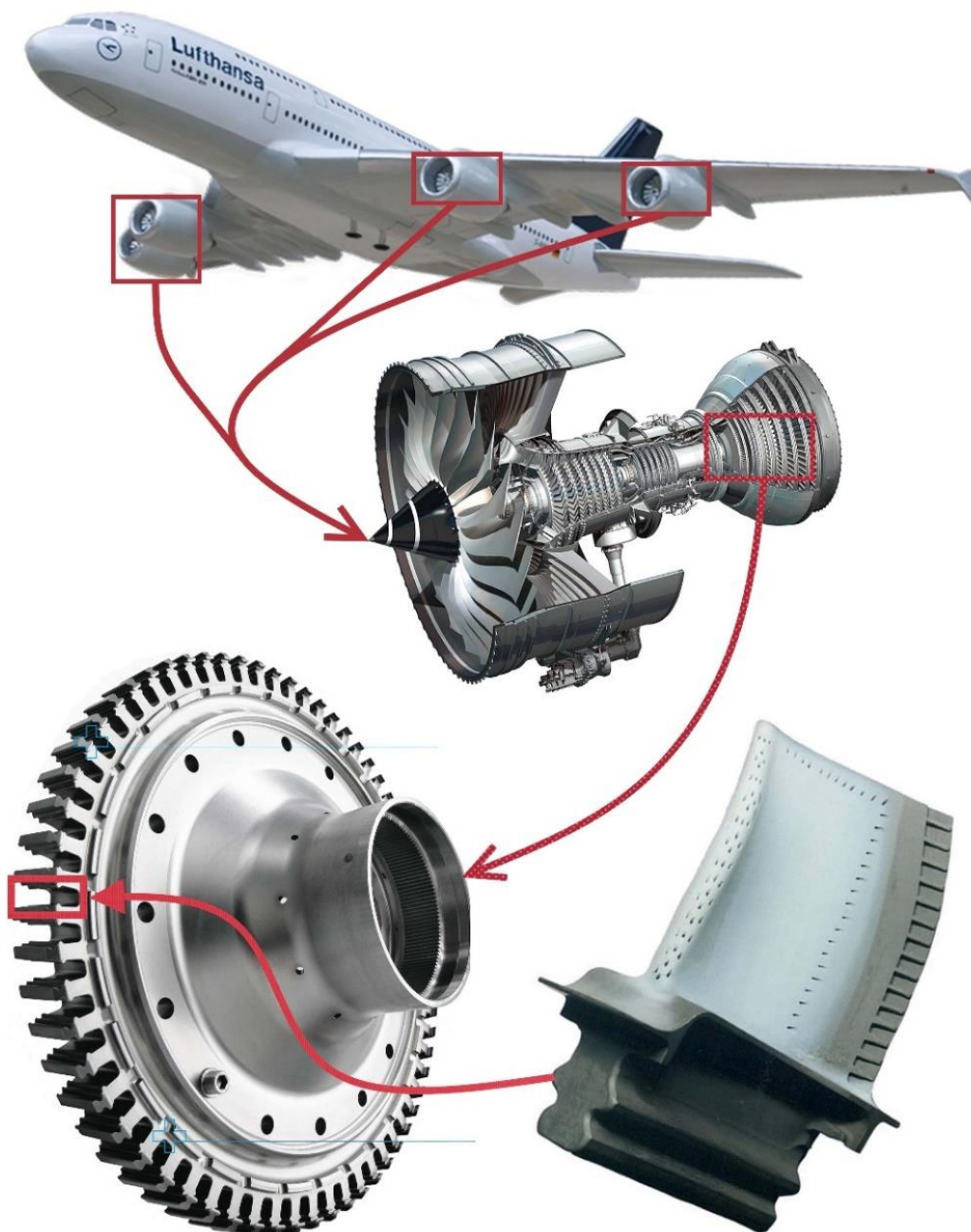
Figure 1.5 WEDM application in manufacturing of aero engine components (Rolls Royce, 2015).

A modern jet engine has more than 40 turbine discs whereas each disc consists of more than 100 turbine blades. WEDM is a capable process to economically manufacture fir tree profiles for turbine blade and turbine disc. Moreover, WEDM process offers low production costs and high process reliability compared to broaching process.

1.3.8 Evaluation of WEDM performance for Turbine disc profile application

Inconel 706 superalloy is best suited for manufacturing of aero engine components, particularly in turbine disc. Further, literature survey revealed that WEDM is a capable process of manufacturing fir tree profiles on turbine disc and turbine blade. Even though, WEDM offers various advantages over conventional/non-conventional machining process, still there are some issues with WED machined components such as recast layer formation, microhardness alteration, microstructural and elemental changes. Hence, there is a need of investigating the WEDM performance characteristics of Inconel 706 while producing the critical aero engine components.

With this impulse, the current study has been conducted to solve the issues related to the WED machined components and to achieve the feasibility in the manufacturing of aircraft components. The research work mainly emphasis on the manufacturing of turbine disc profile slots as per the standard of gas turbine industries and to evaluate the various WEDM performance characteristics such as the material removal rate (MRR), cutting speed, surface roughness (SR), surface topography, subsurface microhardness, recast layer thickness, profile accuracy, microstructural and elemental changes.

1.3.8.1 Investigation of WEDM performance characteristics

An initial experimental design was based on the one factor at a time approach. This approach helped to determine the individual effect of pulse on time, pulse off time, servo voltage, servo feed, wire feed and flushing pressure on WEDM performance characteristics such as material removal rate, surface roughness. Experimental results revealed that pulse on time, servo voltage and pulse off time are the major factor influencing the material removal rate and surface roughness. Further, the effect of

these control factors on microhardness, surface topography, recast layer thickness and microstructure have been investigated.

To determine the optimum diameter wire, significant control parameters such as pulse on time, pulse off time, servo voltage and wire feed have been considered based on earlier investigation. The comparison of different diameter wires such as 150 μm, 200 μm and 250 μm was obtained by defining the different discharge energy modes. All these wires are made of hard brass. Further, the effect of different diameter wires on cutting speed, surface roughness, surface topography, recast layer thickness, microstructural and elemental changes have been investigated. The experimental investigation revealed that smaller diameter is best suited to improve the productivity and surface quality of the machined components. Further, efforts have been made to determine the optimum wire material by considering the different discharge energy mode. The effect of wire materials on WEDM performance characteristics such as residual stresses, cutting speed, surface roughness, surface topography, recast layer thickness, microhardness, microstructural and elemental changes have been evaluated. The experimental results indicated that zinc coated wire is best suited for improved productivity, however it affects the surface quality of the machined components. Hard brass wire has shown improved surface quality in terms of lower surface roughness, smoother topography, lower recast layer thickness, minimum hardness alteration and lower residual stresses within WED machined components.

For evaluation of WEDM performance characteristics of turbine disc profile slots, all six categories of wires such as hard brass wire of diameter 150 μm, 200 μm and 250 μm; zinc coated wire of diameter 200 μm and 250 μm; diffused wire of diameter 250 μm were considered. The geometrical data of turbine disc slots were obtained from the literature (Klocke et al., 2014). The profile slot geometry was drawn in AutoCAD and simulated in ELCAM to generate the corresponding CNC program. Then, profile slots were machined using a different category of wires and WEDM performance characteristics such as residual stresses, profile accuracy, microhardness, recast layer thickness, surface topography and surface roughness were evaluated. The experimental investigation revealed that hard brass wire diameter 150 μm, 200 μm and 250 μm are best suited for machining of turbine disc profile slots whereas zinc

16

coated wire and diffused wire were disqualified from the quality checklist of turbine disc issued by gas turbine industries. However, hard brass wire of diameter 150 µm has shown the minimum hardness alteration, almost negligible recast layer, profile accuracy within ±5 µm, surface roughness of 0.65 µm and residual stresses of 597.8 MPa in second trim cut mode and confirm the requirements of gas turbine industries.

1.3.8.2 Modeling and optimization of WEDM performance characteristics

For modeling and optimization of WEDM performance characteristics, optimum wire diameter and wire materials were considered. The mathematical models for material removal rate (MRR) and surface roughness (SR) were developed using response surface methodology (RSM). In different modules of RSM, central composite design is quite popular to investigate the linear, squared and interaction terms. The insignificant terms have been removed from the model based on backward elimination approach. The developed mathematical models were used as a fitness function for teaching learning based optimization (TLBO) algorithm. In this study, TLBO algorithm was used for individual as well as multiple objective optimization. For multiple objective optimization, a combined objective function was developed by normalizing the MRR and SR. Finally, Pareto optimal solutions were obtained which are believed to be a global optimal solution.

1.4 OUTLINE OF THE THESIS

To achieve the feasibility in WED machining of advanced turbine disc alloy (Inconel 706), the current thesis work has been divided into seven chapters. The detail of individual chapter has been described below:

CHAPTER 1

In this chapter, background of superalloys, introduction of nickel-iron-based superalloys and their applications have been described. The chapter also discusses the machinability of nickel-iron-based superalloys followed by introduction of WEDM, principle of WEDM, workpiece materials, wire materials, dielectric fluid, control parameters and application of WEDM.

CHAPTER 2

This chapter presents the comprehensive literature review which is closely related to the WED machining of Nickel-based superalloys. The literature review has been classified based on the influence of wire materials, control parameters, dielectric fluids, surface and subsurface characteristics, advancement in WEDM process, modeling and optimization of WEDM process. Moreover, various researchers' contributions and experimental conditions used by earlier researchers have been tabulated. Finally, the motivation of a literature survey and objective of current research work has been presented.

CHAPTER 3

This chapter deals with the material selection, material preparation, experimental setup, procedure and methodology involved in the research work. This chapter also mentions the steps involved in measurement of WEDM performance characteristics. Moreover, the details of equipment used for measurement of WEDM performance have also been described in this chapter.

CHAPTER 4

This chapter is associated with the evaluation of WEDM performance characteristics such as material removal rate (MRR), surface roughness (SR), recast layer formation, microhardness, surface topography, microstructural and elemental changes based on one factor at a time (OFAT) approach. Further, WEDM performance has been studied by considering the different discharge modes in order to investigate the optimum wire diameter as well as optimum wire material.

CHAPTER 5

This chapter deliberates with the manufacturing of turbine disc profile slots using WEDM process and its characterization for gas turbine application. In this chapter, various WEDM performance characteristics of turbine disc profile slots such as cutting speed, surface roughness, microstructure, recast layer formation, subsurface microhardness, surface topography, residual stresses, crystal structure, profile

accuracy, microstructural and elemental changes have been studied. Also, the comparison of rough cut mode and trim cut mode with respect to WEDM performance characteristics has been presented in this chapter.

CHAPTER 6

This chapter discusses the mathematical modeling of WEDM performance characteristics using RSM followed by a backward elimination approach. The interaction effect of WEDM control parameters has been studied with the help of surface plot and significant control factors have been determined using analysis of variance (ANOVA). This chapter also deals with optimization of WEDM performance characteristics using TLBO algorithm. Finally, Pareto optimal solutions have been obtained in contrast to multi-objective optimization.

CHAPTER 7

In this chapter, conclusions have been derived based on the performance of WED machining of turbine disc alloy. This chapter also addresses the future scope based on the present study.

CHAPTER 2

LITERATURE REVIEW

2.1   INTRODUCTION

This chapter presents the review of research work which is associated with the machining performance of nickel-based superalloys. The effect of wire materials, dielectric fluids and control parameters on WEDM performance characteristics has been defined clearly. Particularly, the effect of WEDM control parameters on surface and subsurface characteristics have been reviewed. An overview of modeling and optimization techniques used for improving the WEDM performance of nickel-based superalloy has been presented. Further, WED machinability of nickel-based superalloys have been reviewed by segregating the various researchers' contributions as shown in Table 2.1.

2.2   MACHINING OF NICKEL-IRON-BASED SUPERALLOYS

Nickel-iron-based superalloys are categorized as a unique class of materials because of their high thermal resistivity and excellent mechanical properties. Also, these superalloys offer high specific strength compared to steel. Therefore, these superalloys are being used in gas turbine, petroleum and nuclear industries. Currently, the gas turbine industries are demanding for precise, complex and irregular shape through these superalloy components for gas turbine engines. Manufacturing of gas turbine components such as turbine discs, turbine blades, turbine vanes, turbine vane rings, and turbine nozzles require advance manufacturing technology which can produce intricate and complex shape components with high precision. Due to higher tool wear rate in conventional machining of these superalloys, it is very difficult to maintain the uniform surface characteristics of the work material and unable to fulfil the current industrial demands. Generally, in conventional machining of nickel-iron-based superalloys, difficulties commonly observed in terms of burr formation at the edge of machined surface, high stresses acting on tool, thermal damage of the tool tip as well as low process stability.

Table 2.1 Contribution of earlier researchers in WEDM process of nickel-based Superalloys.

No.	Author(s)	Process	Material	Brief Contribution
1.	Hewidy et al. (2005)	WEDM	Inconel 601	Statistical models were developed using response surface methodology (RSM) to correlate the WEDM control factors with machining characteristics. The developed models have shown its adequacy under acceptable range.
2.	Aspinwall et al. (2008)	WEDM	Inconel 718	The surface integrity of WEDM process such as surface roughness, microstructure and microhardness were analyzed using MDGT. The technology offers an extremely low level of workpiece damage.
3.	Ramakrishnan and Karunamoorthy (2008)	WEDM	Inconel 718	Artificial neural network (ANN) models were developed based on back-propagation algorithms and, then multiple parameter optimization was attempted to determine the optimum cutting parameters of WEDM process.
4.	Newton et al. (2009)	WEDM	Inconel 718	The effect of energy per spark, peak current, and pulse duration on the recast layer formation were investigated. Within the range of parameters selected, the average recast layer thickness was observed between 5 to 9 μm.
5.	Antar et al. (2011)	WEDM	Udimet 720	The surface roughness and residual stresses produced by uncoated and coated brass wire were compared during WEDM process. The minimum recast layer thickness was achieved using coated wire.
6.	Klocke et al. (2012)	WEDM	Inconel 718	WEDM technology was developed for production of fir tree slots in turbine disc made of Inconel 718 superalloy.

7.	Antar et al. (2012)	WEDM	Udimet 720	Improvements in fatigue performance of Udimet 720 were obtained using trim cut technology and MDGT.
8.	Li et al. (2013)	WEDM	Inconel 718	The surface roughness, surface topography, microstructure and white layer of WED machined surface were evaluated under rough cut mode and trim cut mode.
9.	Rajyalakshmi and Ramaiah (2013)	WEDM	Inconel 825	WEDM process parameters were optimized using combination of Taguchi technique and grey relational analysis (GRA) for maximization of MRR, minimization of SR and spark gap.
10.	Klocke et al. (2014)	WEDM	Inconel 718	New wire electrodes were developed to improve the productivity of WEDM process. However, best surface integrity and accuracy were obtained with standard brass wire.
11.	Li et al. (2014)	WEDM	Inconel 718	MRR, SR, microhardness and subsurface microstructure of WEDM processed Inconel 718 were investigated under one rough cut and three trim cut mode.
12.	Garg et al. (2014)	WEDM	Inconel 718	Effect of wire materials on WEDM cutting performance was evaluated using RSM.
13.	Jakhar et al. (2015)	WEDM	Inconel 600	WEDM control parameters were optimized using Taguchi method with prediction error of 0.46 % and 6.02 % for cutting speed and SR respectively.
14.	Aggarwal et al. (2015)	WEDM	Inconel 718	Mathematical models were developed for cutting speed and surface roughness. The developed models were found to be reliable for representation of experimental results with minimum prediction errors.
15.	Rao and Venkaiah (2015)	WEDM	Nimonic 263	The control parameters of WEDM process were optimized using RSM and particle swarm optimization (PSO) approach.

16.	Kumar et al. (2016)	WEDM	Nimonic 90	The comparison of dielectric fluid with/without Al and Si power was presented in WEDM of Nimonic 90. Al and Si power shows reduction in machining rate in trim cut operation while surface roughness decreases with a concentration of 1 g/L of Al and Si powder additives.
17.	Rao and Venkaiah (2016)	WEDM	Inconel 690	The mathematical model was developed using a feed forward back propagated neural network to predict the circularity error. The developed model was found to be useful to predict the circularity error with acceptable deviation.
18.	Mandal et al. (2016)	WEDM	Nimonic 263	The statistical models were developed for cutting speed, surface roughness, spark gap and wire wear ratio. The optimal machining conditions were obtained using desirability function approach.
19.	Dabade and Karidkar (2016)	WEDM	Inconel 718	WEDM machining conditions were studied for MRR, SR, kerf width and dimensional deviation and, significant control parameters have been evaluated using analysis of variance (ANOVA).

Ezugwu et al. (1998) have found that nickel-based superalloys exhibit poor performance during conventional machining. Since, these alloys are capable to maintain their strength at high temperature. Choudhury et al. (1998) have conducted the extensive study on nickel-based superalloys and concluded that machinability of these superalloys are very inferior using conventional techniques because of their high strength at elevated temperature, tendency to react with tool materials and low thermal conductivity. Ezugwu et al. (2003) have studied the machinability of aero engine alloys and concluded that due to improved properties of aero engine alloys, the life of all tool materials is limited by extreme temperature and pressure conditions encountered during machining operation.

The issues, which are responsible for the poor machining of nickel-based superalloys, are given below (Choudhury et al., 1998; Ezugwu et al., 2003):

- High work-hardening tendency of these alloys leads to high cutting force.
- These alloys lead to abrasive wear due to existence of hard abrasive particles.
- They also have a high tendency to built up edge formation.
- These alloys exhibit low thermal diffusivity and specific heat, which leads to high thermal gradient in cutting tool due to precipitation of hard secondary phase (γ").
- They can maintain their strength at elevated temperature.
- The conventional machining of these alloys results in formation of tough and continuous chip which is difficult to remove during machining.
- These alloys exhibit high chemical affinity towards many tool materials which leads to diffusion and attrition wear.

All these factors associated with nickel-iron-based superalloys make them inadequate and incapable to machine using conventional machining methods. To overcome these machining limitations, non-conventional machining processes such as electrochemical machining (ECM), laser beam machining (LBM), electrical discharge machining (EDM) and abrasive water jet machining (AWJM) were successfully using and yield good capability to machine these superalloy components irrespective of their mechanical properties. Still, there are few concerns with non-conventional machining processes. The usage of AWJM process is limited to brittle materials. The

components produced by AWJM process include several issues such as impingement of abrasive particles into the matrix, crack propagation and burr formation at the edge (Singh and Jain, 1995). LBM process results in micro-cracking, poor surface quality, low dimensional accuracy and significant recast layer formation (Zhong et al., 2005). ECM process results in more chance of corrosion due to acidic electrolyte, comparatively low material removal rate (MRR) and require special shaped electrode (El-Hofy, 2005). EDM process results in less recast layer formation compare to LBM and require special shaped electrode (Rasheed, 2013).

Looking into the current stringent economy, gas turbine manufacturing industries are forced to search for alternatives to achieve better quality, lower production cost and faster delivery time. However, the Wire electrical discharge machining (WEDM) was found to best alternative over EDM. WEDM is an advance version of EDM which eliminate the need of special shaped electrode and reduce the recast layer thickness significantly with the use of low discharge pulse. Additionally, WEDM is more efficient than the EDM in terms of flexibility and offers low residual stresses on the machined component. High dimensional accuracy and improved surface quality of the machined components make WEDM most valued. In the past few years, WEDM proved and got success in the production of gas turbine components which require complex shape profiles with high precision. Turbine disc is amongst the most critical components in gas turbine engine which requires a number of complex profile slots to attach the turbine blades. The typical geometry of these profile slots is dovetail or fir tree profiles. For the current study, the fir tree profile has been selected which is commonly employed for turbine disc of aircraft engines.

Nowadays, manufacturing of these complex slots through the turbine disc is one of the most important aspect because of their high demand in terms of geometry, shape, surface finish and dimensional accuracy. Bez'yazychnyi et al. (2008) have suggested some machining processes (i.e., broaching, milling, electro erosion milling, electrochemical machining) to produce the turbine disc profile slots. In order to substitute the conventional broaching process, Curtis et al. (2008) have used novel machining techniques to produce the complex profile slots. WEDM process is found to be an alternative to conventional broaching process for turbine disc slots

production. Even though, high MRR and good surface quality can be achieved in broaching process, the process offers high tool wear rate and high maintenance cost which prevents the continuous production of gas turbine components. Moreover, broaching process is highly inflexible if the workpiece geometry is frequently changing. While producing fir tree slot through Inconel 718, Welling (2014) has exposed the good strength of WED machined components compared to the conventional broaching process. Only a few researchers (Klocke et al., 2012; Klocke et al., 2014) have attempted to produce these complex slots through turbine disc alloy using WEDM process. Therefore, in this study, an attempt will be made to manufacture the complex profile slots through advanced turbine disc alloy (Inconel 706) using WEDM process to meet the standards set by gas turbine industries such as surface roughness less than 0.8 μm, dimensional accuracy within the range of ±5 μm and residual stresses less than 850 MPa (Klocke et al., 2014).

2.3   WED MACHINING OF NICKEL-BASED SUPERALLOYS

WEDM is a popular industrialized non-conventional machining process. In this process, productivity of the components greatly depends upon the MRR and cutting speed whereas the surface quality of the machined component depends on the surface roughness, surface topography, subsurface microstructure, elemental changes and residual stresses. There are several factors in WEDM process such as wire material, dielectric fluid, control parameters, generator technology and trim cut strategy which affects its performance. Based on the available literature, the effect of these factors on WEDM performance characteristics of nickel-based superalloys has been studied under the following sections. The machining conditions, which are used by the various researchers during the WEDM process of nickel-based superalloys, have been segregated and presented in Table 2.2.

Table 2.2 Summary of machining conditions used by earlier researchers during WEDM process of nickel-based superalloys.

No.	Author(s)	Material	Control parameter(s)	Dielectric Fluid(s)	Wire Material(s)	Wire Diameter
1.	Hewidy et al. (2005)	Inconel 601	Discharge energy, depth and speed	Deionized water	Uncoated brass	200 μm
2.	Ramakrishnan and Karunamoorthy (2008)	Inconel 718	Pulse on time, delay time, wire feed speed, and ignition current	Deionized water	Uncoated brass	250 μm
3.	Aspinwall et al. (2008)	Inconel 718	Depth and speed	Deionized water	Zinc coated brass and uncoated brass	200 μm and 250 μm
4.	Newton et al. (2009)	Inconel 718	Wire diameter, table feed speed, spark cycle, spark energy	Deionized water	Hard brass	100 μm
5.	Antar et al. (2011)	Udimet 720	Voltage, ignition current, on time, off time, flushing pressure, wire speed, wire tension, wire offset	Deionized water	Copper coated brass	250 μm
6.	Antar et al. (2012)	Udimet 720	Constant process parameters	Deionized water	Uncoated brass	250 μm
7.	Klocke et al. (2012)	Inconel 718	Open voltage, discharge duration, pulse interval time, discharge current, wire offset	Deionized water	Standard brass wire	250 μm
8.	Rajyalakshmi and Ramaiah (2013)	Inconel 825	Voltage, gap voltage, on time, off time, and flushing pressure, wire speed, wire tension, servo feed rate	Deionized water	Brass	250 μm

9.	Li et al. (2013)	Inconel 718	Discharge energy, depth, speed	Deionized water	Uncoated brass	200 μm
10.	Li et al. (2014)	Inconel 718	Voltage, current, pulse on time, pulse off time, wire feed, wire tension, and flushing pressure	Deionized water	Brass	250 μm
11.	Klocke et al. (2014)	Inconel 718	Pulse rise time, pulse interval time, open voltage, servo voltage	Deionized water	Standard brass wire, coated high-speed-cutting wire and Nickel coated wire	250 μm
12.	Aggarwal et al. (2015)	Inconel 718	Pulse on time, pulse off time, pulse current, spark gap voltage, wire feed rate, wire tension	Deionized water	Zinc coated brass wire	250 μm
13.	Kumar et al. (2016)	Nimonic 90	Discharge energy, concentration of dielectric fluid	Distilled water + Al and Si mixed distilled water	Copper coated brass	250 μm
14.	Mandal et al. (2016)	Nimonic 263	Pulse on time, pulse off time, servo voltage, dielectric flow rate	Deionized water	Zinc coated brass	250 μm
15.	Dabade and Karidkar (2016)	Inconel 718	Pulse on time, pulse off time, peak current, wire feed, wire tension, servo voltage	Deionized water	Zinc coated brass	250 μm

2.3.1 Influence of wire materials

WED machinability of nickel-based superalloys has been affected by the several wire electrode parameters (i.e., type of wire materials, diameter of wire, and the type of coating used on the wire). For effective utilization of WEDM, wire material should have adequate tensile strength, high electrical resistivity, good flushability, low melting temperature and minimum energy required to melt and vaporize the workpiece material. Klocke et al. (2014) have explored the WEDM capability using different wire materials. The manufacturing time has been reduced to almost one-third using high speed cutting wire. However, the best surface quality of machined component was obtained using standard brass wire. Maher et al. (2014) have shown the various improvements in wire material properties for its better utilization in WEDM process. It was reported that productivity increases with increase in zinc content in wire. The high zinc content allows lower servo voltage which makes short circuiting difficult. Additionally, evaporation of zinc coating produces a heat-sink effect which leads to a cooling of the core material. Therefore, allowing a more thermal flow due to reduction in wire temperature and hence leading to a higher cutting speed. When zinc coating evaporates, it stabilizes the plasma channel of spark and increases the spark gap which leads to a better dielectric flushing. Even though, zinc coated wire has shown improved cooling ability and better flushability compared to conventional brass wire, high cost, straightness issues and environmental hazards have been recorded.

Antar et al. (2011) have conducted the extensive study on coated and uncoated brass wire during WED machining of Udimet 720. It was observed that up to a 40 % increase in productivity was observed while substituting the standard brass wire by diffusion annealed coated wires under the similar operating conditions. The change of wire electrodes significantly affects the surface roughness (SR) and residual stresses produced during the operation as shown in Figure 2.1. The variations of SR may be due to the imperfect sparks caused by wire erosion. Up to a 25 % thinner recast layer was observed for Udimet 720 when coated wire was used. Further, Garg et al. (2014) have studied the influence of wire materials on WEDM machining characteristics while cutting Inconel 718 alloy. It was found that zinc coated brass wire is best suited

for high productivity. Manjaiah et al. (2015) have also studied the effect of wire materials on WEDM performance characteristics. It was observed that zinc coated wire produces better MRR compared to the brass wire.
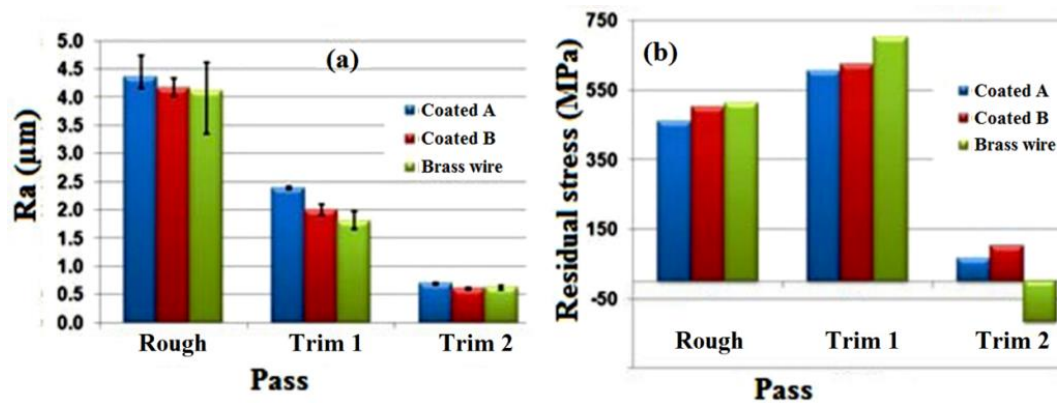
Figure 2.1 Effect of wire materials on: (a) surface roughness; (b) residual stresses
(Antar et al., 2011).

2.3.2 Effect of control parameters

The selection of WEDM control parameters plays crucial role in achieving higher productivity and improved surface quality of the machine parts. However, an inappropriate selection of control parameters in WEDM process may result in unstable machining condition such as wire breakage and gap shortage issue. In WEDM, servo voltage, servo feed, pulse on time, wire feed, pulse off time, pulse current, wire offset and wire tension are the commonly used control parameters. However, in Electronica Eco-cut WEDM there is a limitation that wire tension cannot be changed. Based on the available literature, some of the important control parameters have been reviewed by discussing their effect on WEDM performance characteristics while machining nickel-based superalloys.

Goswami and Kumar (2014) have investigated that with an increase in pulse off time and servo voltage, MRR and cutting speed decreases. But, with increase in pulse on time and pulse current, MRR and cutting speed increases. This is due to increased discharge energy at high pulse on time and pulse current; however, discharge energy supplied to workpiece material is decreasing with an increase in pulse off time and servo voltage. Li et al. (2013) have studied the effect of WEDM control parameters on

SR, surface topography, microstructure, micro hardness and elemental changes during the WEDM process of Inconel 718. It was observed that when pulse current or discharge energy decreases, then less thermal energy would be transferred to the material. Consequently, less material will be melted. This, in turn, reduces the formation of craters and micro cavities on the machined surface and hence improves the SR. The effect of discharge energy on SR with parallel and perpendicular direction of wire has been shown in Figure 2.2. Manjaiah et al. (2016) have observed that MRR increases with increased pulse on time within the range of 4–8 mm^3/min.
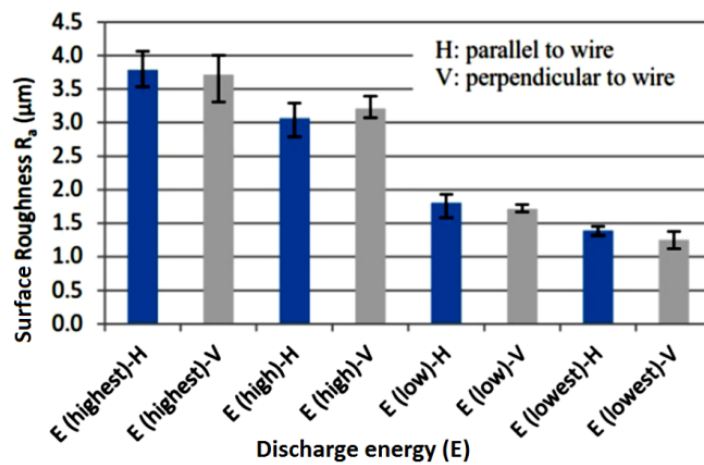
Figure 2.2 Variation of SR at different level of discharge energy (Li et al., 2013).

According to Hewidy et al. (2005), with an increase in wire tension, SR gradually decreases as shown in Figure 2.3 (a). Because, an increase of wire tension minimizes the bending effect of wire and provide the dynamic stability to the wire which reduces the depth of craters formed on machined surface and thus reduces the SR. Figure 2.3 (b) shows that volumetric material removal rate (VMRR) is nearly constant at all specified levels of wire tension and water pressure which indicate that wire tension has little impact on VMRR. Further, Manjaiah et al. (2016a) have investigated that SR of WED machined surface decreases with increased pulse off time due to formation of shorter ignition ratio which induces smaller craters on the machined component.
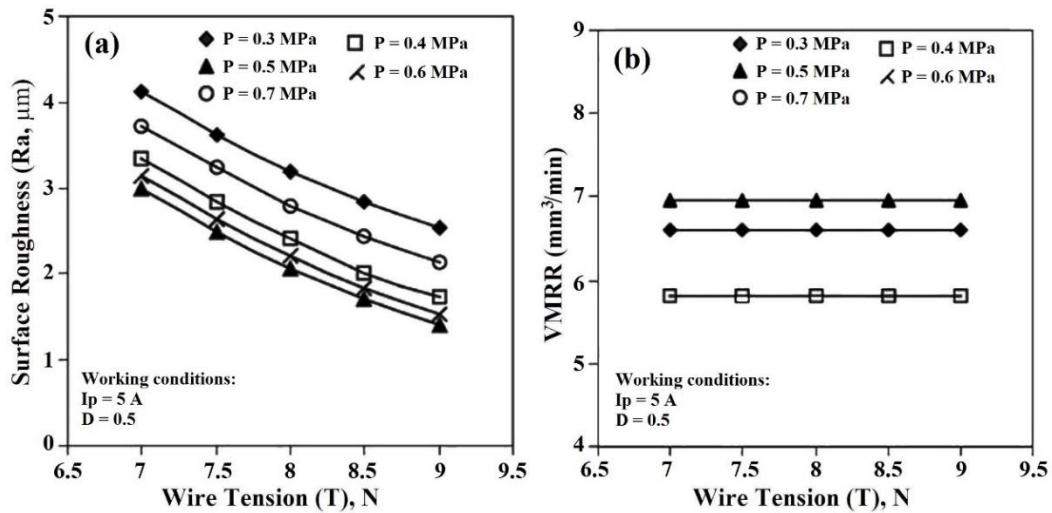
Figure 2.3 Effect of wire tension on: (a) surface roughness; (b) volumetric MRR (Hewidy et al., 2005).

The selection of duty factor has an important role to enhance the WEDM performance. Generally, duty factor is defined as the ratio of pulse duration to total cycle time. According to Hewidy et al. (2005), VMRR increases with increase in duty factor up to 0.5 then thereafter it decreases. That's because, at high duty factor, same amount of thermal energy transferred to the material for longer time. Therefore, it will increase the melting and evaporation of workpiece material and remove large volume of molten metal and thus increases the MRR.

2.3.3 Influence of dielectric fluid

De-ionized water is generally employed as a dielectric medium in WEDM process. Recently, Kumar et al. (2016) have made an attempt to investigate the WEDM performance in trim cut operation using Al and Si powder mixed dielectric fluid. The effect of concentration of Al and Si powder in distilled water on machining rate and surface roughness has been shown in Figure 2.4. From the Figure 2.4 (a–b), it was observed that addition of Al and Si powder in dielectric fluid reduces the machining rate in trim cut operation, however, it also reduces the surface roughness with a concentration of 1 g/L of Al and Si powder. Also, recast layer becomes denser and micro hardness increases after replacing the dielectric fluid with Al and Si powder mixed dielectric fluid. Moreover, nano impingements were observed on the machined

surface while using Al and Si powder mixed dielectric fluid. Micro cracks free machined surface were observed due to the absence of carbon in Nimonic 90 whereas nano impingements were observed due to Al and Si powders which is not completely evaporated during WEDM process.
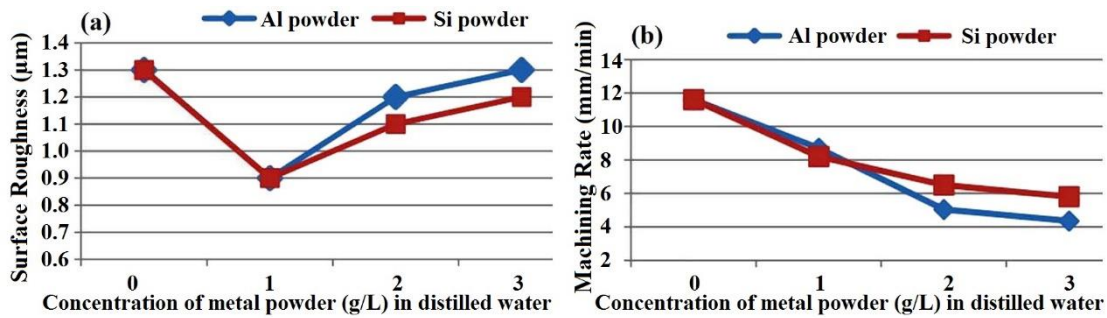
Figure 2.4 Effect of concentration of Al and Si powder in distilled water on: (a) machining rate; (b) surface roughness (Kumar et al., 2016).

Similarly, Yeh et al. (2013) have tried to mix sodium pyrophosphate powder into dielectric fluid to achieve the feasibility in the WED machining of semiconductor materials. It was observed that sodium pyrophosphate powder mixed dielectric fluid increases the cutting speed by 1.48 times and decreases the surface roughness by 12% compared to distilled water based dielectric fluid.

2.3.4 Effect on surface and subsurface characteristics

In WEDM, surface and subsurface characteristics of the machined components are influenced by various machining conditions. Based on the available literature, surface characteristics such as microstructure, surface roughness, microhardness, recast layer, elemental changes and residual stress of the WED machined surface have been studied and reported in the following paragraph.

Li et al. (2014) have studied the SR of Inconel 718 during the WEDM using statistical distribution which deliver the spectrum of SR over a wide variety of the machining conditions. They observed that the average SR was reduced significantly by trim cut strategy as shown in Figure 2.5. It was also found that the low carbon content of Inconel 718 would not make the white layer harder, even being quenched by dielectric fluid.

33
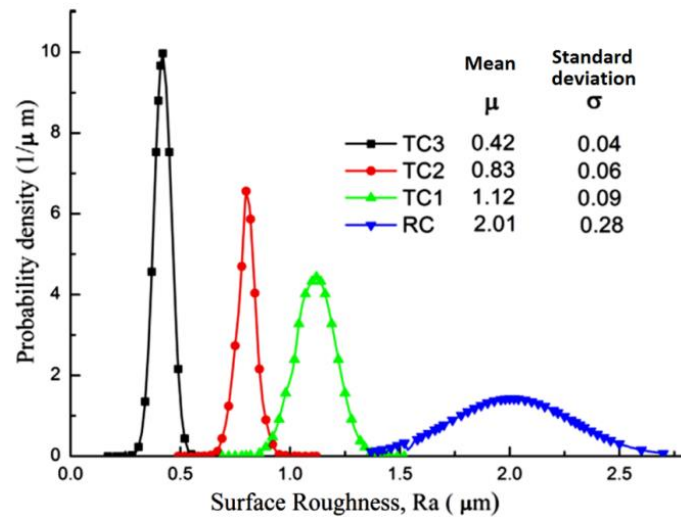
Figure 2.5 Surface roughness distribution from rough cut (RC) to trim cuts (TC1, TC2, TC3) in the WEDM process of Inconel 718 (Li et al., 2014).

Newton et al. (2009) have studied the recast layer formed on WEDM processed Inconel 718. To determine recast layer thickness, area of recast material has been calculated, and then divided by length. The average recast layer thickness of Inconel 718 varied from 5.10 to 8.51 µm during all machining conditions as shown in Figure 2.6. The recast layer formation on machined component is highly undesirable for aerospace application. That's because, aircraft components are subjected to a high amount of stresses during operation, and need to maintain safety even at high cost.
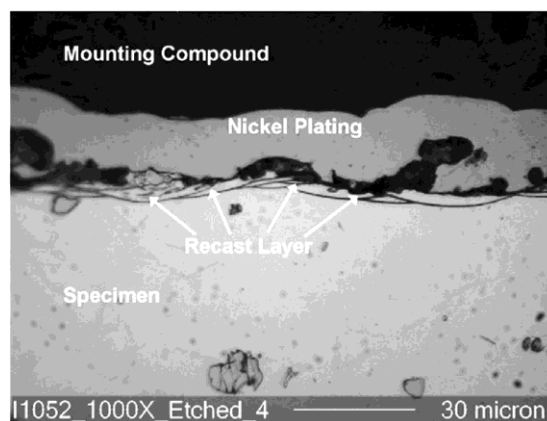
Figure 2.6 Microscopic image of WED machined surface of Inconel 718 specimen under following machine settings: wire diameter of 250 µm, table feed rate of 2.22 mm/min, spark cycle of 28 µs, and spark energy setting of 18 (Newton et al., 2009).

34

Further, the recast layer formation has been studied by Antar et al. (2011) during WEDM process of Udimet 720. Under second trim cut, no recast layer was detected due to low pulse energy. Instead, the white layer formation has been studied by Li et al. (2013). It was observed that white layer thickness increases with increase in pulse current as well as pulse duration. That's because of larger pulse duration and pulse current which allows higher thermal energy to penetrate into the subsurface. An average white layer of 13.3 μm was observed in rough cut mode, whereas the white layer thickness has been reduced significantly up to 3.3 μm in third trim mode due to lowest discharge energy.

Further, Li et al. (2014) have studied the subsurface microhardness of WEDM processed Inconel 718 under rough cut mode as well as trim cut mode. It was observed that microhardness of the white layer was decreased in each case compared to the bulk material. Unlike carbon steel, it won't make the surface harder due to low carbon content of Inconel 718. Additionally, multiple thermal loading during WEDM has softened effect on the material. From the Figure 2.7, it was observed that thermal affected zone is decreasing from rough cut to trim cut. It is possibly due to higher thermal damage produced by high discharge energy in rough cut mode while in trim cut mode, workpiece material is subjected to comparatively low discharge energy which leads to a lower thermal damage. However, the low microhardness of heat affected zone was obtained because of thermal degradation occurred during WEDM process.
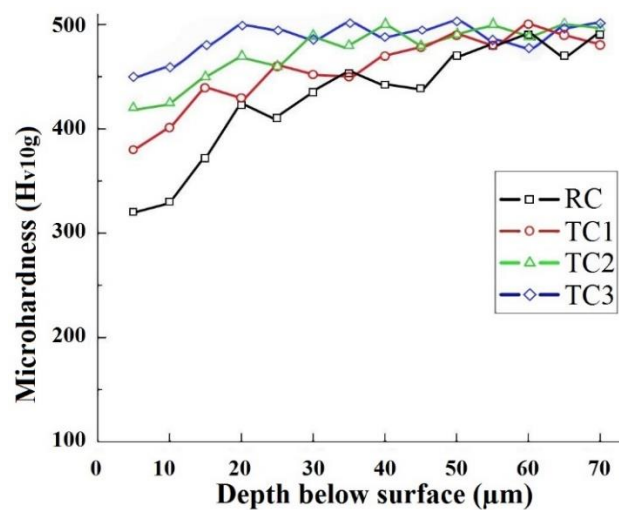
Figure 2.7 Microhardness profile of WED subsurface (Li et al., 2014).

Aspinwall et al. (2008) have obtained microhardness profile of WEDM processed Inconel 718. While comparing the microhardness in rough cut and trim cut mode, minimum alteration was observed, which leads to extremely low recast layer thickness.

Antar et al. (2012) have compared the surface residual stresses of Udimet 720 under WEDM roughing, WEDM finishing and milling operation. It was observed that milling suggests a better fatigue life. However, the fatigue life of WEDM finishing has been improved significantly compared to WEDM roughing as shown in Figure 2.8.
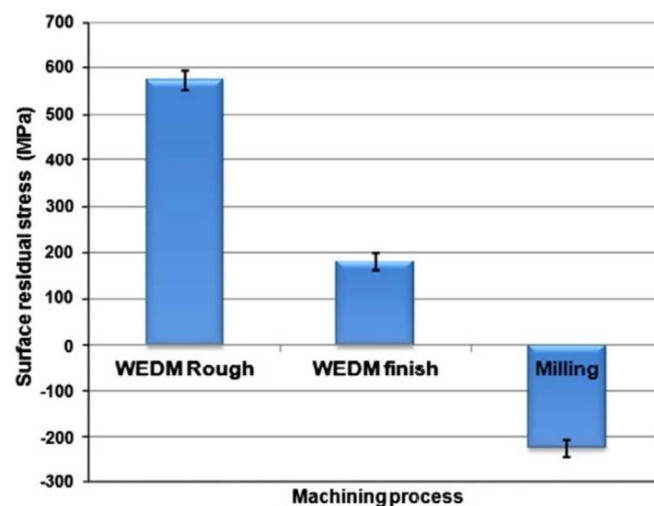
Figure 2.8 Surface residual stresses for fatigue components of Udimet 720 (Antar et al., 2012).

During WEDM operation, complex chemical reaction will take place among workpiece material, wire material and dielectric fluid due to extremely high temperature of plasma heat flux (up to 12000 °C). Due to this high temperature, elemental changes may occur in the surface layer of the workpiece. Li et al. (2013) have measured the elemental composition of white layer produced by WEDM process while machining Inconel 718. Energy Dispersive X-Ray Spectroscopy (EDS) analysis of white layer exposed the presence of Cu element under rough cut mode as shown in Figure 2.9(a) due to diffusion of wire material and workpiece material. However, Cu element is almost nil in trim cut mode as shown in Figure 2.9(b) possibly due to low discharge energy. Moreover, O was also detected in rough cut and trim cut mode,

which is more in the rough cut mode. That's because, decomposition of de-ionized water under rough cut mode is more.
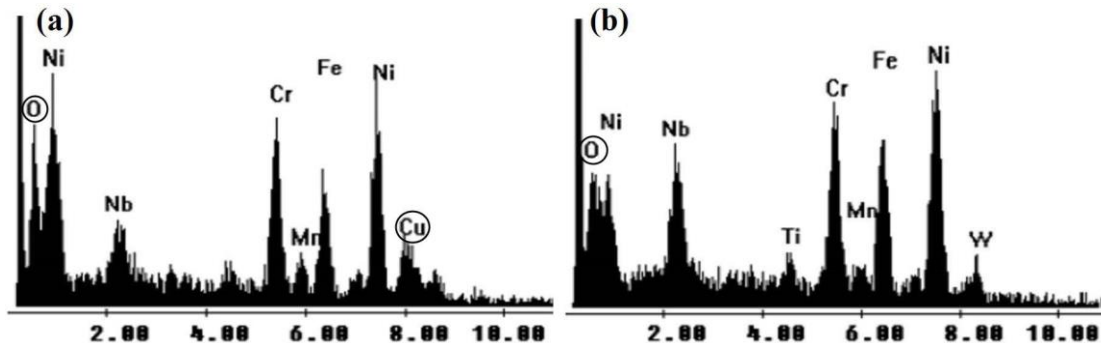
Figure 2.9 Effect of discharge energy on EDS spectra of white layer formed by: (a) Rough cut mode; (b) Trim cut mode (Li et al., 2013).

2.3.5 Advancement in WEDM process

WEDM process has been undergoing continuous technological development since last 10 years. Due to development made in generator technology and wire electrode materials, it has become possible to achieve cutting rates approximately 5 times higher than usual. Through the usage of minimum damage generator technologies, Aspinwall et al. (2008) has reported the recast layer thickness less than 11 μm during WEDM process of Inconel 718. With the usage of appropriate trim pass strategy, recast layer became nearly invisible. No variation in microhardness was observed with cracking confined to recast layer. The fatigue performance of machined components of Udimet 720 alloy has been improved significantly in WEDM using a combination of minimum damage generator technology (MDGT) and appropriate trim cut strategies (Antar et al., 2012). Klocke et al. (2012) and Klocke et al. (2014) have attempted to produce the fir tree slots though Inconel 718 using WEDM equipped with clean cut generator technology followed by appropriate trim pass strategy. Further, Mandal et al. (2016) have investigated that multiple cut strategy minimizes the surface roughness and also diminishes the recast layer significantly.

Atzeni et al. (2014) have evaluated the subsurface alteration of Inconel 718 during the WEDM process, but no thermal modification was observed on machined surface using the proper setting of discharge energy and wire feed rate. For the further improvement in WEDM process, process monitoring tool has been developed by

Klocke et al. (2014 a) to correlate the surface integrity of the WEDM process while producing fir tree slots. Schwade (2014) studied the high recurrent electrical signal to improve the existing WEDM technology. They have recorded the actual value of pulse on time, pulse current, pulse off time and voltage using a 'Tektronix digital oscilloscope'. Then, the quality of WEDM process has been determined in terms of actual discharge frequency, percentage of multi-discharge and duty cycle. Further, these parameters were linked to cutting speed and SR.

Zhang et al. (2016) have investigated the WEDM performance characteristics of aerospace alloys with magnetic field assisted techniques and ultrasonic vibration. It was detected that magnetic field-assisted WEDM increases the stability of the plasma channel by generating Lorentz force and Ampere force. Moreover, it increases the current density as well as resultant force to eject the melted debris and hence improve the MRR and SR. In order to improve the profile accuracy in WEDM process, an analytical model has been developed by Sarkar et al. (2011) to determine wire lag and gap force during WEDM process. Based on this model, wire lags compensation technique was developed to minimize the profile inaccuracy.

2.4   MODELING AND OPTIMIZATION OF WEDM PROCESS

Due to the complexity mechanism in WEDM, there are several control parameters which influence the productivity and surface features of the machined component. A slight change in control factor settings may affect the WEDM performance. Earlier researchers have developed mathematical models, and also used various optimization techniques to select the optimum combination of control parameters to improve the WEDM efficiency and machined surface quality. Hewidy et al. (2005) have established the mathematical models for correlating the inter-relationships between WEDM control factors (i.e., peak current, duty factor, wire tension, water pressure) and performance characteristics (i.e., VMRR, SR, wear rate). Response surface methodology (RSM) was found to be advantageous for identifying the effect of control factors on output responses.

Ramakrishnan and Karunamoorthy (2008) have used Artificial Neural Network (ANN) model to predict the WED machining characteristics more precisely. Further,

the effect of various control factors such as pulse on time, wire feed, delay time and ignition current on machining characteristics of Inconel 718 were investigated. After that, multi-response optimization technique was employed to determine the optimum setting of control parameters of WEDM process. It was observed that Taguchi-based multiple performance optimization is quite simple, efficient, systematic and reliable for optimizing the WEDM performance. In the same way, Taguchi method has been employed by Dabade and Karidkar (2016) to study the various response variables of WEDM process such as MRR, SR, kerf width and dimensional deviation. And, the significant control factors have been determined at 95% confidence level using Minitab. Further, Rao and Venkaiah (2016) have developed the mathematical model to predict the circularity error during WED machining of Inconel 690. The model has been developed using a feed forward back propagated neural network, which is found to be useful to predict the circularity error with acceptable deviation.

Towards the journey of WEDM process optimization, Sharma et al. (2015) have used one factor at a time approach to understand the effect of various WEDM control parameters on machining characteristics. Aggarwal et al. (2015) have developed the mathematical models for cutting speed and surface roughness of WEDM processed Inconel 718. These RSM based models were found to be reliable for representation of experimental results with minimum prediction error. Similarly, Mandal et al. (2016) have developed statistical models for cutting speed, surface roughness, spark gap and wire wear ratio using RSM. And, also optimum machining conditions were predicted using desirability function approach. Kumar et al. (2016 a) have used the RSM approach to develop the quadratic model for cutting speed, surface roughness and radial overcut during WED machining of Nimonic 90. Moreover, desirability function was used for multi-objective optimization of WEDM performance characteristics.

Grey relational analysis, which is proposed by Deng (1989), has found to be useful for solving the problems with inadequate and uncertain data. Muthu et al. (2010) have used GRA based on L_9 Taguchi orthogonal array to optimize the WEDM parameters. Further, Taguchi method has been combined with the GRA for multiple process parameter optimization of WEDM process while cutting Inconel 825 (Rajyalakshmi and Ramaiah, 2013). Next, Taguchi-Fuzzy-GRA approach has been proposed by

Rajyalakshmi and Ramaiah (2015) to optimize the WEDM performance of Inconel 825. The approach was found to be useful to improve the existing WEDM performance.

Due to stochastic nature of WEDM, conventional techniques of optimization can only yield local optimum solution. Therefore, evolutionary algorithms such as genetic algorithm (GA), artificial bee colony (ABC), particle swarm optimization (PSO), teaching learning based optimization (TLBO) and differential evolution (DE) are successfully implemented to overcome the limitation of conventional optimization techniques. Rao and Venkaiah (2015) have used RSM and PSO techniques to optimize WEDM performance. Rao et al. (2014) have used the TLBO algorithm to optimize the parameters of the selected casting process. Rao and Kalyankar (2014) have shown the importance of TLBO while optimizing the modern manufacturing processes. An overview of optimization techniques which are used to improve the EDM/WEDM performance of nickel-based superalloy has been presented in Table 2.3.

2.4.1 Teaching learning based optimization

Among all the evolutionary algorithms, TLBO evolve as a promising technique which has shown reasonably competitive performance. Rao and Kalyankar (2014) have found that TLBO outperforms for modern manufacturing application. According to Satapathy and Naik (2013), TLBO algorithm provides improved results in comparison to GA, PSO, ABC and DE. Therefore, there is a scope to use the evolutionary algorithm for optimizing the control parameters of WEDM process.

Table 2.3 An overview of modeling and optimization techniques used by earlier researchers during EDM/WEDM process of nickel-based superalloys.

No.	Author(s)	Material	Modeling/Optimization tool(s)	Type of optimum results	Responses of EDM/WEDM process
1.	Hewidy et al. (2005)	Inconel 601	RSM	Single response	MRR and SR
2.	Kuppan et al. (2008)	Inconel 718	RSM	Single response	MRR and SR
3.	Ramakrishnan and Karunamoorthy (2008)	Inconel 718	ANN	Multi-response	MRR and SR
4.	Muthu et al. (2010)	Incoloy 800	GRA + Taguchi method	Multi-response	MRR, SR and Kerf
4.	Rajesha et al. (2012)	Inconel 718	RSM	Single response	MRR and SR
5.	Mustafa et al. (2013)	Inconel 718	GRA + Regression model	Multi-response	MRR and SR
6.	Sengottuvel et al. (2012)	Inconel 718	Desirability Approach	Multi-response	MRR, SR and electrode wear rate (EWR)
7.	Prabhu and Vinayagam (2013)	Inconel 825	Taguchi Method	Single response	MRR, SR and Micro cracks
8.	Dhanabalan et al. (2013)	Inconel 718	Taguchi Method + GRA	Multi-response	MRR, EWR, Perpendicularity and Straightness
9.	Lin et al. (2013)	Inconel 718	Taguchi Method + GRA	Multi-response	MRR, EWR and Working gap
10.	Uhlmann and Domingos (2013)	Nickel-based alloy	Design of experiment (DOE) method	Single response	MRR and SR

11.	Ayesta et al. (2013)	C1023	RSM	Single response	Machining time and EWR
12.	Rajyalakshmi and Ramaiah (2013)	Inconel 825	Taguchi Method + GRA	Multi-response	MRR, SR and Spark gap
13.	Garg et al. (2014)	Inconel 718	RSM	Single response	MRR
14.	Jakhar et al. (2015)	Inconel 600	Taguchi Method	Single response	Cutting speed and SR
15.	Rajyalakshmi and Ramaiah (2015)	Inconel 825	Taguchi + Fuzzy + GRA	Multi-response	MRR, SR and Spark gap
16.	Aggarwal et al. (2015)	Inconel 718	RSM	Single response	Cutting speed and SR
17.	Rao and Venkaiah (2015)	Nimonic 263	RSM + PSO	Single response	MRR and SR
18.	Karidkar and Dabade (2016)	Inconel 718	Taguchi Method + GRA	Multi-response	SR, Kerf width and Dimensional deviation
19.	Kumar et al. (2016)	Nimonic 90	RSM + Desirability approach	Multi-response	Cutting speed, SR and Radial over cut
20.	Rao and Venkaiah (2016)	Inconel 690	Feed forward back propagated Neural Network	Single response	Circularity error
21.	Mandal et al. (2016)	Nimonic 263	RSM + Desirability approach	Multi-response	Cutting speed, SR, Spark gap and Wire wear ratio
22.	Dabade and Karidkar (2016)	Inconel 718	Taguchi method	Single response	MRR, SR, kerf width and dimensional deviation

2.5   SUMMARY AND MOTIVATION FROM LITERATURE SURVEY

Due to the requirement of advanced manufacturing industries, the usage of nickel-based superalloys are increasing day by day. Therefore, it is necessary to understand the machining behavior of these superalloys. Looking into continuous improvement in the manufacturing process of aero engine components, Inconel 706 superalloy was selected as a workpiece material which is more recently industrialized for manufacturing of turbine discs to substitute the Inconel 718. In the field of WEDM, most of the available literature discussed about the optimization of performance characteristics, investigation of surface integrity and mechanical properties while machining nickel-based superalloys. But, only a few researchers have concentrated on the manufacturing of intricate and complex shape components with acceptable tolerance. Therefore, there is a scope to study the dimensional and geometrical tolerance while manufacturing complex profiles through critical gas turbine components such as turbine disc profile slot, turbine blade root profile etc.

Even though, earlier literatures have shown the various improvements in WEDM process using modified generator technology, trim pass strategy, different wire material and various optimization approaches, no significant number of literature has been found by the author which is related to the effect of wire diameter on the WEDM performance characteristics. Therefore, there is a scope to examine the effect of different wire diameters on WEDM performance characteristics.

However, earlier literatures have shown the usage of various optimization techniques (i.e., Taguchi techniques, desirability approach, ANN modeling, GRA, RSM and DOE approach) in the field of WED machining of nickel-based superalloys. These conventional techniques of optimization can only yield local optimum solution because experimental design is based on the discrete levels, although, in reality, control parameters are changing continuously. The global optimum solution may lie outside the experimental domain. In order to obtain global optimum solutions, some evolutionary algorithms such as GA, ABC, PSO, TLBO and DE have been described in literature. According to the literature, TLBO perform better compared to other evolutionary algorithm. Hence, in the current study, TLBO algorithm has been used to

predict the optimum performance of WEDM process while manufacturing of complex turbine disc slots with acceptable tolerance.

2.6   OBJECTIVES OF THE RESEARCH WORK

Looking at the continuous development in manufacturing of gas turbine components with improved productivity as well as better surface quality, the following main objectives have been derived from the literature survey.

1. To investigate the effect of WEDM control parameters (i.e., pulse on time, pulse off time, servo voltage, servo feed, wire feed, dielectric pressure) on performance characteristics (i.e., material removal rate, surface roughness, microhardness, recast layer thickness, microstructure, surface topography) using one factor at a time (OFAT) approach.

2. To carry out the WED machining of Inconel 706 using three different materials (i.e., hard brass wire, diffused wire, zinc coated wire) as well as wires of three different diameters (i.e., 150 μm, 200 μm, 250 μm) and to investigate the optimum wire material and wire diameter suitable for the WED machining of Inconel 706.

3. To manufacture the turbine disc profile slots through Inconel 706 as per the requirement of gas turbine industries and to evaluate the WEDM performance characteristics of profile slots.

4. To develop the mathematical models to predict the MRR and SR within the experimental range of control parameters using response surface methodology (RSM) and to optimize the WEDM control parameters using teaching learning based optimization (TLBO) algorithm.

2.7   COMPARISON OF CURRENT STUDY WITH PREVIOUS LITERATURE

Earlier Klocke et al. (2012) and Klocke et al. (2014) have demonstrated the WEDM capability to manufacture the fir tree slots through Inconel 718 and to meet the minimum requirement of turbine disc slot in terms of surface integrity and geometry. And, it was suggested to use nickel-coated wire in order to avoid the unwanted

contamination of Cu and Zn. However, in the current study, WEDM technology has been developed to manufacture the turbine disc profile slots as per the standard of gas turbine industries and to fulfill the minimum requirement of turbine disc profile slots. To achieve this, various WEDM control parameters, different wire materials and wire diameters are taken into consideration and efforts have been made to select the best operating parameters that are recommended for WEDM process of Inconel 706.

CHAPTER 3

EXPERIMENTAL WORK

3.1   INTRODUCTION

This chapter outlines the detail description of Inconel 706 superalloy, its composition, properties, preparation of samples for WEDM operation and the experimental procedure for conducting the experiments. The experimental plan based on one factor at a time approach and response surface methodology also has been discussed. Further, the chapter also deliberates the measurement of MRR, SR, recast layer formation, microhardness, surface topography, residual stresses, recast layer formation and elemental changes on WED machined components.

3.2   TRIAL EXPERIMENTS

The trial experiments were conducted on Inconel 625 and Inconel 600 superalloy to obtain the feasible range of WEDM control parameters. During experimentation, it was observed that inappropriate selection of control parameter may result in wire rupture and gap short during WEDM process. The gap short issue was generally observed at high servo voltage (more than 60 V) and at low pulse on time (less than 105 μs), however wire rupture was observed at low servo voltage (less than 20 V) and high pulse on time (more than 125 μs). With the help of trial experiments conducted by the author (Sharma et al., 2014), feasible range of control parameters was identified and considered for further investigation. Inconel 706 was considered for actual experimentation to machine complex shape profiles for gas turbine application.

3.3   MATERIAL SELECTION AND PREPARATION

Inconel 706, which is a newly developed nickel-based superalloy, was selected as a workpiece material. This alloy was mainly developed to substitute the Inconel 718 for turbine disc application. The alloy was procured in the form of plate (200 mm × 200 mm × 10 mm) from Special Metals, India. The chemical composition of Inconel 706, which has been verified by Energy dispersive X-ray spectroscopy

(EDS) analysis, is presented in Table 3.1. EDS analysis of as received Inconel 706 has been shown in Figure 3.1.

Table 3.1. Chemical composition of Inconel 706 superalloy.

Alloy (%)	Inconel 706 superalloy	
	Minimum	Maximum
Ni+Co	39	44
Cr	14.5	17.5
Fe	Balance	
Nb+Ta	2.5	3.3
Ti	1.5	2
Co		1
C		0.06
Mn		0.35
Si		0.35
S		0.015
Cu		0.3
Al		0.4
P		0.02
B		0.006
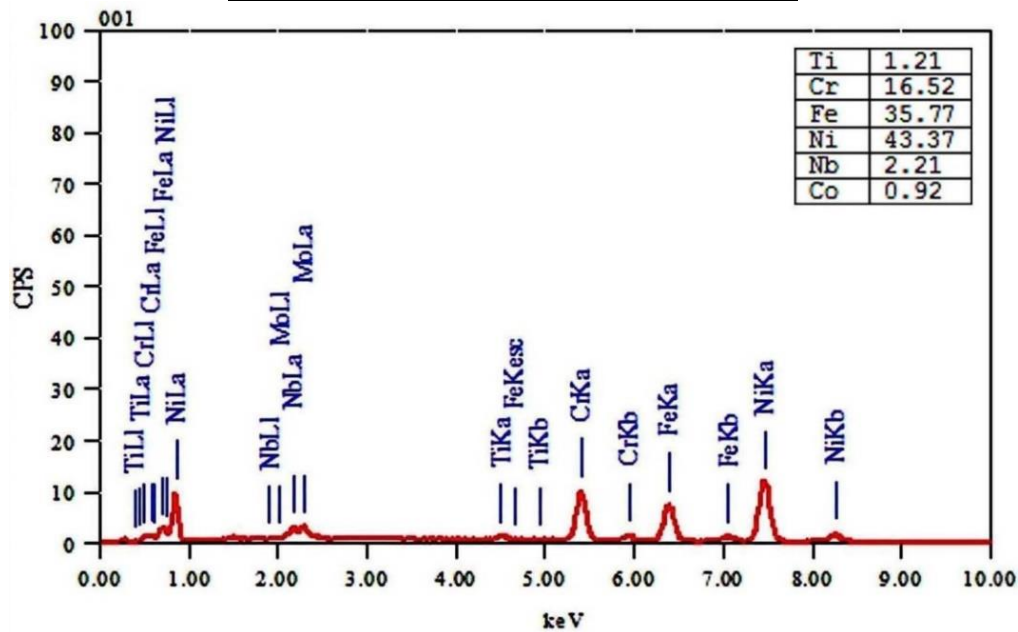
Figure 3.1 EDS analysis of the as-received Inconel 706 superalloy.

onel 706 alloy is evolved as a substitute of Inconel 718 for manufacturing of aero and land-based turbine discs. Some physical and mechanical properties of Inconel 706 have been listed in Table 3.2. Molybdenum was excluded from Inconel 706 to increase forgability and niobium was reduced to decrease the propensity for segregation and freckle formation. To avoid the rapid age hardening, a low level of aluminum was chosen. The chromium content was selected to achieve good oxidation resistance and low magnetic permeability. The nickel level was selected as low as possible to reduce the cost, however, maintain phase stability and avoid the formation of sigma phase. Moreover, carbon content was kept minimum to improve machinability (Schilke et al., 1994).

Table 3.2. Physical and mechanical properties of Inconel 706 (Technical bulletin).

Properties of Inconel 706	Specification
Density	8.05 g/cm³
Melting range	1334–1371°C
Thermal conductivity	12.5 W/mK
Modulus of elasticity	210 kN/mm^2
Tensile strength	1282 MPa
Yield strength (0.2% offset)	993 MPa
Elongation	19%

The microscopic study of as-received Inconel 706 superalloy was carried out using scanning electron microscope (SEM). Figure 3.2 shows the SEM image of as-received Inconel 706 superalloy which indicates the fine and stable equiaxed grains. The grain size analysis was done using BIOVIS software as per the ASTM E112 standard which uses the liner intercept method. The average grain size of the polished Inconel 706 specimen was found to be ASTM 5 (56.6 μm). It can be observed that precipitates with circular and squared morphology are arbitrarily dispersed within the microstructure. EDS analysis of precipitates shows them to be Nb-rich carbide (NbC) and Ti-rich carbide (TiC).
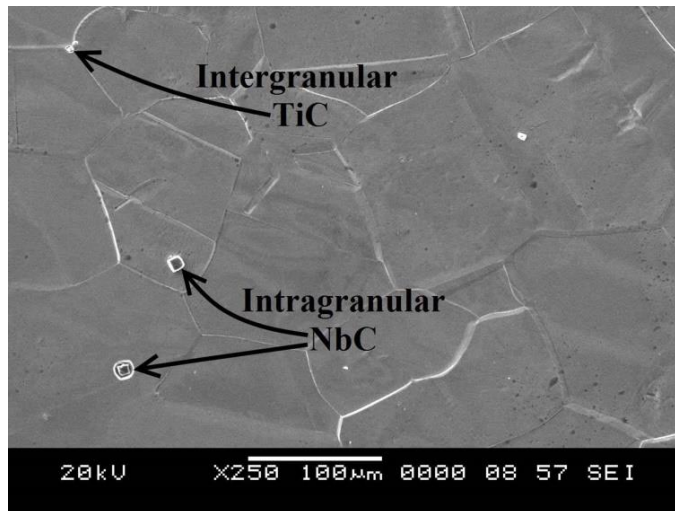
Figure 3.2 Microstructure of as-received Inconel 706 superalloy.

Before proceeding to machining operation, it needs to be ensured that the workpiece material should be clean and rust free which is essential for edge finding. Moreover, the superalloy was stress relieved to avoid the distortion during WEDM process. Without heat treatment, distortion may occur due to the presence of residual stresses within the material which may lead to the failure of machined components. To avoid this, the alloy was heat treated at a temperature of 800 °C in a tubular induction furnace for 1 hour in a closed chamber followed by cooling down to room temperature.

3.4   EXPERIMENTAL SETUP

The experiments were conducted on a WED machine (Model: ECOCUT from Electronica Machine Tools, PUNE, INDIA) as shown in Figure 3.3. The machine comprises of a main table where workpiece is mounted. The main table can be moved in a step of 1 μm in X and Y direction. The machine also comprises of an auxiliary table which can be used for taper cutting operation. The auxiliary table also can be moved in a step of 1 μm in U and V direction where U and V axes are parallel to the X and Y axes respectively. The machine is capable to load a workpiece up to 300 kg. A fresh wire, which is continuously fed from the wire spool, is supported by upper and lower wire guide. Both lower and upper wire guide can be displaced along X–Y axes. Moreover, the upper wire guide can also be moved along U–V axes with respect to lower wire guide. Usually, this WED machine is only made for the use of wire

diameter of 250 µm. To utilize the wire diameter of 200 µm and 150 µm for the same experimental setup, separate wire guides were procured. The wire guides are comprised of very fine tolerance of 5 µm to minimize the wire vibration and wire deflection between upper and lower wire guide.

Figure 3.3 Experimental setup of WED machine.

The machine has two distinct options as it can be operated either in power pulse mode (pulse current of 12 A) or fine pulse mode (pulse current of 1 A). Generally, the power pulse mode is used for basic cutting operation while fine pulse mode is employed for finishing operation of machined surface. The WEDM setup has been shown in Figure 3.3. In order to minimize the wire vibration and deflection, the distance between the upper wire guide and workpiece were kept around 0.5 mm. In case of complex profile as shown in Figure 3.4, dwell time is recommended to achieve better profile accuracy. In the current study, dwell (delay) time of 2 sec has been selected and maintained constant. De-ionized water has been used as a dielectric

fluid. Based on the trial experiments, feasible range of various WEDM control parameters such as pulse on time, pulse off time, servo voltage, servo feed, wire feed, wire offset and flushing pressure were identified. Corner control factor of 3 is used in the current study as shown in Figure 3.4, which means that cutting speed is reduced to 30 % at the corner of the geometry. Moreover, cutting speed override is kept 50 %, which provide 50 % lower cutting speed compared to normal cutting speed.
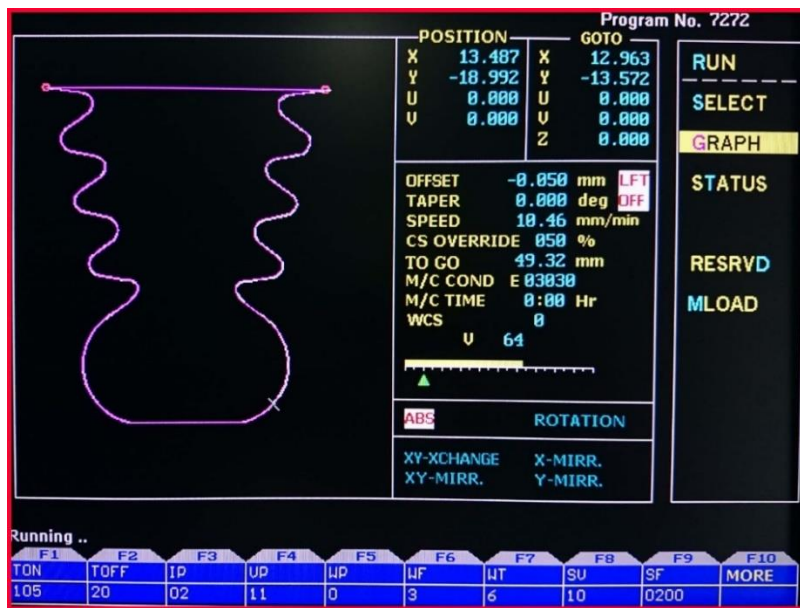
Figure 3.4 WEDM program window.

3.5 EXPERIMENTAL PROCEDURE

The initial experimental design is based on the one factor at a time approach to understand the effect of various WEDM control parameters on WEDM performance characteristics. Further, optimum wire diameter and optimum wire materials have been identified by performing the experiment under different discharge mode and comparison has been made under similar experimental conditions. The flow chart of experimental plan has been shown in Figure 3.5, however a detailed experimental procedure has been described below:

- Based on the requirement of aircraft manufacturing industries, Inconel 706 is selected as the workpiece material which is recently developed for turbine disc applications. Further, control parameters and their levels were selected based on the trial experiments.

51

- The experiments were performed on Inconel 706 based on the one factor at a time approach (OFAT) to study the effect of various WEDM control parameters on the WEDM performance characteristics. Then, significant control parameters are considered for further investigation.

- The significant control parameters are considered to evaluate the effect of different wire diameters on the WEDM performance characteristics such as cutting speed, surface roughness, surface topography, recast layer formation, subsurface microhardness, microstructural and elemental changes.

- The effect of different wire materials on WEDM performance characteristics such as cutting speed, surface roughness, surface topography, recast layer thickness, residual stresses, subsurface microhardness, microstructural and elemental changes were evaluated.

- The turbine disc profile slots were machined using WEDM process as per the standard of gas turbine industries. Moreover, WEDM performance characteristics of turbine disc profile slots such as cutting speed, surface roughness, surface topography, subsurface microhardness, recast layer thickness, residual stresses, profile accuracy, crystal structure, microstructural and elemental changes have been evaluated.

- The statistical models of WEDM performance characteristics such as material removal rate and surface roughness have been developed using response surface methodology (RSM) followed by backward elimination approach.

- The developed RSM models were used as a fitness function in TLBO algorithm. To achieve multi-objective optimization using TLBO, a combined objective function has been developed by normalizing the material removal rate (MRR) and surface roughness (SR) which satisfy both the objectives.

- Finally, RSM based models and TLBO predicted results are validated using experimental results. Also, Pareto optimal solutions were obtained at different weightage which might be useful to modern manufacturing industries.

```
                    ┌─────────────────┐
                    │   WEDM Setup    │
                    └─────────────────┘
                             │
        ┌────────────────────────────────────────────────┐
        │  Selection of workpiece material (Inconel 706)  │
        │    and heat treatment for 1 hour at 800 °C      │
        └────────────────────────────────────────────────┘
                             │
    ┌────────────────────────────────────────────────────────┐
    │  Selection of feasible range of control parameters such as │
    │  pulse on time, pulse off time, servo voltage, servo feed, wire feed │
    │    and flushing pressure based on trial experiments     │
    └────────────────────────────────────────────────────────┘
                             │
    ┌────────────────────────────────────────────────────────┐
    │  Evaluation of significant control parameters using OFAT approach │
    └────────────────────────────────────────────────────────┘
                             │
            ┌────────────────────────────────────┐
            │   Selection of optimum wire material │
            └────────────────────────────────────┘
                             │
     ┌──────────────┐  ┌──────────────┐  ┌──────────────┐
     │  Hard brass  │  │   Diffused   │  │ Zinc coated  │
     └──────────────┘  └──────────────┘  └──────────────┘
                             │
            ┌────────────────────────────────────┐
            │   Selection of optimum wire diameter │
            └────────────────────────────────────┘
                             │
       ┌──────────┐    ┌──────────┐    ┌──────────┐
       │ 150 μm   │    │ 200 μm   │    │ 250 μm   │
       └──────────┘    └──────────┘    └──────────┘
                             │
    ┌────────────────────────────────────────────────────────┐
    │  Measurement of WEDM performance characteristics such as │
    │  cutting speed, surface roughness, surface topography, recast layer │
    │  thickness, microhardness, microstructural and elemental changes │
    └────────────────────────────────────────────────────────┘
    ┌────────────────────────────────────────────────────────┐
    │  Development of Turbine disc profile slots as per the standard of gas │
    │  turbine industries and evaluation of recast layer, profile accuracy, │
    │  residual stresses, surface roughness and subsurface hardness │
    └────────────────────────────────────────────────────────┘
    ┌────────────────────────────────────────────────────────┐
    │  Development of mathematical models using RSM and optimization │
    │       of WEDM performance using TLBO algorithm          │
    └────────────────────────────────────────────────────────┘
                             │
    ┌────────────────────────────────────────────────────────┐
    │  Validation of RSM based models and TLBO predicted results │
    │              using experimental results                 │
    └────────────────────────────────────────────────────────┘
                             │
       ┌────────────────────────────────────────────────┐
       │  Analysis of experimental results and conclusion │
       └────────────────────────────────────────────────┘
```

Figure 3.5 Flow chart of the experimental plan.

3.6   ONE FACTOR AT A TIME APPROACH

One factor at a time (OFAT) is considered as a classical engineering approach for optimization. In OFAT approach, any one factor or variable is varied at a time while others are kept constant. The approach is best suited to determine the individual effect of each control factors on the performance characteristics. To understand the effect of various control factors on WEDM performance characteristics of Inconel 706 superalloy, the OFAT approach has been used in the current study. Six control parameters, namely, pulse on time, pulse off time, servo voltage, wire feed, servo feed and flushing pressure were considered. Each control factor was varied at five different levels, whereas others control factors were kept constant at their average level. Further, the effect of these control factors on the material removal rate (MRR), surface roughness (SR), recast layer thickness, microstructure and microhardness have been investigated.

3.7   RESPONSE SURFACE METHODOLOGY

Response surface methodology (RSM) is one of the statistical tools which are used to obtain the linear, squared and quadratic models. In the field of manufacturing, one can optimize the response which is influenced by several control factors of the WEDM process. According to Mayer et al. (2016), initially orthogonal design was used Box and Wilson (1951) for first order model. Then, second order models such as central composite design and 3 levels design has been proposed by Box and Behnken (1960). Further, the RSM was developed to model experimental responses which are proposed by Box and Draper (1987), then a full factorial design was presented by Montgomery (1997) to construct the approximation model. The developed model was based on a full factorial design and can capture interaction terms between design variables. If number of design variables become larger, then fractional factorial design can be used to minimize the experimental time.

For the current study, four control parameters has been selected based on the preliminary investigation. The relationship between control factors and output response can be expressed as:

$$y = f(x_1, x_2, x_3, x_4) \pm \varepsilon \tag{3.1}$$

The variables x_1, x_2, x_3 and x_4 are the control parameters of WEDM process whereas y is the response surface which needs to be analyzed. The output response y is the function of control parameter and experimental error as given in Eq. (3.1). The experimental error may corresponds to measurement error involved in response. However, in most of the RSM problems, true response function is unknown. In order to develop an approximating function, experimenter can start with a linear function of independent control factors which is also known as the first order model. The first order model with 4 control parameters is shown in Eq. (3.2).

$$y = \beta_0 + \beta_1 x_1 + \beta_2 x_2 + \beta_3 x_3 + \beta_4 x_4 \pm \varepsilon \tag{3.2}$$

Where β_0 is constant and β_1, β_2, β_3, β_4 represents the coefficient of linear function. If response surface involves a curvature, then approximating function can be given by second order polynomial equation expressed as:

$$y = \beta_0 + \beta_1 x_1 + \beta_2 x_2 + \beta_3 x_3 + \beta_4 x_4 + \beta_{11} x_1^2 + \beta_{22} x_2^2 + \beta_{33} x_3^2 + \beta_{44} x_4^2 + \beta_{12} x_1 x_2 + \beta_{13} x_1 x_3 + \beta_{14} x_1 x_4 + \beta_{23} x_2 x_3 +$$
$$\beta_{24} x_2 x_4 + \beta_{34} x_3 x_4 \pm \varepsilon \tag{3.3}$$

Where β_{12}, β_{13}, β_{14}, β_{23} β_{24} and β_{34} represents the coefficient of interaction terms and β_{11}, β_{22}, β_{33}, and β_{44} represents the coefficient of squared terms. As WEDM involves a complex inter-relationship between control parameters and performance characteristics, second order model is best suited to determine the main effect, quadratic effects and two-way interaction effects among control factors (Khuri, 2006). This design contains both factorial and fractional factorial design with center points which allow the estimation of individual as well as interaction effect (Myers et al., 2003). In different modules of RSM, central composite design (CCD) is quite popular for fitting second order surface model. Generally, most of the engineering problems, such as non-conventional machining process involves a complex inter-relationship between control factors and its responses. Using CCD, a second order model can be developed efficiently and most suited for such application.

3.8 MEASUREMENT OF WEDM PERFORMANCE CHARACTERISTICS

3.8.1 Material removal rate

The MRR has been calculated using the weight loss method and computed using Eq. (3.4).

$$MRR = \frac{(w_b - w_a)}{\rho \times t} \qquad (3.4)$$

Where,

w_a = Weight of the workpiece after machining (g),

w_b = Weight of the workpiece before machining (g),

ρ = Density of the workpiece (g/mm^3), and

t = machining time (sec).

The weight of each sample was measured using precision weighing balance (Model: BT 224 S from SARTORIUS, GERMANY). This weighing balance offers an accuracy of 0.1 mg and weight capacity of 220 g. Before weighing the samples, hot air blower was used to remove the moisture from the samples. The machining time was calculated using a digital stopwatch.

3.8.2 Cutting speed

A material having a low melting temperature exhibits slightly higher cutting speed in WEDM process. Besides, a thicker workpiece material in WEDM process shows comparatively lower cutting speed. This is because, in case of thick material, comparative longer length of wire is required to produce the sparking and thus require longer time to cut the material. In the current study, the cutting speed of the specimen was calculated using Eq. (3.5). Total path length was calculated using the CNC program, whereas total machining time was calculated using a digital stopwatch (accuracy of 0.01 s).

$$\text{Cutting speed (mm/min)} = \frac{\text{Total path length (mm)}}{\text{Total machining time (min)}} \qquad (3.5)$$

3.8.3 Surface roughness

The surface roughness (SR) of WED machined components were measured using surface roughness tester (Model: SURFTEST SJ-301 from MITUTOYO, JAPAN) which has been shown in Figure 3.6. The roughness tester uses a differential inductance method as a detection technique. The tester consists of a hard needle shape

stylus made of diamond. The stylus includes a tip radius of 2 µm and apply a force of 0.75 mN to measure the surface roughness. The evaluation length of measurement has been determined based on the component size, however stylus speed was maintained constant (0.25 mm/sec). The average surface roughness (Ra) which is commonly accepted in manufacturing industries, are considered for the current research work. Moreover, roughness depth mean (Rz) values were considered for evaluation of peak to valley height of profile slot surface. The Ra and Rz value of WED machined surface was directly recorded using roughness tester.

Figure 3.6 Surface roughness tester.

3.8.4 Surface topography

The topography of the WED machined surface was obtained using a 3D laser microscope (Model: LEST OLS4000 from OLYMPUS, JAPAN) available in Nano Manufacturing Technology Centre at CMTI, Bangalore which is shown in Figure 3.7. This microscope uses a laser scanning to measure the surface profile of the machined components. This microscope can measure surface texture more accurately due to low laser spot diameter of 0.4 µm. However, contact type surface roughness tester can't measure the micro asperities less than the stylus tip diameter. For the current study, scan area of 1.28 mm × 1.28 mm was selected for topographic evaluation of WED machined components followed by OFAT approach. Also, a scan area of 107 µm ×

107 μm was selected for topographic investigation of turbine disc profile slots and 3D images were captured at 2592 X magnification.
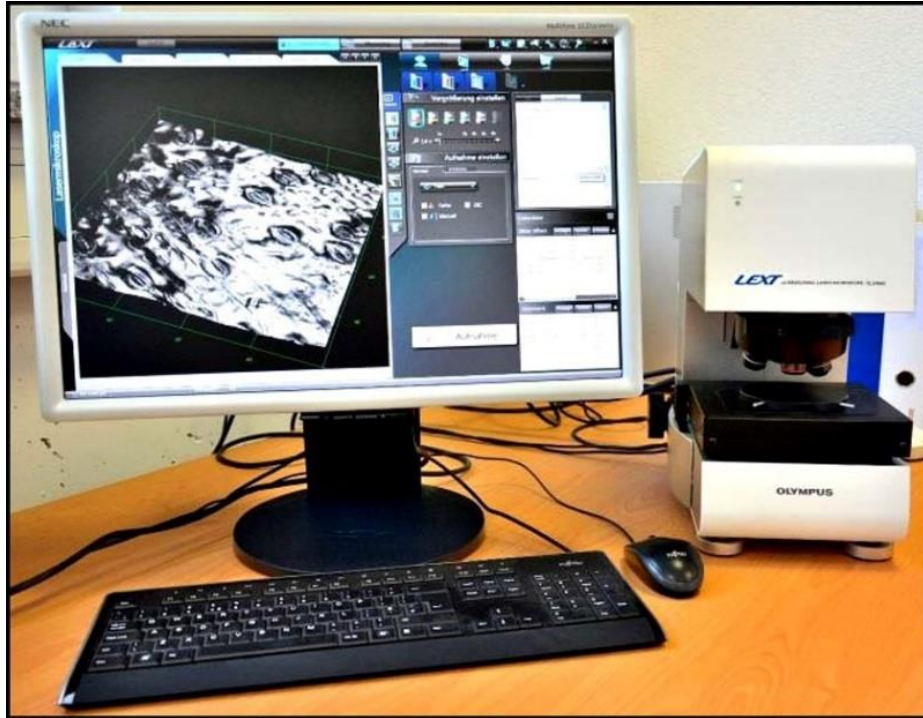
Figure 3.7 3D laser microscope.

3.8.5 Surface and subsurface microstructure

In order to obtain the grain structure and recast layer, samples were ground and polished using 'METKON' grinder and polisher. The mechanical polishing was carried out at a rotational speed of 300 rpm using progressive grade of silicon carbide (SiC) papers. Then, diamond paste polishing was done at rotation speed of 150 rpm to obtain mirror finish on the cross-section of the component. The polished samples were etched using Marble's reagent (10 g $CuSO_4$ + 50 ml HCl + 50 ml H_2O + few drops of H_2SO_4) to expose the grain structure. The etching time of the specimens was kept around 110 to 120 sec.

Before microscopic investigation, all samples are subjected to ultrasonic cleaning process. For this purpose, all samples were immersed in acetone, then kept into the ultrasonic cleaner for 40 minutes. The scanning electron microscope (Model: JEO JSM–638OLA from JEOL, USA) was used to obtain the microstructure images at a suitable magnification as shown in Figure 3.8. The equipment has a maximum

resolution of 3 nm however maximum magnification is limited to 3,00,000 X. Aperture size of 30 µm and acceleration voltage of 20 kV was used to obtain secondary electron images (SEI). The SEM can be operated either in high vacuum or low vacuum mode as per the requirement. However, in the current study, high vacuum mode was used which is generally employed for high density material.

Figure 3.8 Scanning electron microscope.

Microstructural images of WED machined surface were captured at 1500 X magnification whereas microscopic images of recast surface was captured at 500 X magnification. EDS analysis was carried out to study the elemental changes on the WED machined surface. For recast layer analysis, the cross-section of WED machined surface was subjected to cold mounting, polishing and ultrasonic cleaning respectively.

3.8.6 Subsurface microhardness

In order to measure the subsurface microhardness, WED machined components were cold mounted cross-sectionally using self-curing liquid and acrylic powder. Then, samples are subjected to grinding, polishing and ultrasonic cleaning. After cleaning,

micro Vickers hardness tester (Model: MVH–S–AUTO from OMNI TECH, PUNE, INDIA) was used to measure the subsurface microhardness of WED machined components as shown in Figure 3.9. For the micro indentations, 10 kgf load was applied for dwell time of 10 sec. The microhardness was calculated using the expression (Dieter and Bacon, 1986) given in Eq. (3.6).

$$\text{Hv} = \frac{2F\sin(136^{o}/2)}{d^{2}} = 1.854\frac{F}{d^{2}} \qquad (3.6)$$

Where,

$\qquad$ Hv = Vickers hardness of the sample,

$\qquad$ d = Mean of diagonals length of a squared pyramid and

$\qquad$ F = Applied load.
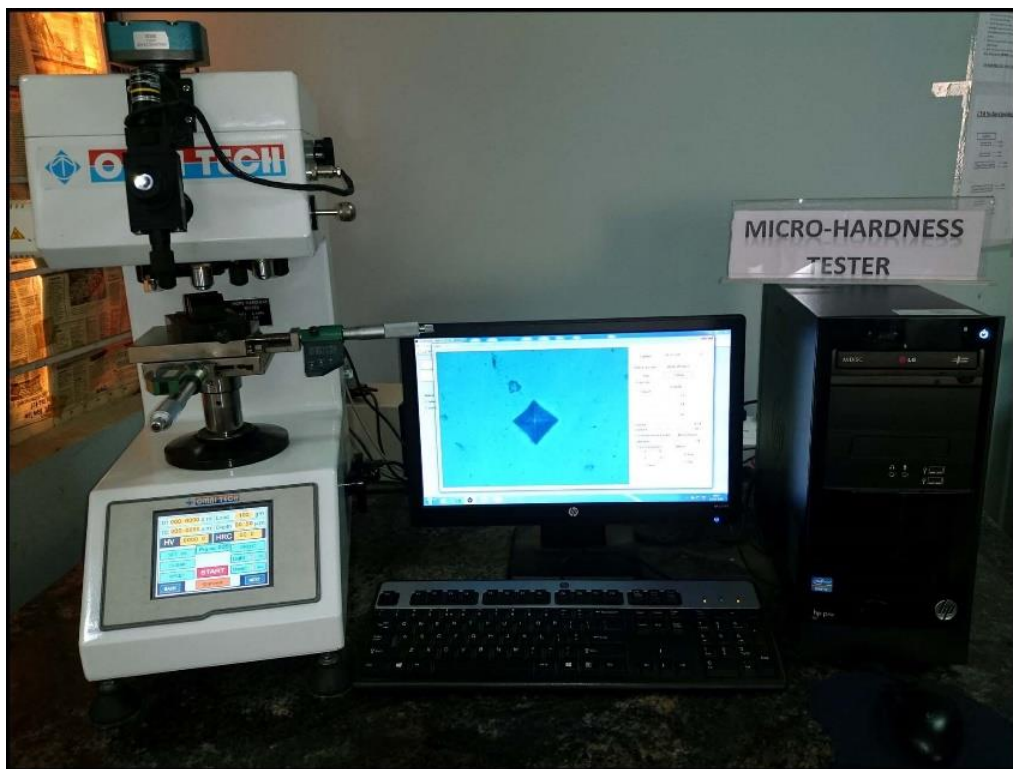
Figure 3.9 Microhardness tester.

3.8.7 Residual stresses

Residual stresses are the stresses which remain in a material after removing thermal or mechanical loads. Generally, these stresses are induced in the material due to material deformation, heat treatment and machining operation which transforms the material properties. In WEDM, residual stresses are induced due to high temperature gradient

and thermal contraction of recast material. The residual stresses present in WEDM machined surface were measured using stress measuring system (Model: PROTO– iXRD MGR40 from Proto Manufacturing Ltd., CANADA) available in Advanced Machine Tool Testing Facility, at CMTI Campus, Bangalore as shown in Figure 3.10. For residual stress measurement of Inconel 706 superalloy, the input variables (i.e., Tube: Mn_K–Alpha, wavelength: 2.103 Å, Bragg angle: 151.88°, exposure time: 6 s, aperture: 1 mm and D spacing: 1.0840460 Å) were used as per the standard.

Figure 3.10 Stress measuring system.

3.8.8 Profile accuracy

The profile accuracy of turbine disc profile slots as shown in Figure 3.4 was measured using coordinate measuring machine (Model: UPMC 850 CAA from ZEISS, GERMANY) available in Ultra Precision Engineering at CMTI, Bangalore which is shown in Figure 3.11. The machine is equipped with rotary axis along with measuring range of X–850 mm × Y–1200 mm × Z–600 mm. It also contains a high speed scanning probe head and can measure the coordinates with minimum resolution of 0.1 μm. To obtain the coordinates of the profile, a step width of 10 μm and probe diameter of 1.5 mm was used. The coordinates of measured profiles were compared with nominal profiles to calculate the deviations. From the experimental analysis, it

was observed that CMM data can be reproduced within the tolerance of $\pm$ 5 μm and is suitable to examine the profile accuracy.

Figure 3.11 Coordinate measuring machine.

3.9   SUMMARY

In this chapter, workpiece material and its properties have been described. WEDM experimental setup, material preparation and experimental procedure have been demonstrated. The research methodology adopted in the current research work has also been described. Finally, the details of the equipments used for measurement of surface roughness, microhardness, recast layer, elemental changes, residual stresses, profile accuracy, microstructure and surface topography of WED machined surface have been described. In case of all equipments, measurements were made with more precisely and accurately. Besides, repeatability was obtained in most of the measurements which confirm the minimum deviation.

CHAPTER 4

EVALUATION OF WEDM PERFORMANCE CHARACTERISTICS

4.1 WEDM PERFORMANCE EVALUATION BASED ON ONE FACTOR AT A TIME APPROACH (OFAT)

4.1.1 Introduction

This chapter outlines the detail description of WEDM control parameters and their effect on the performance characteristics. The experimental methodology based on one factor at a time (OFAT) approach was adopted to finalize the control parameters and their levels for further experimentation. The chapter also discusses the investigation of MRR, SR, microstructure, recast layer formation, microhardness, surface topography and elemental changes on the WED machined surface.

4.1.2 Experimental details

In the current study, efforts have been made to investigate the effect of WEDM control parameters on performance characteristics using power pulse mode. Six control parameters, namely, pulse on time, pulse off time, servo voltage, servo feed, wire feed and flushing pressure were identified and the range of control parameters was estimated through preliminary trials. In the range of parameters selected, no wire breakage and gap short problem were recorded. The control parameters and their levels have been shown in Table 4.1.

All the control parameters have been examined at five different levels to study the linear/non-linear effect of control parameters with respect to the machining characteristics (i.e. MRR, SR). One factor at a time (OFAT) approach has been adopted for the current investigation in which one factor was varied at one time and other factors were maintained at their average level (Level–3). This approach helped to determine the individual effect of each control parameter on the machining characteristics. The standard brass wire of diameter 250 μm was selected as the tool

electrode because this wire offers the best surface integrity of the machined components compared to the coated wire (Antar et al., 2011).

Table 4.1 Control parameters and their levels.

SL No.	Control parameters	Level–1	Level–2	Level–3	Level–4	Level–5
1.	Pulse on time (µs)	105	110	115	120	125
2.	Pulse off time (µs)	18	27	36	45	54
3.	Servo voltage (V)	20	35	50	65	80
4.	Wire feed (m/min)	2	4	6	8	10
5.	Servo feed (mm/min)	5	10	15	20	25
6.	Flushing pressure (bar)	1.37	1.67	1.96	2.25	2.55

Figure 4.1(a-b) shows the complex profile and slots machined using WEDM process. The geometry has been selected based on the complexity of aero engine components. The preferred geometry consists of straight as well as curved profiles. Moreover, the geometry has been designed in such a way that it is easy to hold while measuring WEDM performance characteristics.
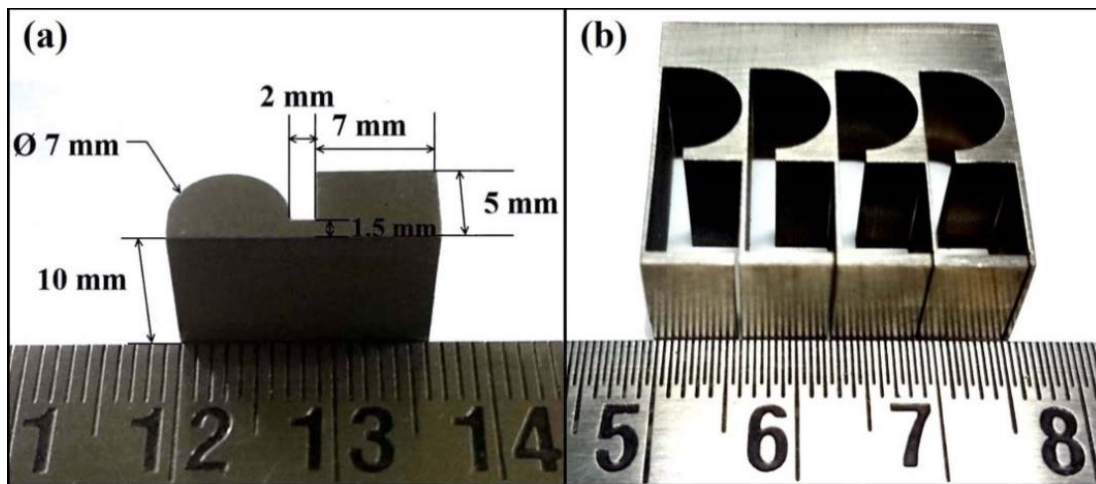
Figure 4.1 (a) Profile of WED machined component of Inconel 706; (b) complex profile slots in Inconel 706.

The experimental values of control parameters and performance characteristics have been shown in Table 4.2.

Table 4.2 Experimental setting of control parameters and performance characteristics.

SL No.	Constant control parameters	Variable control parameter	MRR (mm³/sec)	SR (µm)
		Pulse on time (µs)		
1.	Pulse off time (36 µs)	105	0.020	1.76
2.	Servo voltage (50 V)	110	0.021	2.34
3.	Wire feed (6 m/min)	115	0.037	2.86
4.	Servo feed (15 mm/min)	120	0.054	3.12
5.	Flushing pressure (1.96 bar)	125	0.085	3.79
		Pulse off Time (µs)		
6.	Pulse on time (115 µs)	18	0.062	2.97
7.	Servo voltage (50 V)	27	0.045	2.89
8.	Wire feed (6 m/min)	36	0.037	2.84
9.	Servo feed (15 mm/min)	45	0.025	2.75
10.	Flushing pressure (1.96 bar)	54	0.021	2.66
		Servo voltage (V)		
11.	Pulse on time (115 µs)	20	0.078	3.35
12.	Pulse off time (36 µs)	35	0.055	2.92
13.	Wire feed (6 m/min)	50	0.037	2.84
14.	Servo feed (15 mm/min)	65	0.018	2.81
15.	Flushing pressure (1.96 bar)	80	0.006	2.62
		Wire feed (m/min)		
16.	Pulse on time (115 µs)	2	0.037	2.98
17.	Pulse off time (36 µs)	4	0.038	2.87
18.	Servo voltage (50 V)	6	0.039	2.76
19.	Servo feed (15 mm/min)	8	0.038	2.81
20.	Flushing pressure (1.96 bar)	10	0.037	2.88
		Servo feed (mm/min)		
21.	Pulse on time (115 µs)	5	0.035	2.77
22.	Pulse off time (36 µs)	10	0.036	2.79
23.	Servo voltage (50 V)	15	0.036	2.81
24.	Wire feed (6 m/min)	20	0.036	2.83
25.	Flushing pressure (1.96 bar)	25	0.036	2.85
		Flushing pressure (bar)		
26.	Pulse on time (115 µs)	1.37	0.037	2.95
27.	Pulse off time (36 µs)	1.67	0.038	2.88
28.	Servo voltage (50 V)	1.96	0.039	2.81
29.	Wire feed (6 m/min)	2.25	0.038	2.87
30.	Servo feed (15 mm/min)	2.55	0.037	2.91

As per the WEDM technology manual, some control parameters were kept constant throughout the experimental work as shown in Table 4.3.

Table 4.3 Constant process parameters used during the WEDM process.

Dielectric fluid	De-ionized water
Polarity	Positive
Discharge current	12 A
Discharge voltage	28 V
Cutting speed over ride (%)	50
Dwell time	2 sec
Corner control factor	3

4.1.3 Material removal rate

The variation of MRR with respect to the control parameters such as pulse on time, pulse off time, servo voltage, servo feed, wire feed, flushing pressure has been shown in Figure 4.2. From the Figure 4.2(a), it was observed that MRR increases with increased pulse on time, whereas MRR decreases with increased servo voltage and pulse off time. A similar trend also has been reported by Manjaiah et al. (2015). This behaviour can be explained by the fact that at high pulse on time, the number of electrical sparks in a specified time will increase, which in turn melts comparatively more amount of material from the workpiece resulting in high MRR. Moreover, MRR decreases with increased pulse off time as shown in Figure 4.2(b). Goswami and Kumar (2014) have also obtained results similar to the current finding. This is due to reduced number of electrical sparks in specified time, which in turn, reduces the number of the crater formed on the machined surface leading to lower MRR. Figure 4.2(c) shows that MRR decreases with increase in servo voltage. This is because, at high servo voltage, the average spark gap gets widened and thus reduces the spark intensity. Consequently, less material will be melted resulting in lower MRR. From the Figure 4.2(d), it was observed that an increase in wire feed up to 6 m/min, more amount of molten material splashed through the machining zone and hence leading to higher MRR. At higher wire feed of more than 6 m/min, wire vibration comes into

play that reduces the dynamic stability of wire and causes the unfavorable sparking condition and hence leading to lower MRR.
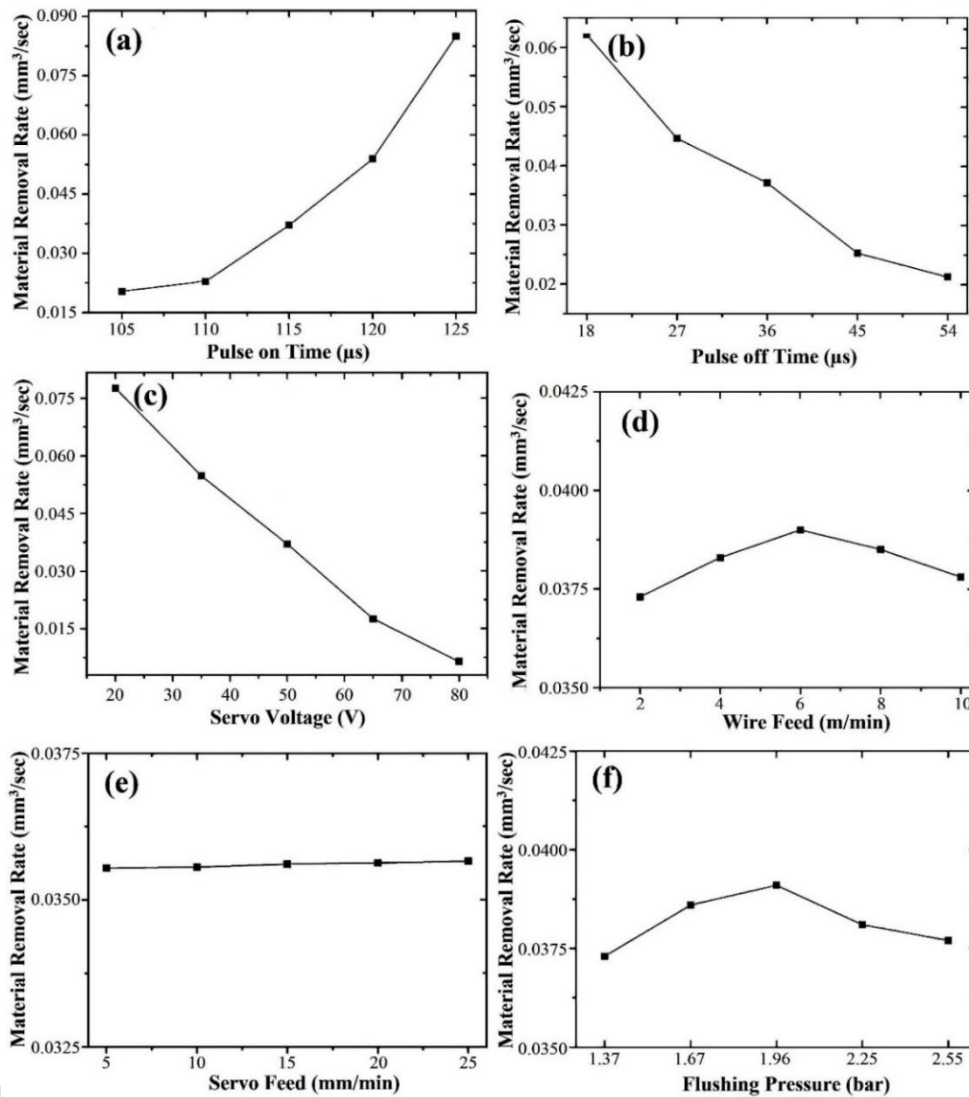
Figure 4.2 Effect of control parameters on material removal rate.

From Figure 4.2(e), it was observed that MRR remains almost constant for all the specified levels of servo feed. This is because, servo feed is the function of workpiece thickness, however in the current study, workpiece height is constant at 10 mm as discussed in chapter 1. Further, MRR increases with the increase in flushing pressure up to 1.96 bar and thereafter it decreases as shown in Figure 4.2(f). Since, an increase in flushing pressure will lead to spilling out the relatively more amount of molten material thus leading to higher MRR. The high flushing pressure (more than 1.96 bar)

causes the unfavorable sparking conditions due to wire deflection and wire vibration, thus affecting the spark intensity which leads to lower MRR (Okada et al., 2015).

4.1.4 Surface roughness

The effect of various control factors on SR have been shown in Figure 4.3. From Figure 4.3(a), it was observed that SR increases with increased pulse on time because at high pulse on time, the number of electrical sparks within a specified time will increase, which in turn increases the number of craters formed on the machined surface leading to higher SR. A similar trend for variation of surface roughness with pulse on time has also been observed by Manjaiah et al. (2015). Figure 4.3(b) shows the reduced SR at high pulse off time. More or less similar results have also been reported by Narendranath et al. (2013). This is because, at high pulse off time, cooling time will increase, which also increases the flushing time of melted debris. This, in turn, tends to spill out comparatively more amount of molten material through the machining zone and hence reduces the SR. The experimental investigation revealed that SR is drastically reduced with an increase in servo voltage as shown in Figure 4.3(c). This is because, an increase in servo voltage tends to widen the spark gap. Therefore, it reduces the spark intensity and increases the flushing and thus forms micro cavities on the machined surface leading to better surface quality (Sharma et al., 2015). Figure 4.3(d) and Figure 4.3(f) have shown an almost similar trend of SR with increased wire feed and flushing pressure.

From the Figure 4.3(d) that SR decreases with an increase in wire feed up to 6 m/min, beyond that SR increases. This behaviour can be explained by the fact that at a higher wire feed up to 6 m/min, SR gets reduced due to improved splashing of molten material. However, beyond 6 m/min, it was observed that SR increases because wire vibration comes into play. This will cause unfavorable sparking conditions and thus create uneven craters on the machined surface which leads to higher SR. Figure 4.3(e) indicates that there is no more variation in SR at specified levels of servo feed. This is because, the effect of servo feed is limited to the workpiece thickness as discussed earlier in chapter 1. From Figure 4.3(f), it was observed that low flushing pressure enhances the contamination of dielectric fluid and contributes to unfavorable sparking

conditions leading to higher SR. The SR decreases with increased flushing pressure up to 1.96 bar and thereafter it increases. Since, an increase in flushing pressure leads to spilling out relatively more amount of molten material and reduces the formation of micro voids on the machined surface leading to lower SR. The higher flushing pressure (more than 1.96 bar) again contributes to the unfavorable sparking conditions and thus create uneven craters on the machined surface leading to higher SR. According to Okada et al. (2015), high flushing pressure leads to more wire deflection and contributes to the wire vibration. Thus, it affects the shape accuracy of the machined components as well as SR and increases the chances of wire breakage.
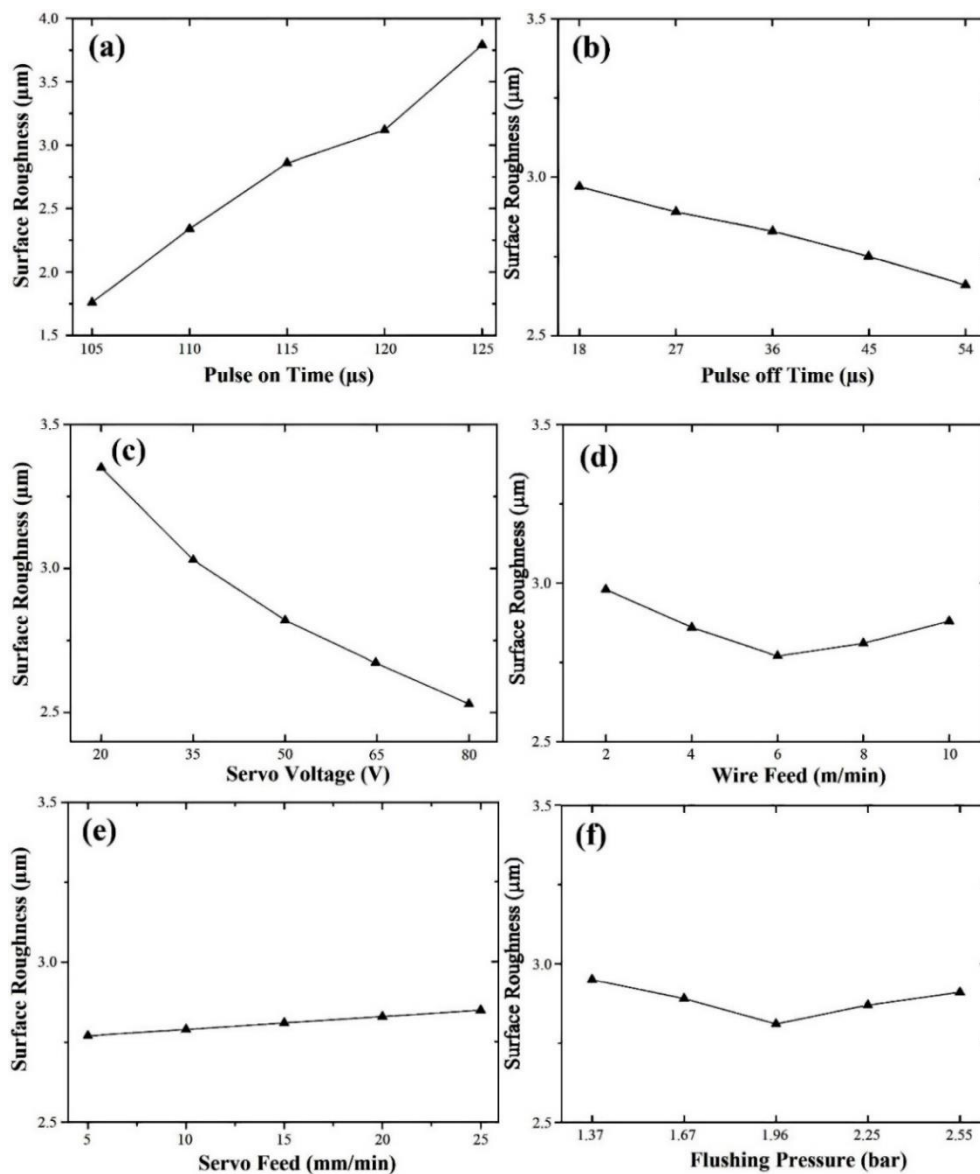
Figure 4.3 Effect of control parameters on surface roughness.

4.1.5 Surface topography of WED machined surface

The surface topography of the WED machined surface has been shown in Figure 4.4.
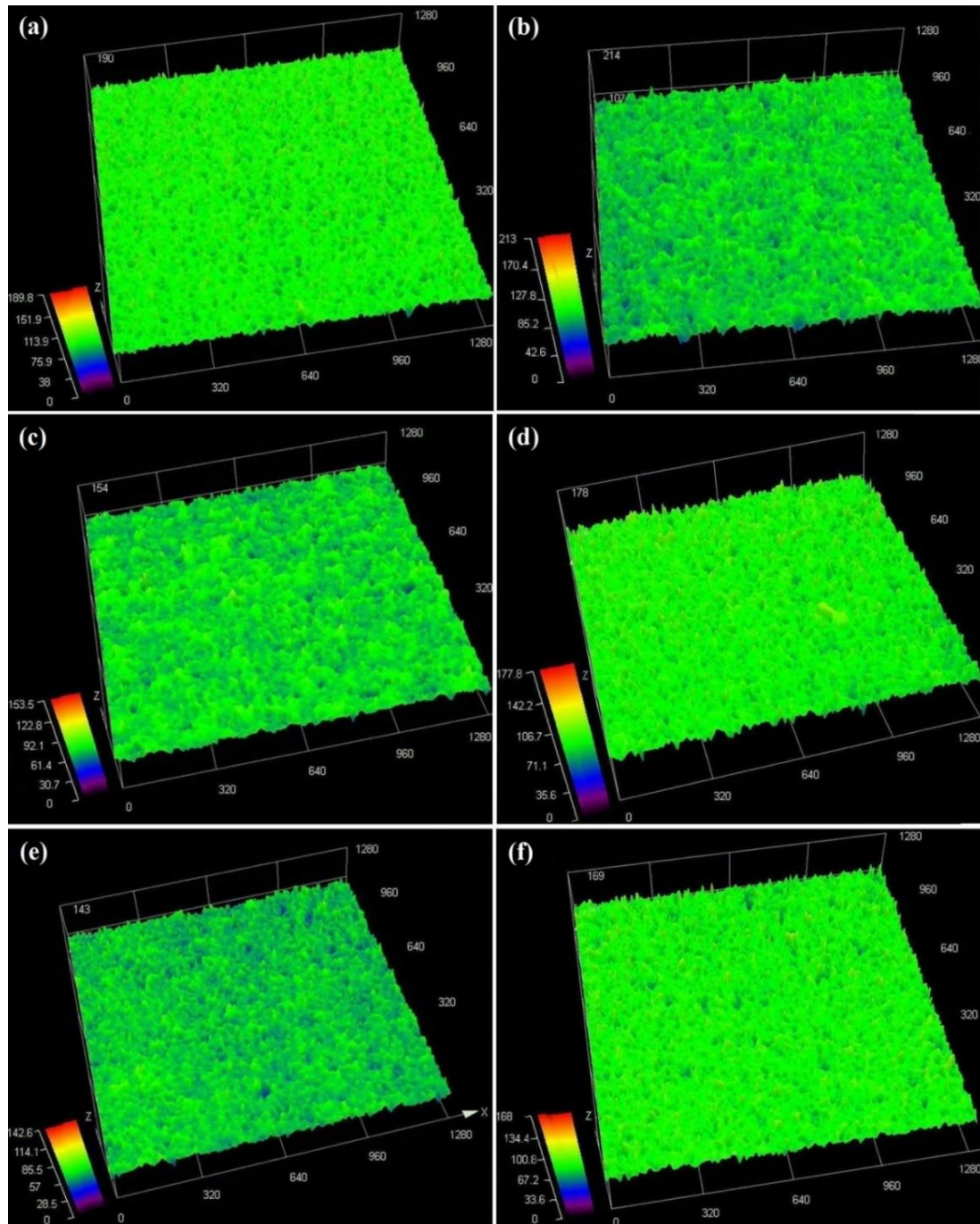
Figure 4.4 Surface topography of WED machined surface under the following machine setting: (a) pulse on time of 105 μs; (b) pulse on time of 125 μs; (c) servo voltage of 20 V; (d) servo voltage of 80 V; (e) pulse off time of 18 μs; (f) pulse off time of 54 μs.

From topography analysis, it was revealed that servo voltage and pulse on time are the major factors affecting the surface quality of the machined components. Higher smoothness and fine surface can be obtained at low pulse on time of 105 µs because of reduced electrical sparks within a specified time as shown in Figure 4.4(a). However, an increased electrical sparks within specified time increases the number of craters formed on the machined surface and hence, offering a rough surface as shown in Figure 4.4(b). After comparing the average SR of WED machined components at pulse on time of 105 µs and 125 µs, the difference of 2.03 µm has been found which indicates that pulse on time has great influence on the SR of WED machined components. Similarly, by comparing the average SR of WED machined components at servo voltage of 20 V and 80 V, the difference of 0.73 µm has been observed which indicates that servo voltage is the another factor affecting the surface quality of the machined components. Figure 4.4(c) shows the rough surface of WED machined components at low servo voltage because of increased spark intensity. But, at higher servo voltage, the spark gap widens and reduces the intensity of the spark. This, in turn, increases the flushing and forms the micro cavities on the machined surface leading to a smoother surface of the machined components as shown in Figure 4.4(d). From Figure 4.4(e), it was observed that a low pulse off time generally offers rough surface on the machined components. This is because, at low pulse off time, cooling time is less which will reduce the amount of molten material to be spilled out from the machining zone and thus forms a rough surface on the machined component. However, at high pulse off time, fine and smooth surface has been detected due to the increased flushing time of melted debris as shown in Figure 4.4(f).

4.1.6 Microstructure of WED machined surface

The microstructure of WED machined surface of Inconel 706 alloy has been studied based on the image obtained through the scanning electron microscope (SEM) at a magnification of 1500X. From Figure 4.5(a-f), it was observed that WED machined surface includes the micro voids, micro globules and melted debris. The formation of micro globules is almost similar to the production of powder via atomization of molten material in water. During the electrical discharge, a large volume of gas is super saturated within the plasma channel. The electrical discharges has the

temperature of around 10,000 °C which is enough to melt and vaporize any conductive material, but it is not sufficient to produce high exploding pressure which can splash all the molten material from the machined surface. When the remaining molten material solidifies on the machined surface, some gas bubbles get entrapped in the melted region and thus produce micro voids on the machined surface (Li et al., 2004).
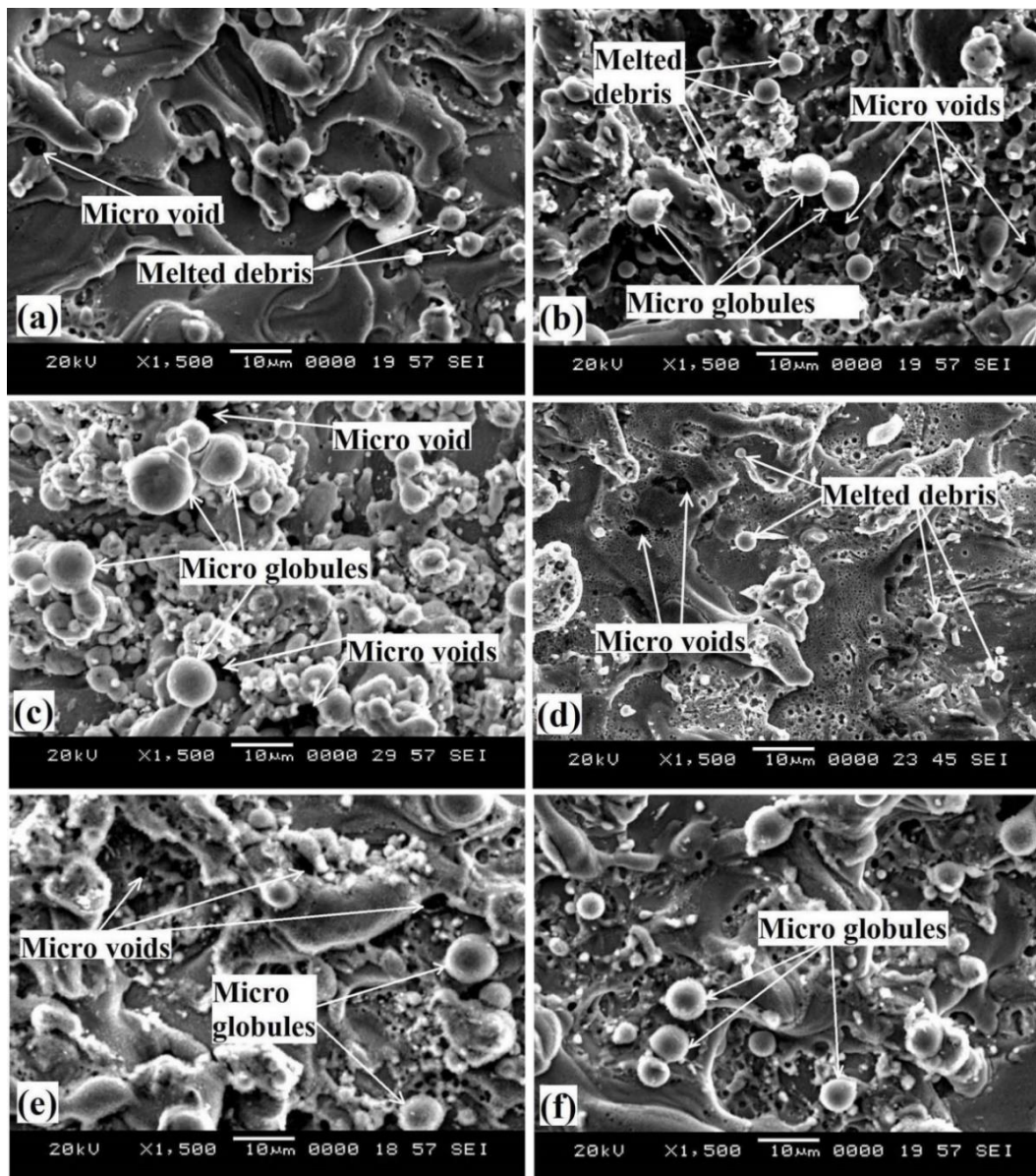
Figure 4.5 SEM graph of WED machined surface under the following machine setting: (a) pulse on time of 105 μs; (b) pulse on time of 125 μs; (c) servo voltage of 20 V; (d) servo voltage of 80 V; (e) pulse off time of 18 μs; (f) pulse off time of 54 μs.

From Figure 4.5(a–b), it was observed that micro globules and micro voids are more prominent at higher pule on time (125 μs) because at higher pulse on time, the amount of thermal energy transferred to the material increases which results in the melting of more amount of material. This, in turn, increases the number of the craters formed on the machined surface and thus produces a rough surface on the machined components. Similarly, micro voids and micro globules are more prominent at low servo voltage of 20 V as shown in Figure 4.5(c). These micro globules and micro voids tend to reduce at high servo voltage of 80 V as shown in Figure 4.5(d). This occurs due to an increased gap voltage which tends to increase the spark gap and consequently increases the flushing and thus reduces the growth of micro voids as well as micro globules. From Figure 4.5(e), it was evident that micro voids and micro globules are more prominent at pulse off time of 18 μs. Since at low pulse off time, the flushing of melted debris is considerably reduced due to less cooling time and thus allowing the formation of micro voids and micro globules and thus leads to poor surface quality of the machined components. Figure 4.5(f) shows that micro voids and micro globules are comparatively reduced at high pulse off time of 54 μs due to increased flushing of melted debris. From Figure 4.5(a–f), it was concluded that servo voltage and pulse on time have an important role to improve the surface features of the machined components. Since micro voids and micro globules are considerably reduced at low pulse on time and high servo voltage.

4.1.7 Subsurface microhardness

Figure 4.6 shows the cross-sectional view of WED machined surface along with indentations. The nearest region of the machined surface was considered as a reference point (0 μm) since it is extremely difficult to measure the microhardness exactly on the machined edge due to improper indentations. The indentation nearest to the machined surface is comparatively bigger, but not exactly a rhombus because of elemental changes that occurred during the WEDM process. Total 25 measurements were taken in a step of 5 μm till 120 μm and each measurement has been repeated 5 times to enhance the measurement accuracy. The standard error corresponding to each measurement has been indicated in Figure 4.6.
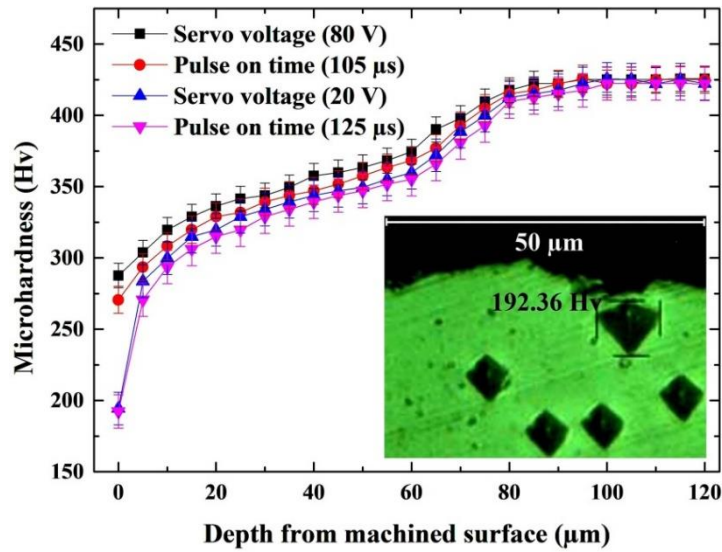
Figure 4.6 Subsurface microhardness profile of WED machined components.

The microhardness of WED machined surface was decreased to a certain depth while machining Inconel 706 superalloy. This is because, Inconel 706 includes very low carbon content (wt. 0.06%) which would make the machined subsurface softer after quenching by dielectric fluid. Almost similar results have been observed by Li et al. (2014) during WEDM process of Inconel 718. From Figure 4.6, it was observed that at high pulse on time of 125 μs and low servo voltage of 20 V, the machined subsurface becomes softer and forms comparatively larger indentation leading to a lower microhardness of the machined components. As a result of WEDM process, the subsurface microhardness of Inconel 706 superalloy was decreased to 192.36 Hv compared to bulk hardness of 425 Hv. The microhardness of subsurface was reduced to a depth of 80 μm due to significant thermal degradation.

4.1.8 Recast layer formation on WED machined Surface

Recast layer is defined as the layer formed on the WED machined surface due to re-solidification of molten material. The recast layer formation may be desirable for some dental applications, but it is detrimental to the aerospace applications. From Figure 4.7(b), and Figure 4.7(c), it was revealed that the high pulse on time and low servo voltage are the major factors contributing to the recast layer formation. Since high pulse on time increases the number of electrical sparks and low servo voltage increases the spark intensity. Therefore, more amount of thermal energy will be

transferred to the material, this in turn, allows more amount of molten material to resolidify on the machined surface leading to thick recast layer on the machined components. Almost similar experimental results have also been reported by Li et al. (2013). It is essential to minimize the recast layer formation as it creates the elemental changes on the machined surface resulting in different material properties. From Figure 4.7(a) and Figure 4.7(d), it was observed that the average recast layer thickness (RLT) has been reduced significantly at low pulse on time and high servo voltage because of reduced number of electrical sparks and low spark intensity. In the range of control factors selected, the average RLT was observed within the range of 10 to 50 μm.
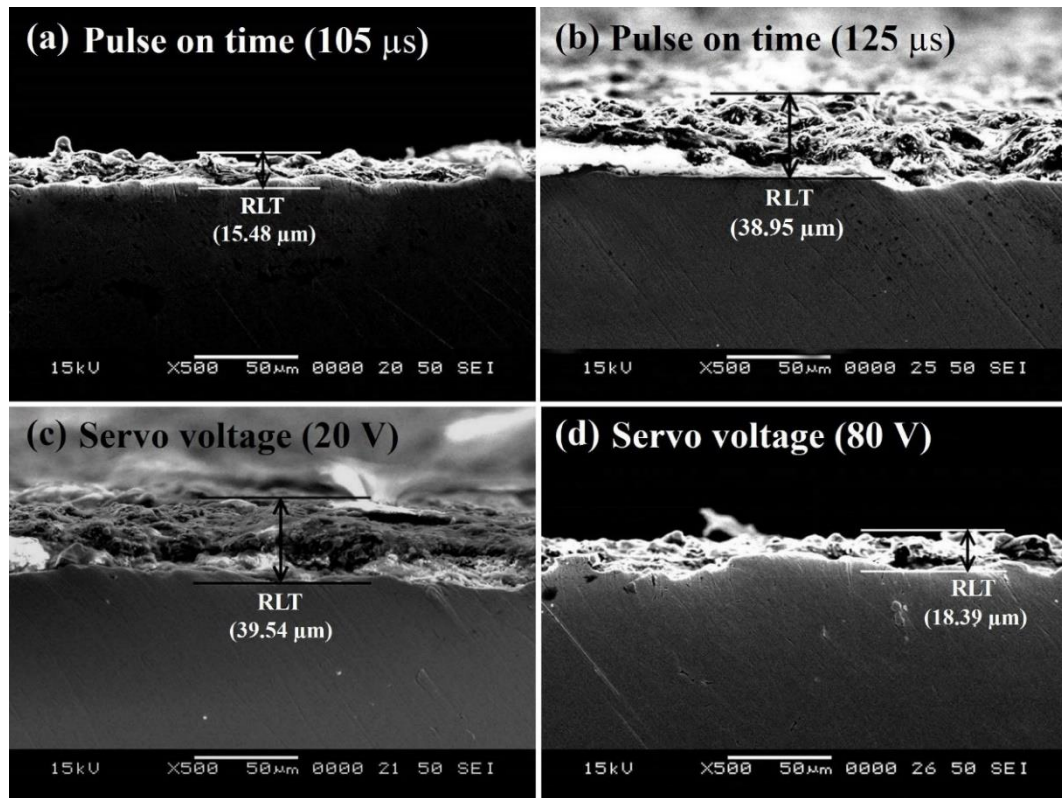
Figure 4.7 Recast layer formed on the WED machined surface.

In the current research work, low hardness of recast layer was observed. This may be due to the fact that the Cu and Zn, which were added to the recast layer during the WEDM process, create the elemental changes and exhibit different material properties. Energy dispersive X-ray spectroscopy (EDS) analysis of recast layer has been shown in Figure 4.8(b). The machining conditions such as pulse on time of 125 μs, pulse off time of 36 μs, servo voltage of 50 V, wire feed of 6 m/min, servo feed of

15 mm/min and flushing pressure of 1.96 bar were used to examine the recast surface. Figure 4.8(a) shows the EDS analysis of Inconel 706 before machining which confirms the presence of major alloying elements but Cu and Zn content are almost nil. However, Figure 4.8(b) indicates the existence of Cu (12.68%) and Zn (3.35%) which was migrated from the brass electrode. Almost similar results have also been observed by earlier researchers (Li et al., 2013; Li et al., 2014) during the EDS analysis of WEDM processed Inconel 718. The presence of these foreign elements lead to altered material properties of WED machined component. Owing to rapid heating and cooling during WEDM operation, the tensile residual stresses may induce within the recast layer and thus reducing the hardness of the recast surface. The relation between hardness and residual stress has already been reported in the previous literature (Sines and Carlson, 1952).
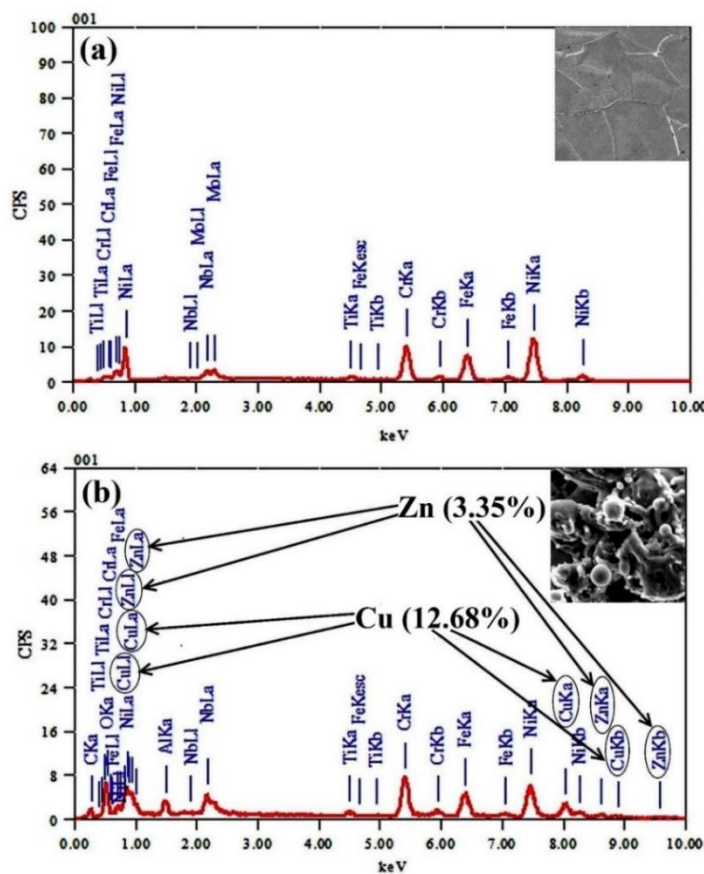
Figure 4.8 EDS analysis of Inconel 706 alloy: (a) surface before machining; (b) recast surface after machining.

4.1.9 Summary based on the effect of WEDM control parameters

The effect of various control parameters such as servo voltage, pulse on time, pulse off time, servo feed, wire feed and flushing pressure on WEDM performance characteristics, namely, MRR and SR of the Inconel 706 alloy components have been investigated. The adopted experimental plan was based on the OFAT approach. Moreover, microstructure and surface topography of WED machined components have been compared at low and high level of servo voltage, pulse on time, and pulse off time. The microhardness and RLT have been examined using the low and high setting of servo voltage and pulse on time. Furthermore, EDS analysis has been carried out to study the elemental changes on WED machined surface. Based on experimental investigation, the following observations are noted:

1. Pulse on time, pulse off time and servo voltage are the major factors influencing the MRR as well as the SR of the machined components whereas the servo feed seems to be ineffective. The wire feed of 6 m/min and flushing pressure of 1.96 bar has shown the improved MRR as well as SR with the average setting of other control parameters.

2. The SEM analysis revealed that micro globules and micro voids are more prominent at high pulse on time of 125 μs and at low servo voltage of 20 V and thus offers rough surface on the machined components. But, no microcracks were detected on the machined surface due to high toughness of Inconel 706.

3. The surface topography analysis exposed that higher smoothness and fine surface can be obtained on the machined components at low pulse on time of 105 μs, at high servo voltage of 80 V and at high pulse off time of 54 μs using power pulse mode. Whereas, high pulse on time and low servo voltage offer poor surface quality because of high discharge energy during the WEDM process.

4. The subsurface microhardness has been decreased to 192.36 Hv due to quenching of dielectric fluid during the WEDM process. Additionally, low carbon content of Inconel 706 would make the machined surface softer. The

subsurface microhardness was decreased to a depth of 80 μm due to multiple thermal loading during the WEDM process.

5. The microstructure of the cross section of WED machined components revealed that recast surface is more frequently observed at high pulse on time of 125 μs and low servo voltage of 20 V. The average RLT was found to be within the range of 10 to 50 μm, even though highly variable in nature. Moreover, minimum RLT was obtained at low pulse on time and high servo voltage.

6. The EDS analysis of recast surface has confirmed the presence of Cu and Zn which creates the elemental alteration on the WED machined surface and also shows lowered hardness of the recast region.

4.2 WEDM PERFORMANCE EVALUATION BASED ON DIFFERENT WIRE MATERIALS

4.2.1 Introduction

This section outlines the effect of different wire materials on WEDM performance characteristics of Inconel 706. For comparison of different wire materials, three different energy modes have been selected based on preliminary experiments. This section also discusses the effect of wire materials on WEDM performance characteristics such as cutting speed, surface roughness, microstructure, recast layer formation, subsurface microhardness, surface topography, residual stresses, microstructural and elemental changes on WED machined surface.

4.2.2 Experimental details

In the current study, efforts have been made to evaluate the performance attributes of WEDM process using different wire materials. For this aim, the experiments were performed on 'Electronica Ecocut' WED machine using power pulse mode followed by different discharge energy settings. As per the pilot experiments, WED machine became unstable at high servo voltage and low pulse on time. The control parameters and their levels as shown in Table 4.4 are selected in such a manner that there is no gap short and wire breakage problem during WEDM process. The complex geometry, which has been machined using WEDM, was shown in Figure 4.9.
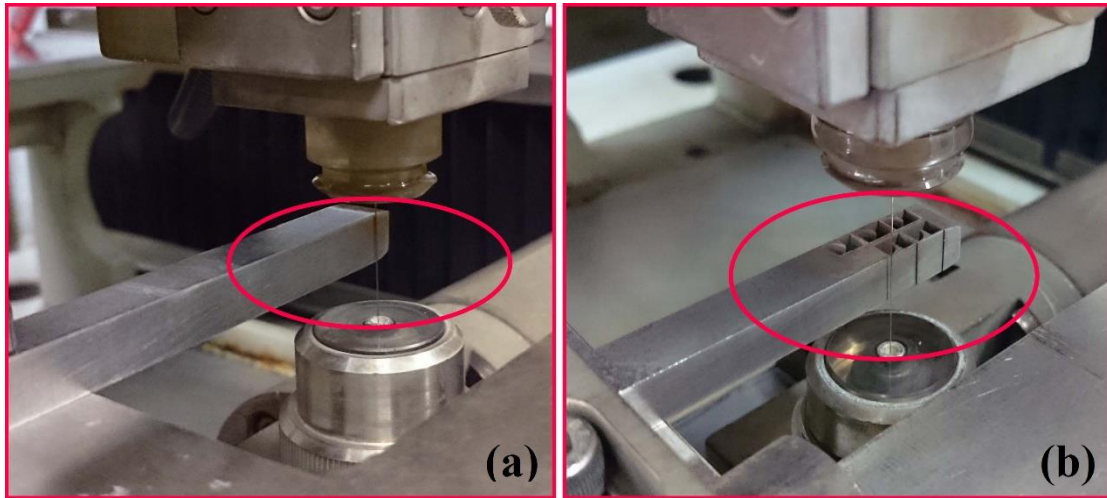
Figure 4.9 Workpiece condition: (a) before machining; (b) after machining.

Table 4.4 Experimental setting of control parameters for different discharge energy.

Discharge energy	Pulse on time (µs)	Pulse off time (µs)	Servo voltage (V)	Wire feed (m/min)
Low (0.035 J)	105	52	60	3
Medium (0.037 J)	110	39	40	6
High (0.039 J)	115	26	20	9

In this section, four control parameters, namely wire feed, servo voltage, pulse off time and pulse on time were chosen based on earlier study presented in section 4.1. A flushing pressure of 1.96 bar and servo voltage of 15 mm/min was kept constant based on the earlier investigation carried out in section 4.1. Further, three different wire materials such hard brass wire (Cu–60% + Zn–40%), diffused wire (Cu–65% + Zn–35%) and zinc coated wire (Cu–63% + Zn–37%) were selected. Each wire material has a diameter 250 µm. To compare the performance of different wire materials within same diameter range, three different discharge energy modes have been selected. The calculation of discharge has been described in section 4.2.3.

4.2.3 Calculation of discharge energy

During WEDM operation, discharge energy is directly converted into thermal energy. Therefore, discharge energy can be determined by an average electrical energy per

pulse which is converted into heat and it can be represented by following governing equation (Gostimirovic et al., 2012):

$$E_e = \int_0^{t_e} u_e(t).\, i_e(t).\, dt \cong U_e.I_e.t_e \qquad (4.1)$$

Where,

E_e = Discharge energy (J),

U_e = Discharge voltage (V),

I_e = Discharge current (A) and

t_e = Discharge duration (sec).

It was assumed that electrical discharge occurs independently during WEDM without any ignition delay. Then, discharge duration became equal to pulse duration. The final expression of discharge energy can be written as:

$$E_e = \int_0^{t_e} u_e(t).\, i_e(t).\, dt \cong U_e.I_e.t_i \qquad (4.2)$$

Where,

t_i = Pulse duration (sec).

According to thermal numerical Equation (4.2), discharge energy depends upon the discharge voltage, discharge current and pulse duration. Due to complex mechanism of material removal in WEDM process, their influence is interrelated and depends on other machining conditions such as pulse off time, servo voltage and wire feed. Therefore, in the present study, pulse on time, servo voltage and pulse off time were taken into consideration. The discharge voltage largely depends on the material of wire electrode and the workpiece. For each combination of wire electrode and the workpiece, there is a certain value of discharge voltage which cannot be influenced under given machining conditions. The control factor which directly influences the discharge energy is pulse current. But, its impact is restricted by the combination of pulse on time, pulse off time and servo voltage. In the current study, all the experiments are conducted under rough cut mode, however pulse current of 12 A is maintained constant throughout the experimentation.

From the above discussion, it is clear that effect of discharge voltage and discharge current on discharge energy is limited by the WED machine capability, materials of

wire and workpiece materials. Further, discharge energy depends on the pulse duration which is defined as the number of electrical spark allowed per cycle. If pulse duration is higher that means more amount of thermal energy is transferred to the material which increases the number of electrical sparks per unit time. Further, pulse off time also influences the discharge energy. If pulse off time is higher means that number of electrical sparks per cycle time will reduce which decreases the discharge energy. Servo voltage, which is also known as spark gap set voltage, is the another factor influencing the discharge energy. In WEDM, servo voltage is used to maintain the spark gap between the wire electrode and the workpiece. Servo voltage is totally independent of discharge voltage, however, it affects the discharge energy. If servo voltage is higher that means spark gap between the wire electrode and workpiece will increase, which reduces the spark intensity and hence decreases the discharge energy. Further, continuity of WEDM operation is maintained by the appropriate wire feed. If wire feed is higher than it will slightly increase the cutting speed of WEDM process by improved splashing of molten metal from the sparking zone.

Based on the earlier investigation carried out in section 4.1, it was revealed that pulse duration is directly proportional to the discharge energy or MRR whereas inversely proportional to the pulse off time and servo voltage. In order to maintain the stability of WEDM process, it is essential to select the appropriate value of pulse duration (pulse on time), pulse off time, servo voltage and wire feed. Based on the preliminary experiments, three different discharge energy modes were selected and efforts have been made to categorize the discharge energy based on pulse on time, pulse off time, servo voltage and wire feed as per the capability of 'Electronica Eco-cut' WED machine. Generally, low wire feed is recommended for finishing operation, whereas high wire feed is recommended for basic cutting operation. According to Gostimirovic et al. (2012), the value of discharge voltage can vary from 15 to 30 V for each combination of workpiece and electrode material. However, for the current study, discharge voltage of 28 V and discharge current of 12 A were kept constant. The pulse duration or pulse on time is only the factor which influences the discharge energy. Further, the numerical value of discharge energy can be calculated by following expression:

$$E_e = U_e.I_e.t_i = P.t_i \qquad (4.3)$$

Where,

$$Power(P) = U_e.I_e = 336 \text{ W}$$

The discharge energy per spark can be calculated using Eq. (4.4). Also, the numerical value of low, medium and high discharge energy per spark was given in Eq. (4.5), Eq. (4.6) and Eq. (4.7) respectively. However, pulse off time, servo voltage and wire feed corresponds to different discharge modes were selected based on their effect on discharge energy as shown in Table 4.4. Further, total discharge energy can also be calculated by determining the number of electrical discharges within specified time. However, for the current study, discharge energy per spark was considered instead of total discharge energy.

$$\text{Discharge Energy per spark } (E_e) = (336 \times t_i) \text{ J} \qquad (4.4)$$

$$\text{Low discharge energy } (E_L) = (336 \times 105 \times 10^{-6}) = 0.035 \text{ J} \qquad (4.5)$$

$$\text{Medium discharge energy } (E_M) = (336 \times 110 \times 10^{-6}) = 0.037 \text{ J} \qquad (4.6)$$

$$\text{High discharge energy } (E_H) = (336 \times 115 \times 10^{-6}) = 0.039 \text{ J} \qquad (4.7)$$

4.2.4 Effect of wire materials on cutting speed and surface roughness

The effect of wire materials on WEDM performance characteristics has been shown in Figure 4.10. Figure 4.10(a) indicates that cutting speed is higher with zinc coated wire. A similar trend for variation of productivity with wire materials has also been observed by earlier researchers (Manjaiah et al., 2015; Garg et al., 2014; Maher et al., 2014). This behaviour can be explained by the fact that during WEDM process, the high temperature electrical discharge tends to blast the zinc from the surface of the wire core. Additionally, zinc has a low melting point and when this additional zinc coating evaporates, it leads to cooling down of core material due to heat-sink effect and slightly improves the flushability leading to higher cutting speed. Instead, the hard brass wire has shown lowest cutting speed whereas diffused wire has a moderate effect on cutting speed. The experimental data of cutting speed has been shown in Table 4.5.
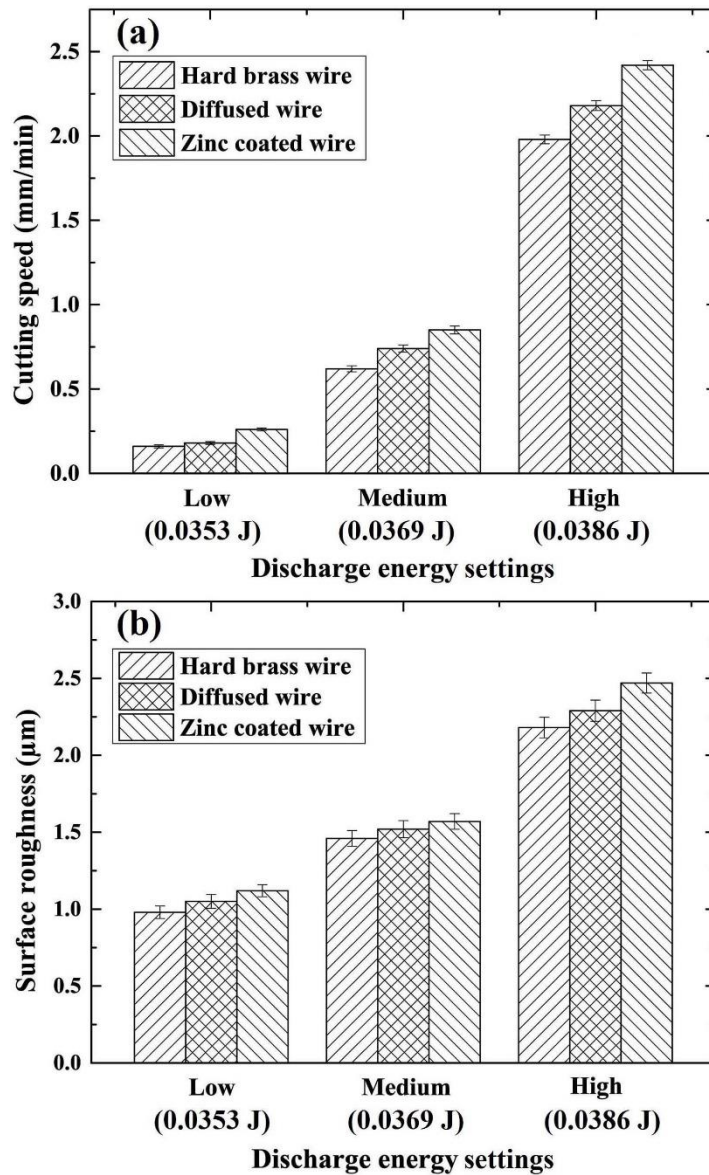
Figure 4.10 Effect of wire materials on: (a) cutting speed; (b) surface roughness.

Table 4.5 Experimental data of cutting speed correspond to different wire materials.

Discharge energy setting	Hard brass wire	Diffused wire	Zinc coated wire	Hard brass wire	Diffused wire	Zinc coated wire
	Cutting Speed (mm/min)			Cutting speed (Error in mm/min)		
Low (0.035 J)	0.16	0.18	0.26	0.009	0.008	0.009
Medium (0.037 J)	0.62	0.74	0.85	0.018	0.021	0.002
High (0.039 J)	1.98	2.18	2.42	0.026	0.029	0.003

On the other hand, hard brass wire has shown improved surface finish at the same level of control parameters as shown in Figure 4.10(b). The behaviour can be explained by the fact that hard brass wire has high tensile strength of 1000 N/mm^2 which resist the bending at the guide pivot and improve the ability to withstand the wire tension imposed upon wire during WEDM process. Therefore, it helps to maintain a vertically straight cut and minimize the wire vibration and hence leading to an improved surface finish of the machined components. Almost similar experimental results have also been reported by Klocke et al. (2014) for brass wire. Instead, zinc coated wire offers comparatively rough surface on the machined components due to its lower conductivity and lower tensile strength (900 N/mm^2) whereas diffused wire has a moderate effect on surface roughness because of its reasonable conductivity and lower tensile strength (900 N/mm^2). The experimental data of surface roughness has been shown in Table 4.6.

Table 4.6 Experimental data of surface roughness correspond to different wire materials.

Discharge energy setting	Hard brass wire	Diffused wire	Zinc coated wire	Hard brass wire	Diffused wire	Zinc coated wire
	Surface roughness (µm)			Surface roughness (Error in µm)		
Low (0.035 J)	0.98	1.05	1.12	0.041	0.045	0.039
Medium (0.037 J)	1.46	1.52	1.57	0.051	0.056	0.051
High (0.039 J)	2.18	2.29	2.47	0.067	0.069	0.065

Moreover, while changing the discharge energy from low to high, cutting speed is increased more than 10 times, whereas surface roughness also increased more than 2 times for all categories of wire materials. From the comparative analysis of wire materials it was observed that zinc coated wire improves the cutting speed by 22 % compared to the hard brass wire. Whereas, hard brass wire reduces the surface roughness by 14 % compared to the zinc coated wire under high discharge energy setting. However, diffused wire has an intermediate effect on cutting speed and surface roughness.

4.2.5 Microstructure analysis of WED machined surface

The microscopic images of the WED machined surface of Inconel 706 has been shown in Figure 4.11 which shows the formation of craters, micro globules, melted debris and micro holes, but no micro cracks were noticed because of high toughness of Inconel 706.
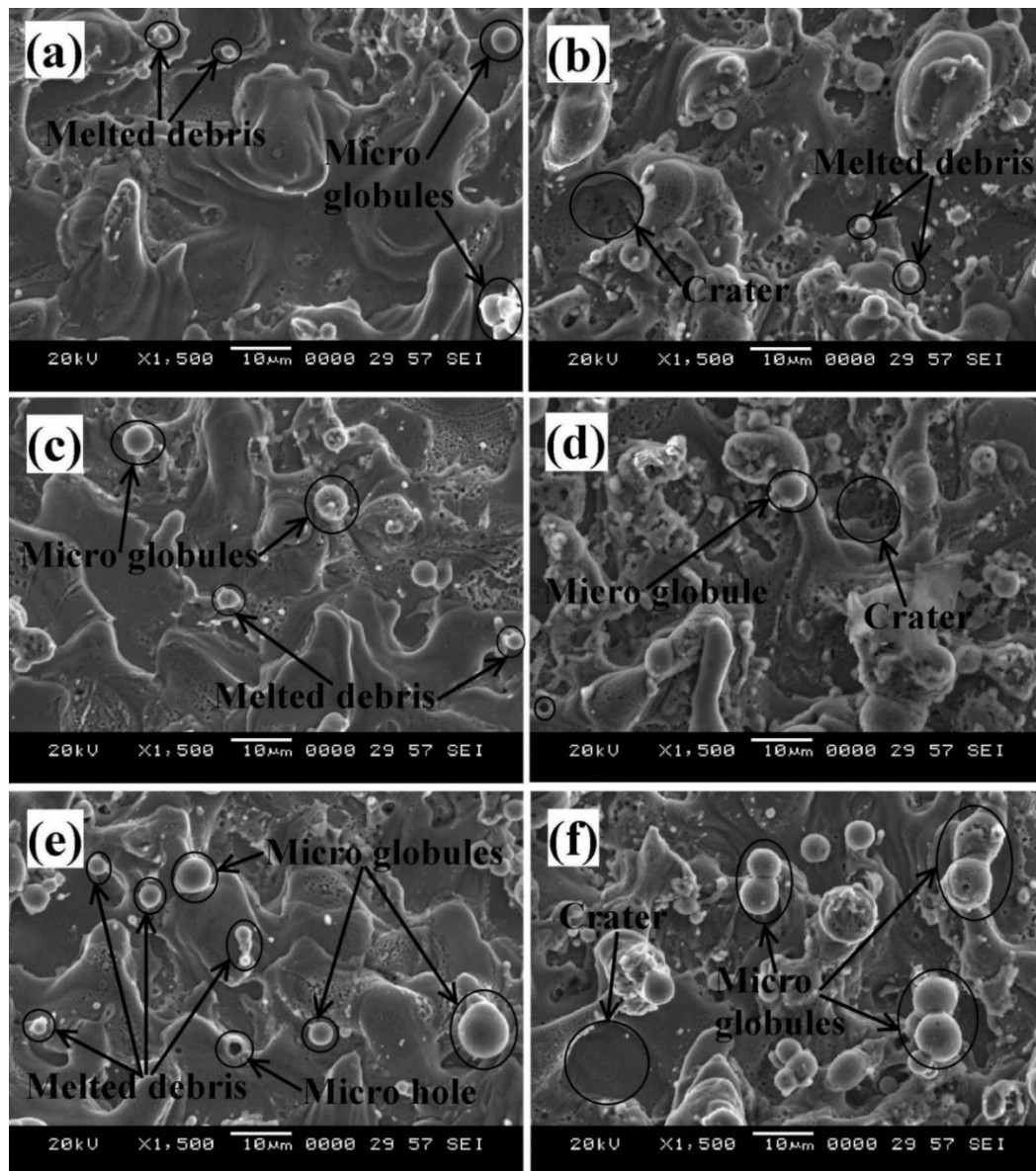
Figure 4.11 SEM graph of WED machined surface of Inconel 706 at: (a) low discharge energy–hard brass wire; (b) high discharge energy–hard brass wire; (c) low discharge energy – diffused wire); (d) high discharge energy – diffused wire; (e) low discharge energy – zinc coated wire; (f) high discharge energy – zinc coated wire).

From the Figure 4.11(b), 4.11(d) and 4.11(f), it can be detected that there is a more propensity of micro globules on the machined surface at high discharge energy. Moreover, crater formation is only visible under high discharge energy setting. This is because, at high discharge energy, comparatively large volume of material is melted. This molten metal is flushed away by pressurized waves which are generated during the absence of plasma channel and forms large crater on the machined surface. With the usage of low discharge pulse, these micro globules and craters have been reduced significantly as shown in Figure 4.11(a), 4.11(c) and 4.11(e). More or less similar results have also been reported by Li et al. (2013). This is because, at low discharge energy, small amount of material is melted which forms nano cavities and nano globules instead of craters and micro globules thus improve the surface quality of the machined component. The formation of micro globules and crater formation can be explained by the fact that during WEDM process, a temperature of around more than 10,000 °C is attained which is sufficient enough to vaporize and melt any conductive materials, but not enough to create high pressure which can splash all melted material. During re-solidification, some gas bubbles get trapped within the melted region when these bubbles collapse, form micro globules and craters on the machined surface. Form Figure 4.11, it can also be observed that hard brass wire slightly reduces the formation of melted debris and micro globules and improve the surface features as explained in section 4.2.4. However, zinc coated wire forms slightly larger crater and higher density of micro globules and thus leading to poor surface quality.

4.2.6   Surface topography analysis

The surface topography of WED machined surface corresponds to different wire materials have been shown in Figure 4.12(a-f) which revealed that there is a slight variation in topography with the wire material. However, poor surface quality was observed with zinc coated wire as shown in Figure 4.12(f). This is because, zinc coated wire produces comparatively rough surface on the machined component as already discussed in section 4.2.4.

Figure 4.12 Surface topography plot of WED machined surface of Inconel 706 at: (a) low discharge energy–hard brass wire; (b) high discharge energy–hard brass wire; (c) low discharge energy – diffused wire); (d) high discharge energy – diffused wire; (e) low discharge energy – zinc coated wire; (f) high discharge energy – zinc coated wire).

87

The experimental investigation revealed that the hard brass wire is well-suited for WED machining of Inconel 706, as it offers comparatively finer and smoother surface when compared at different discharge energy as shown in Figure 4.12(a–f). It can be better explained by the fact that hard brass wire offers lower SR on WEDM processed Inconel 706 as discussed in section 4.2.4. Thus, it improves the surface quality of the machined component. From Figure 4.12(b), 4.12(d) and 4.12(e), it was observed that the surface topography of machined surface is coarser at high discharge energy compared to low discharge energy. This is because at high discharge energy, more amount of material melts and resolidify on the machined surface. However, a part of molten metal is flushed away by pressurized waves which are generated due to absence of plasma channel. When remaining molten metals resolidify, then it forms craters and micro globule on the machined component leading to rough surface.

4.2.7 Recast layer thickness

Before microscopic investigation of recast surface, samples are subjected to ultrasonic cleaning. Then, SEM images of recast surface were captured at 500X magnification. The recast layer formation corresponds to different wire material at different discharge energy settings has been shown in Figure 4.13. The formation of recast layer can be explained by the fact that electrical discharge has a temperature of more than 10,000 °C which is sufficient enough to melt and evaporate any conductive material. During WEDM process, the material is subjected to rapid heating and cooling. A part of melted material is flushed away by the dielectric fluid when remaining molten material resolidifies on WED machined surface and forms recast layer.

From Figure 4.13(a), 4.13(c) and 4.13(e), it was observed that there is a less affinity of recast layer formation at low discharge energy whereas recast layer become thicker at high discharge energy. The experimental results shown in Figure 4.13(f) exposed that the recast layer is slightly thicker with zinc coated wire whereas relatively thin recast layer was detected with hard brass wire as shown in Figure 4.13(a). Since, zinc coated wire offer comparatively rough surface on the machined components and thus, leading to relatively thicker recast layer. Moreover, white layer was detected at high

discharge energy as shown in Figure 4.13(b), 4.13(d) and 4.13(f) which was absent at low discharge energy.

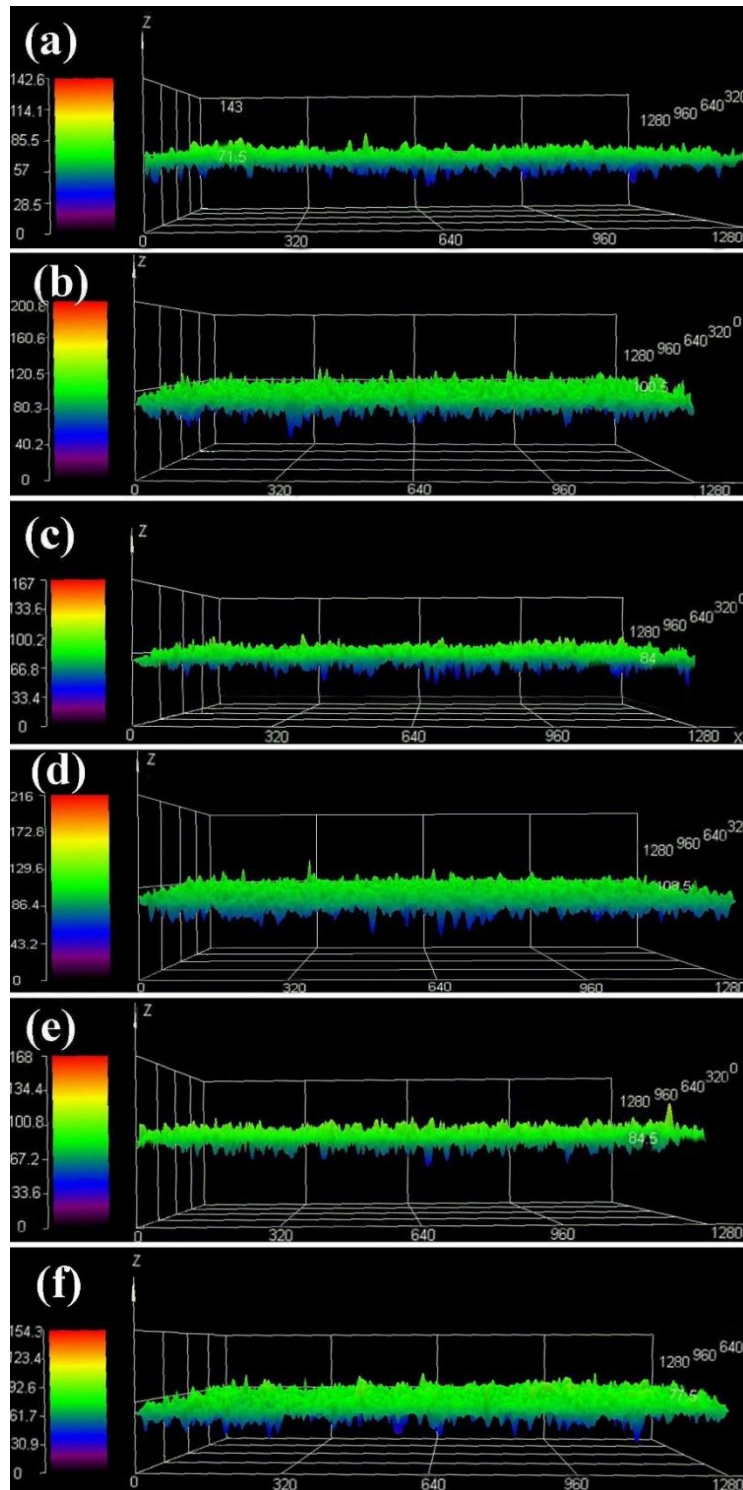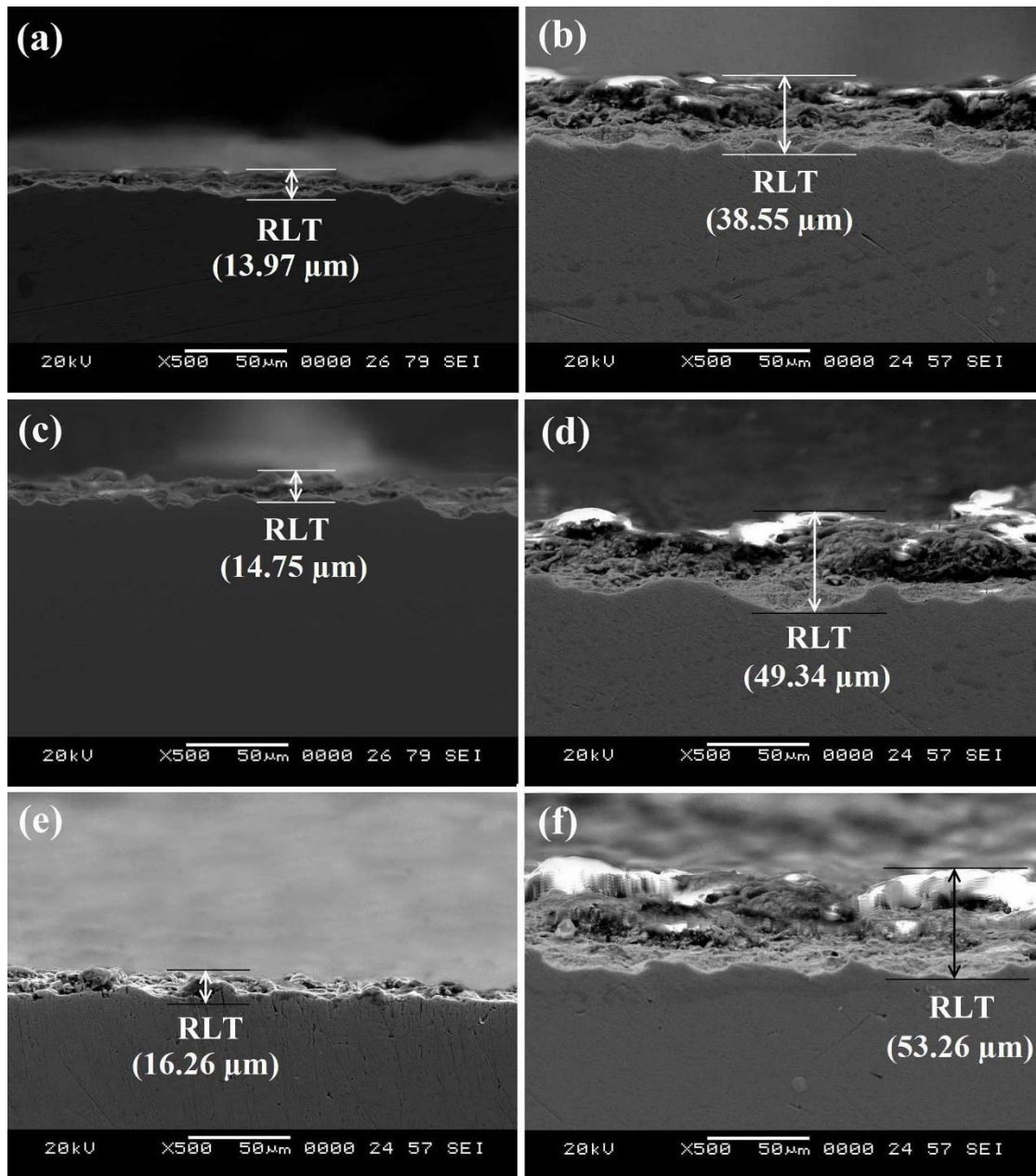**Figure 4.13** Recast layer formed on WED machined surface of Inconel 706 at: (a) low discharge energy–hard brass wire; (b) high discharge energy–hard brass wire; (c) low discharge energy – diffused wire); (d) high discharge energy – diffused wire; (e) low discharge energy – zinc coated wire; (f) high discharge energy – zinc coated wire).

4.2.8 Microhardness analysis

The changes in subsurface microhardness of WED machined components for different wire materials have been shown in Figure 4.14. The microhardness was measured in a step of 5 μm till 90 μm and total 19 observations were taken where each observation is repeated 3 times to increase the measurement accuracy. First observation, which is recorded nearer to the WED machined surface, was considered as 0 μm. The standard error bars corresponding to each observation has also been indicated in Figure 4.14.
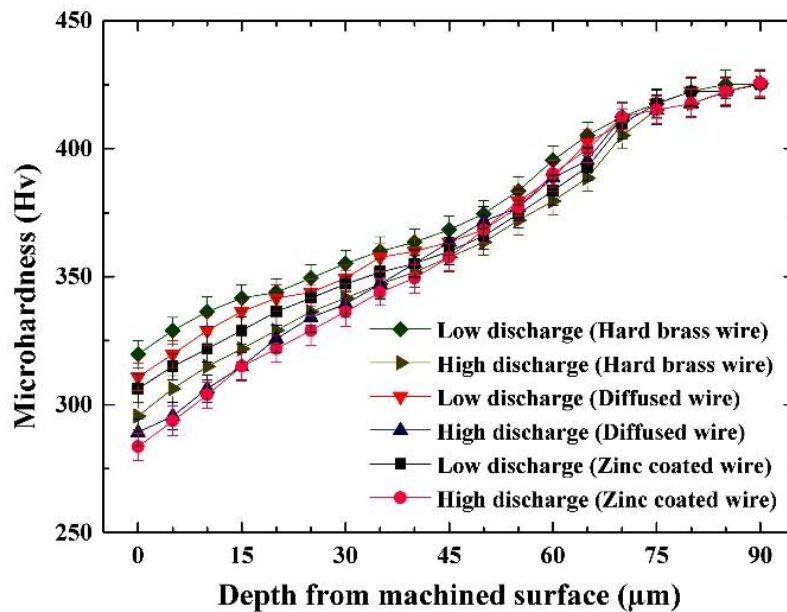
Figure 4.14 Subsurface microhardness of WED machined surface at different discharge energy followed by different wire materials.

Due to cyclic thermal loading during WEDM process, the microhardness of machined component has been affected significantly. The changes in microhardness of WED machined components for different wire material has been shown in Figure 4.14. It was observed that microhardness for WEDM processed sample has been decreased from 425.62 Hv to 283.62 Hv below the depth of 90 μm. Almost similar experimental results have also been reported by Li et al. (2014) for Inconel 718. Since, Inconel 706 has very low carbon content, it doesn't make the surface harder. Figure 4.14 also shows that the microhardness is significantly changing when increasing the discharge energy. Under low discharge energy setting, less reduction in microhardness was observed due to less thermal damage during WEDM process. Further, subsurface

90

microhardness is widely influenced by high discharge energy which creates metallurgical changes on the machined surface and thus leading to lower hardness. Moreover, a minimum hardness alteration was observed using hard brass wire at low discharge energy, whereas zinc coated wire has a significant effect on the subsurface microhardness at high discharge energy.

4.2.9 Analysis of elemental changes

Based on earlier studies in section 4.2.4, it was concluded that zinc coated wire offers poor surface quality on machined component compared to hard brass wire and diffused wire. Therefore, zinc coated wire was selected for further investigation of metallurgical changes on the WED machined surface.
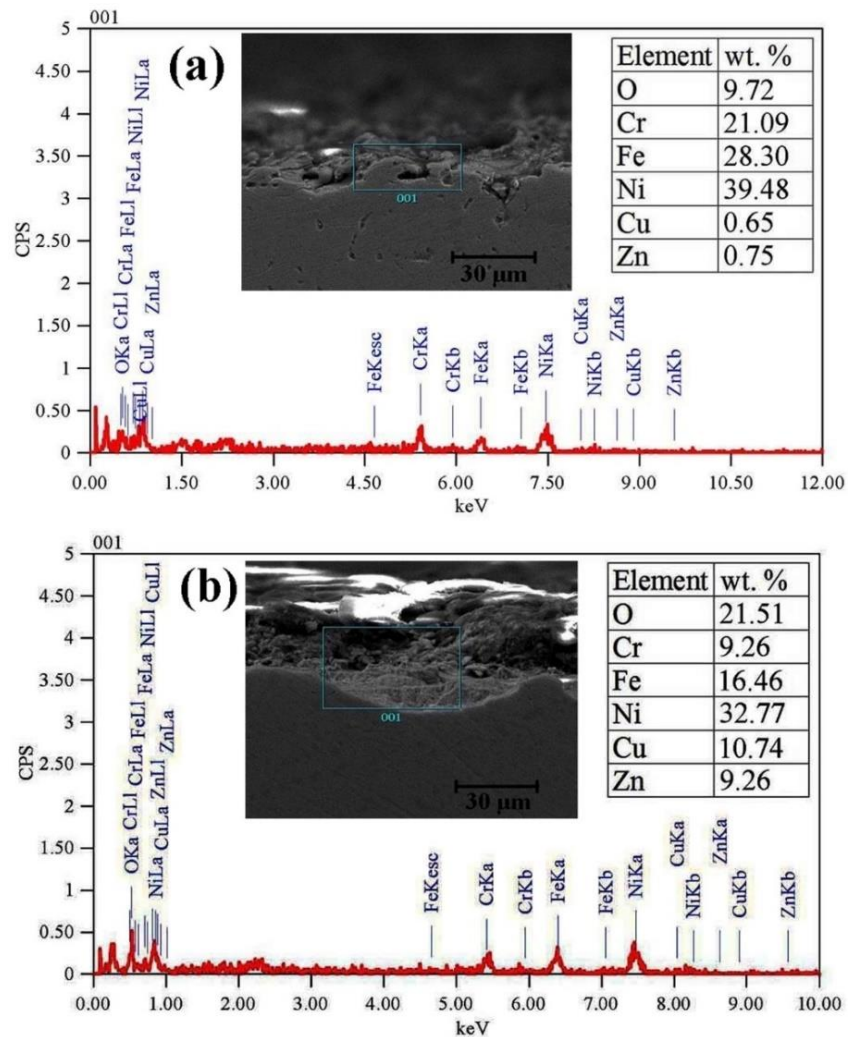
Figure 4.15 EDS analysis of recast surface produced by zinc coated wire at: (a) low discharge energy (b) high discharge energy.

91

The EDS analysis of recast surface exposed that at high discharge energy, WED machined surface is subjected to higher elemental changes. This is because, under high discharge energy setting, workpiece material is subjected to higher thermal energy which melts more amount of wire and workpiece material. Therefore, complex chemical reactions will take place between wire, workpiece and dielectric fluid. As a result, elemental changes were observed on WED machined surface. Further, EDS analysis exposed the presence of foreign elements such as Cu, Zn and O on the WED machined surface in considerable quantities. These elements have been migrated from zinc coated wire during WEDM process. Li et al. (2014) have also observed similar results from the EDS analysis of WEDM processed Inconel 718. From the Figure 4.15(a) and Figure 4.15(b), it was observed that when discharge energy is changing from low to high, the content of Ni, Cr and Fe are decreasing and the content of Cu, Zn and O are increasing. The nickel content has been decreased by 17 % in the recast layer. Moreover, iron and chromium content has been dropped by 42 % and 56 % respectively. This will lead to altered material properties of the recast layer. Moreover, the microhardness of recast surface has been reduced significantly due to elemental changes that occurred during WEDM process.

4.2.10 Analysis of residual stresses

Due to multiple thermal loading during WEDM process, there is a possibility of generation of tensile residual stresses which may lead to a reduction in microhardness of recast layer. There is a well-known relationship between hardness and residual stresses which has already been stated in earlier literature (Sines and Carlson, 1952). Further, generation of residual stresses can be explained by the fact that due to the extreme rise in temperature of electrical discharge (more than 10,000 °C), high thermal gradient are acting on WED machined components. This, in turn, melts and vaporizes the workpiece material. Some part of molten metal is flushed away by pressurized waves. When, remaining molten material starts to resolidify until it won't reaches to the bulk workpiece temperature, then its shrinkage is opposed by the bulk material. As a result, recast material exhibits tensile residual stresses. The presence of these residual stresses can cause premature failure of aircraft components. Earlier study carried out by Antar et al. (2012) have also that WEDM processes surface of

Inconel 718 exhibits tensile residual stresses. Almost similar experimental results also have been reported in the current study. The investigation carried out in section 4.2.4 revealed that zinc coated wire is best suited for higher productivity, whereas hard brass wire improves the surface quality. However, diffused wire has a moderate effect on productivity and surface quality. Therefore, zinc coated wire and hard brass wire are selected for further investigation of residual stresses. The experimental results shown in Figure 4.16 revealed that zinc coated brass wire offers higher residual stress (more than 6 %) compared to the hard brass wire. But, tensile residual stresses are highly detrimental to aircraft application as it will reduce the fatigue life of the components. Hence, the hard brass wire is well-suited for manufacturing of aircraft components using WEDM process.
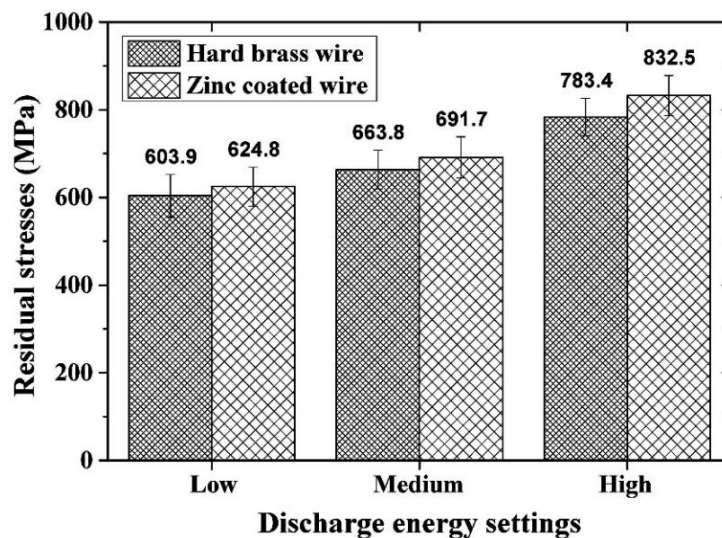
Figure 4.16 Residual stresses generated within WED machined material.

4.2.11 Summary based on the effect of different wire materials

In this chapter, the effect of different wire material on WEDM performance characteristics such as cutting speed, surface roughness, recast layer thickness, microstructure, microhardness, surface topography, residual stresses and elemental changes of Inconel 706 have been evaluated. Based on the experimental investigation, the following observations are noted:

- The hard brass wire improves the surface quality of the machined components in terms of low surface roughness, comparatively smoother topography, lesser recast layer thickness and minimum hardness alteration under the same setting of

control parameters while zinc coated wire has shown improved productivity in terms of higher cutting speed. Instead, diffused wire has a moderate effect on productivity and surface quality.

- Microstructure analysis of the WED machined surface revealed the high density of micro globules and crater formation at high discharge energy setting, but no micro cracks were detected due to high toughness of Inconel 706 alloy. Moreover, hard brass wire offers low density of micro globules and melted debris under low discharge energy setting and improves surface quality of the machined component compared to the zinc coated wire.

- The topography analysis revealed that hard brass wire offers comparatively smoother surface and most suited for WED machining of Inconel 706. Zinc coated wire produces a comparatively rougher surface since it produces comparatively higher surface roughness. Moreover, topography of WED machined surface turns out be coarser at high discharge energy.

- Thin recast layer was detected at low discharge energy setting, whereas recast layer becomes thicker at high discharge energy. Moreover, hard brass wire produces a thin recast layer compared to the zinc coated wire. Additionally, white layer was noticed only at high discharge energy setting, however, no white layer was detected under low discharge energy setting.

- The subsurface microhardness of WED machined Inconel 706 has been changed below the depth of 80 μm due to repeated thermal loading that occurred during WEDM process. Moreover, subsurface microhardness is greatly influenced by high discharge energy which creates metallurgical modifications on the WED machined surface. However, a minimum hardness alteration was detected with hard brass wire at low discharge energy.

- The EDS analysis of recast surface shows higher elemental changes with the increase in discharge energy. Further, foreign elements such Cu, Zn and O are present on WEDM machined surface in substantial quantities which confirms altered material properties of recast surface. The change in material properties has contributed to lower hardness of recast region.

- The residual stress analysis revealed that hard brass wire offers comparatively less residual stresses on the machined components and suitable for manufacturing of aircraft components using WEDM process.

4.3 WEDM PERFORMANCE EVALUATION BASED ON DIFFERENT DIAMETER WIRES

4.3.1 Introduction

This section outlines the effect of different diameter wires on WEDM performance characteristics. The chapter also discusses the investigation of MRR, SR, microstructure, recast layer formation, microhardness, surface topography, microstructural and elemental changes on the machined surface.
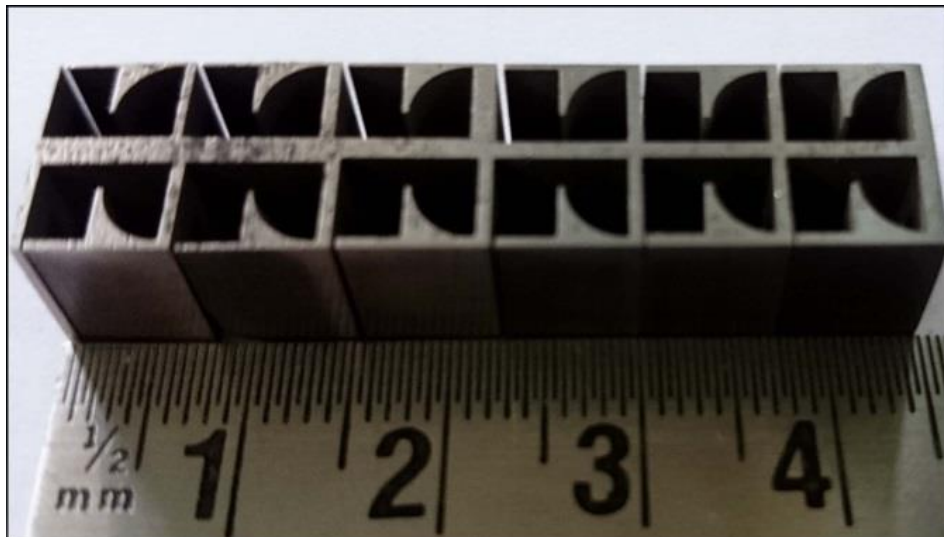
Figure 4.17 Complex slots in Inconel 706 machined by WEDM process.

4.3.2 Experimental details

The experimental work was carried out to investigate the effect of different diameter wires and evaluate the WEDM performance characteristics of Inconel 706 to achieve the feasibility in manufacturing of complex shape components for gas turbine applications. The WED machine has two distinct modes of operation, power pulse mode and fine pulse mode. Usually, the power pulse mode is employed for the basic cutting operation, whereas fine pulse mode is used for finishing of machined surface. As per the experimental record, the WED machine turns out to be unstable with the

usage of smaller diameter wire at low discharge setting while cutting the complex shape through Inconel 706. Therefore, control parameters and their levels are selected in such a way that there is no wire rupture and gap short issue during the WEDM operation. The complex profile slot, which is shown in Figure 4.17, has been selected based on the complexity of aircraft components.

Based on the earlier investigation carried out in section 4.1, it was observed that pulse on time, pulse off time and servo voltage are the major factor affecting the MRR and SR whereas servo feed is almost ineffective. The wire feed of 6 m/min and flushing pressure of 1.96 bar was found to be optimum for improved productivity as well as better surface quality. Therefore, in this section, the optimum value of servo feed and flushing pressure were considered. It must be noted that insufficient flushing in WEDM process creates gap short problem while inadequate wire feed results in wire rupture. However, the wire rupture is the more critical issue than the gap short issue. This is because, wire rupture during the machining process significantly increases the production time and also affects the surface quality of the machined component. Therefore, four control parameters such as servo voltage, pulse on time, pulse off time and wire feed are selected for the current investigation.

The experimental investigation carried out in section 4.2 revealed that hard brass wire improves the surface integrity of WED machined component and best suited for manufacturing of aircraft components. Therefore, hard brass wire has been selected to investigate the effect of different diameter wires on WEDM performance characteristics. For the comparative investigation of different diameter wires, low, medium and high discharge energy modes were selected as shown in Table 4.7. Further, the calculation of discharge energy has already been described in section 4.2.3. Based on the low and high discharge energy setting, microstructural changes, surface topography, microhardness and recast layer thickness have been evaluated for different diameter wires. The current study mainly focuses on the selection of optimum diameter wires based on various performance criteria. All wires are made up of hard brass with elongation of 1%. The 150 µm wire has a tensile strength of 900 N/mm^2 while 200 µm and 250 µm wires offer a tensile strength of 1,000 N/mm^2. It must be noted that 150 µm, 200 µm and 250 µm wires are unable to sustain the pulse

on time of more than 118 μs, 123 μs, and 127 μs respectively with an average setting of other control parameters. Because of low tensile strength of 150 μm wire, there is more propensity of wire breakage at pulse on time more than 118 μs.

Table 4.7 Experimental setting of control parameters for different discharge energy.

Discharge energy setting	Pulse on Time (μs)	Pulse off Time (μs)	Servo Voltage (V)	Wire Feed (m/min)
Low (0.035 J)	105	52	60	3
Medium (0.037 J)	110	39	40	6
High (0.039 J)	115	26	20	9

4.3.3 Effect of wire diameter on cutting speed and surface roughness

The effect of different diameter wires on cutting speed as well as surface roughness has been shown in Figure 4.18. From Figure 4.18(a), it was observed that with the smaller diameter wire, cutting speed is 20 % higher compared to larger diameter wire under similar experimental condition. This behaviour could be explained by the fact that with a smaller diameter wire of 150 μm, the wire transport speed is relatively higher. This, in turn, slightly improves the wire feed compared to the large diameter wire. Therefore, more amount of molten metal will be splashed through the machining zone and hence leading to higher cutting speed. Generally, a higher cutting speed resembles lesser time for cutting the profile through the component. Although, smaller diameter wire offers high cutting speed, it removes comparatively less amount of material from the machined component. This can be better explained by the fact that 0.4337 g material has been removed in 717 sec in case of wire diameter of 150 μm whereas 0.6887 g material has been removed in 824 sec in case of wire diameter of 250 μm under high discharge energy setting. It means that MRR is comparatively lower for smaller diameter wire, but cutting speed is higher. The experimental data of cutting speed and surface roughness have been shown in Table 4.8 and Table 4.9 respectively.

Even though, smaller diameter wire has shown the various improvements in WEDM process such as higher cutting speed, minimum corner radius, minimum spark gap and better surface quality. However, there is a more propensity of wire breakage because

of its lower tensile strength of 900 N/mm^2 as that of larger diameter wire of 1000 N/mm^2. Earlier study carried out by Antar et al. (2011) have shown the improvement in WEDM process using the coated wire, however coated wires are restricted to their minimum diameter of 200 μm. Below 200 μm, no coated wires are commercially available because of wire straightness issue and difficulties in processing of smaller diameter coated wire.

Table 4.8 Experimental data of cutting speed correspond to different diameter wires.

Discharge energy setting	150 μm	200 μm	250 μm	150 μm	200 μm	250 μm
	Cutting speed (mm/min)			Cutting speed (Error in mm/min)		
Low (0.035 J)	0.21	0.19	0.16	0.009	0.009	0.009
Medium (0.037 J)	0.74	0.68	0.62	0.017	0.016	0.018
High (0.039 J)	2.45	2.32	1.98	0.031	0.029	0.026

Table 4.9 Experimental data of surface roughness correspond to different diameter wires.

Discharge energy setting	150 μm	200 μm	250 μm	150 μm	200 μm	250 μm
	Surface roughness (μm)			Surface roughness (Error in μm)		
Low (0.035 J)	1.46	1.51	1.54	0.037	0.033	0.041
Medium (0.037 J)	2.34	2.48	2.51	0.044	0.048	0.051
High (0.039 J)	3.28	3.46	3.57	0.064	0.058	0.067

Figure 4.18(b) indicates that surface roughness (SR) of larger diameter wire is 8 % higher compared to smaller diameter wire under similar experimental condition. This behaviour can be explained by the fact that with larger diameter wire, the relative wire transport speed is lower. This, in turn, marginally reduces the wire feed and the amount of molten metal to be splashed out from the machining zone is considerably reduced. Hence, allowing the formation of micro holes and micro globules on the machined surface leading to slightly higher SR. The similar trend for the variation of surface roughness with the different diameter wires are reported in previous literature (Newton, 2008). Based on the experimental investigation, it was concluded that the smaller diameter wire is well-suited for cutting the complex shape profile with

improved cutting speed as well as the better surface finish and found to be useful to maintain the minimum corner radius. The smaller diameter wire is also the best choice for cutting the profile through thin and delicate specimen with minimum spark gap.
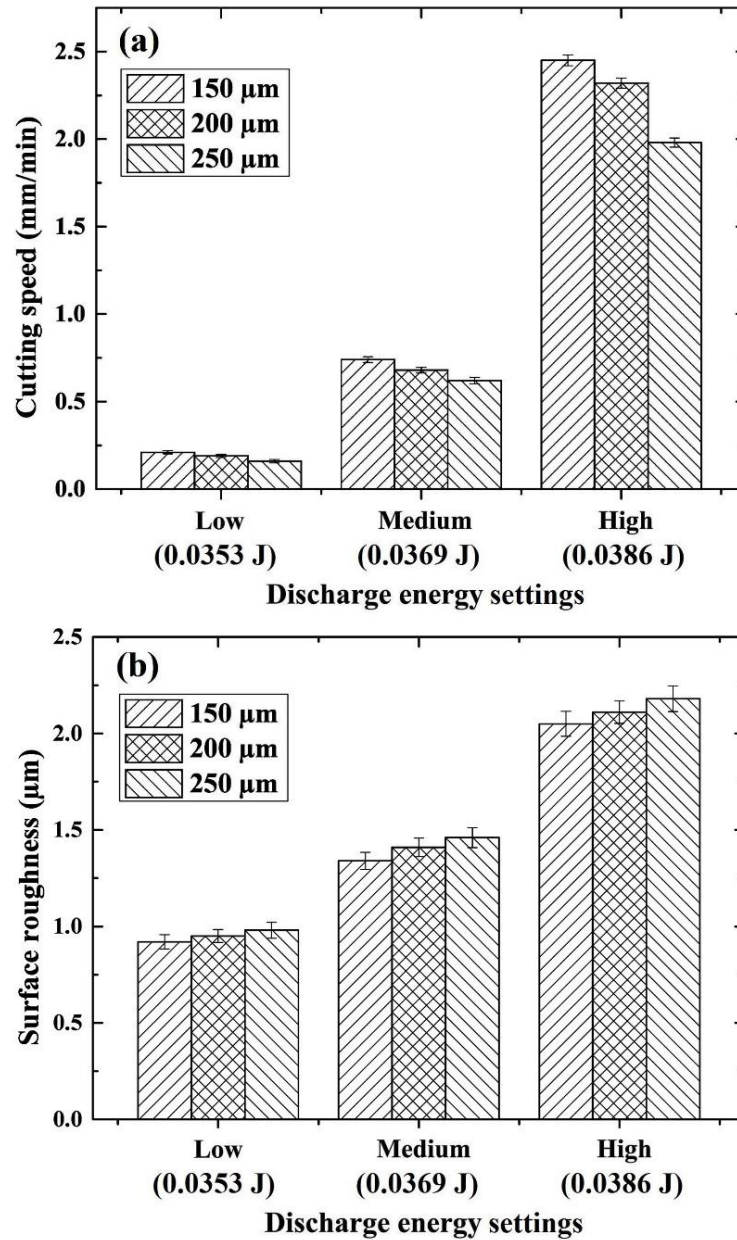
Figure 4.18 Effect of discharge energy setting on: (a) cutting speed; (b) surface roughness.

4.3.4 Microstructure study of wire surface

With the usage of high discharge energy setting along with smaller diameter wire, the more frequent wire breakage would take place due to its lower tensile strength of 900 N/mm^2. The experiment results revealed that pulse on time and servo voltage are the major factors contributing to the wire rupture during the WEDM process. The microscopic images of wire surface have explored the formation of crater, rupture, recast layer, and melted debris and micro holes as shown in Figure 4.19.
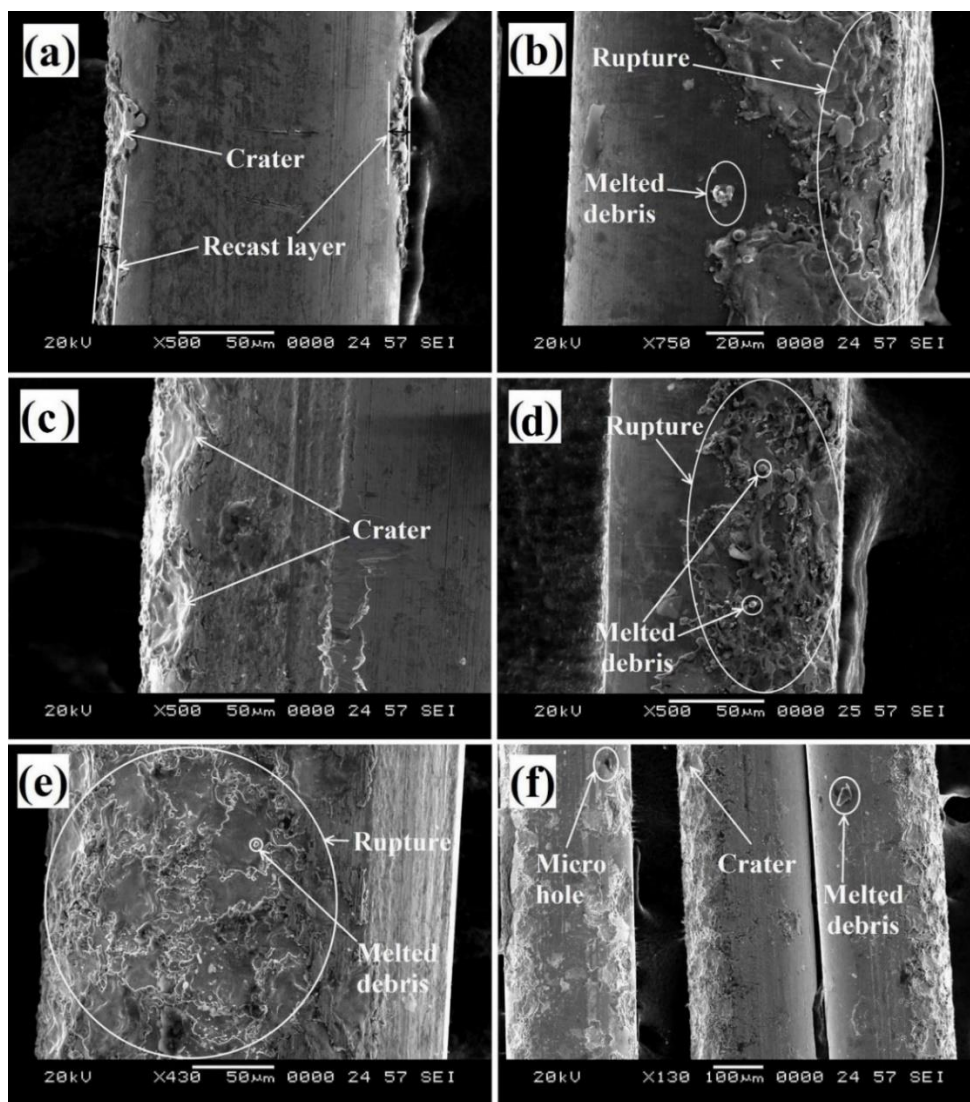
Figure 4.19 Microstructure graph of wire surface during WEDM of Inconel 706: (a) low discharge energy – 150 μm wire; (b) high discharge energy – 150 μm wire; (c) low discharge energy – 200 μm wire; (d); high discharge energy – 200 μm wire; (e) low discharge energy – 250 μm wire ; (f) high discharge energy – 250 μm wire.

The EDS analysis of wire surface as shown in Figure 4.20 exposed the presence of O, Ni and Cr on the wire surface resulting in altered material properties of wire surface. Owing to insufficient pulse off time, melted debris may stick to the wire surface and reduces the spark gap thus making the spark unstable. This situation leads to an arcing between wire and workpiece resulting in wire breakage.

Element	wt. %
O	15.25
Cr	1.23
Ni	3.26
Fe	2.04
Cu	49.24
Zn	28.98
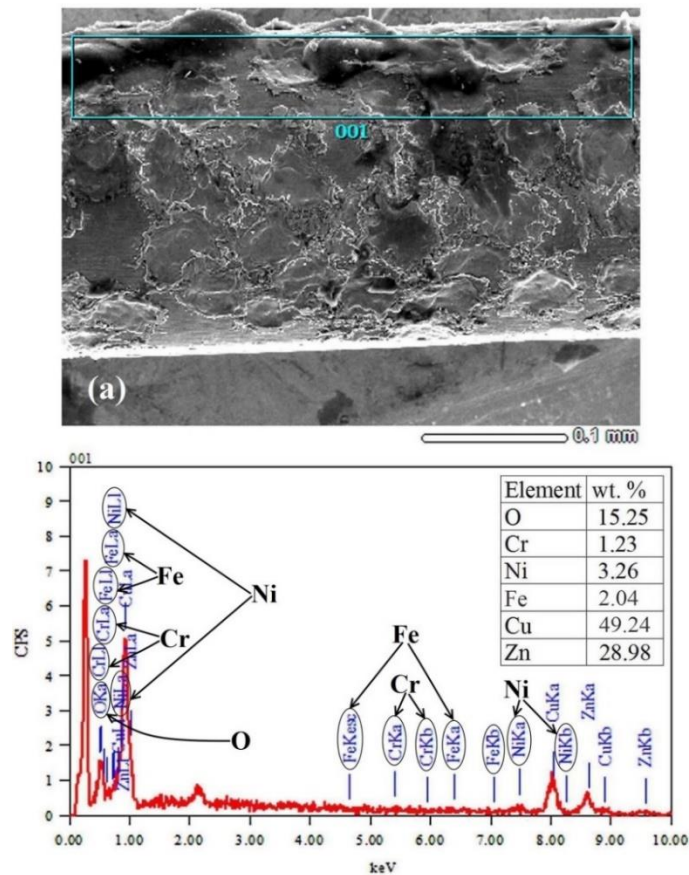
Figure 4.20 (a) Recast wire surface; (b) EDS analysis of wire surface.

4.3.5 Microstructure study of WED machined surface

The SEM images of WED machined surface of Inconel 706 has revealed the formation of micro holes, micro globules, craters and melted debris as shown in Figure 4.21. But, no micro crack was detected on the machined surface due to high toughness of Inconel 706 alloy. From Figure 4.21(b), 4.21(d) and 4.21(f), it was observed that micro voids, craters and micro globules are commonly observed due to the high discharge energy of the spark. Li et al. (2013) have also observed similar results under high discharge energy settings.

The experimental investigation revealed that with the appropriate setting of pulse on time, servo voltage and flushing pressure, the formation of micro voids and micro globules can be reduced significantly.
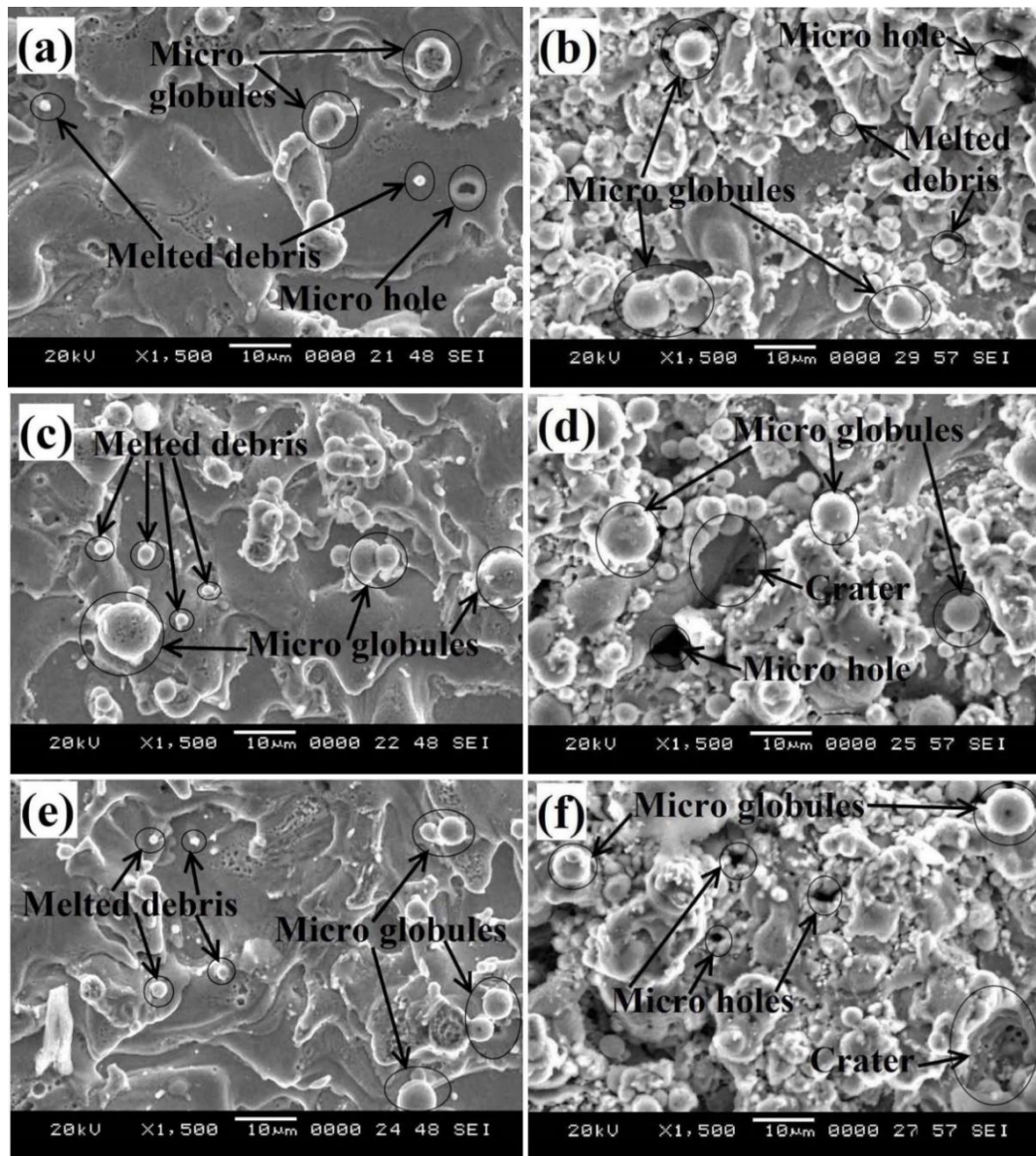
Figure 4.21 Microstructure graph of WED machined surface of Inconel 706 at: (a) low discharge energy – 150 μm wire; (b) high discharge energy – 150 μm wire; (c) low discharge energy – 200 μm wire; (d); high discharge energy – 200 μm wire; (e) low discharge energy – 250 μm wire ; (f) high discharge energy – 250 μm wire.

Figure 4.21(a), 4.21(c) and 4.21(e) shows the reduced micro void and micro globules due to the low discharge energy of the spark. The formation of micro holes and craters can be explained by the fact that the electrical spark has a temperature of around 10,000 °C which is more than sufficient to melt and vaporize the any conductive material, but not enough to create high exploding pressure which can splash all the melted material from the machining zone. When remaining molten material resolidify on the machined surface, some gas bubbles get entrapped in the melted area and thus, forming micro holes and craters on machined surface.

4.3.6 Surface topography of WED machined surface

The experimental results revealed that the topography of WED machined surface is slightly varied with the wire diameter. From Figure 4.22(a) it was observed that a smaller wire diameter relatively offers fine and smooth surface on the machined components with the use of low discharge energy setting. This behaviour can be explained by the fact that the smaller diameter wire generally offers lower SR on the machined component as discussed in the previous section. Therefore, improves the surface features of the WED machined components.

From Figure 4.22(a), 4.22(c) and 4.22(e), it was observed that the topography of machined surface is fine textured compare to Figure 4.22(b), 4.22(d) and 4.22(f) because of low discharge energy setting. At higher discharge energy setting, more amount of material melts and resolidifies on the machined surface, and allow less time for the splashing of molten metal through machining zone leading to the rough surface on the machined component. A more or less similar results for variation of surface topography have also been observed by Li et al. (2013).

Figure 4.22 Surface topography of WED machined surface of Inconel 706 at: (a) low discharge energy – 150 μm wire; (b) high discharge energy – 150 μm wire; (c) low discharge energy – 200 μm wire; (d); high discharge energy – 200 μm wire; (e) low discharge energy – 250 μm wire ; (f) high discharge energy – 250 μm wire.
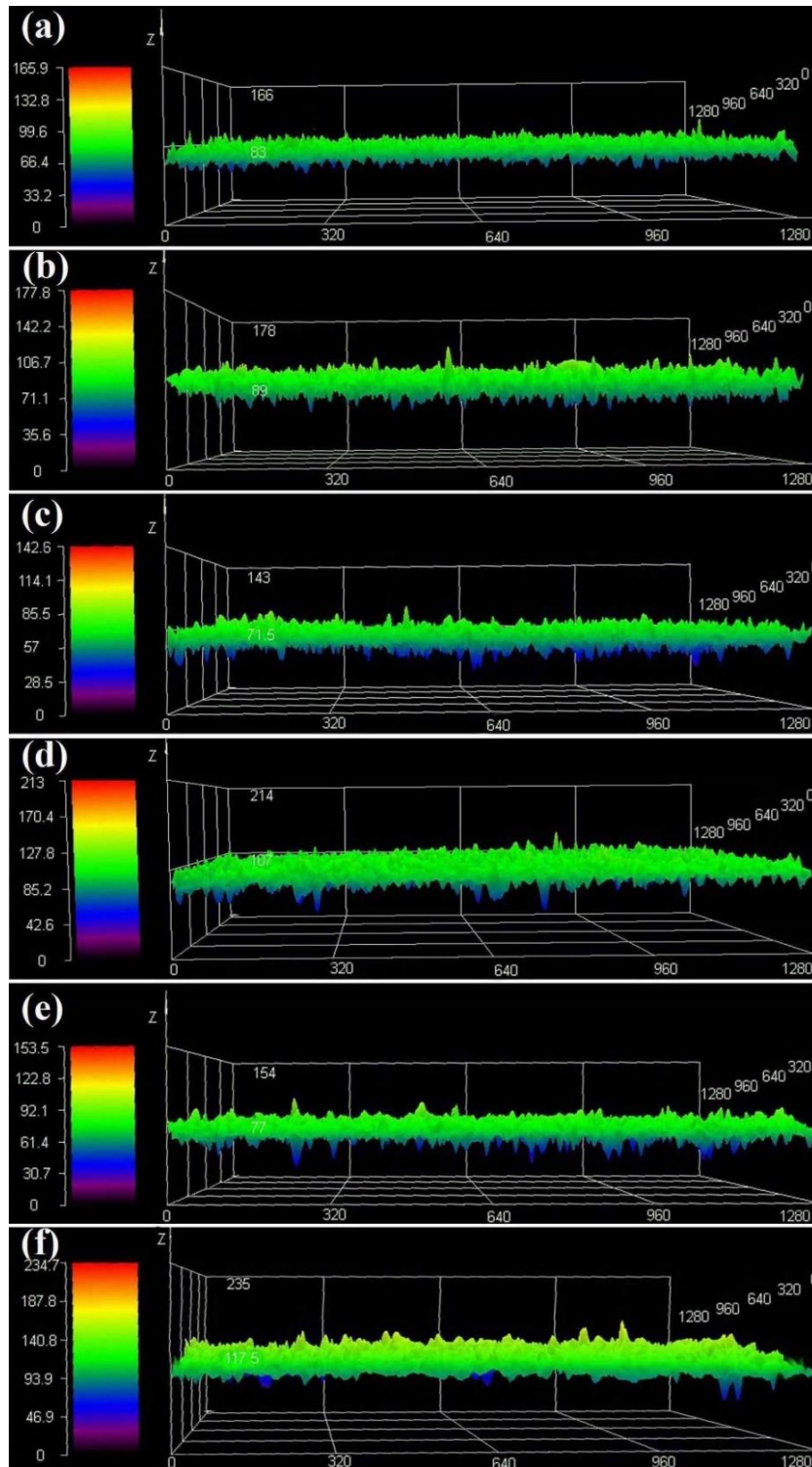
4.3.7 Microhardness of WED machined surface

Microhardness of machined surface is mainly affected due to sudden heating and cooling occurred during the WEDM process. The experimental investigation revealed that subsurface microhardness has been reduced to a depth of 80 μm owing to altered material properties. Due to low carbon content (wt. 0.06%) of Inconel 706, it doesn't make the WEDM surface harder. In addition, the electrolysis may occur during the WEDM process and also contributes to the softening of machined surface. Figure 4.23 shows the microhardness profile for different diameter wires as well as different discharge energy setting. It was observed that with the larger diameter wire, there is a higher tendency of microhardness reduction compared to the smaller diameter wire. The microhardness of machined surface has been decreased to 270.6 Hv due to high thermal gradient on the machined component during WEDM process. Under high discharge energy setting, more reduction in microhardness was observed due to significant thermal degradation that occurred during WEDM process. Aspinwall et al. (2008) have also found similar experimental observations during WEDM process of Inconel 718 under rough cut mode.
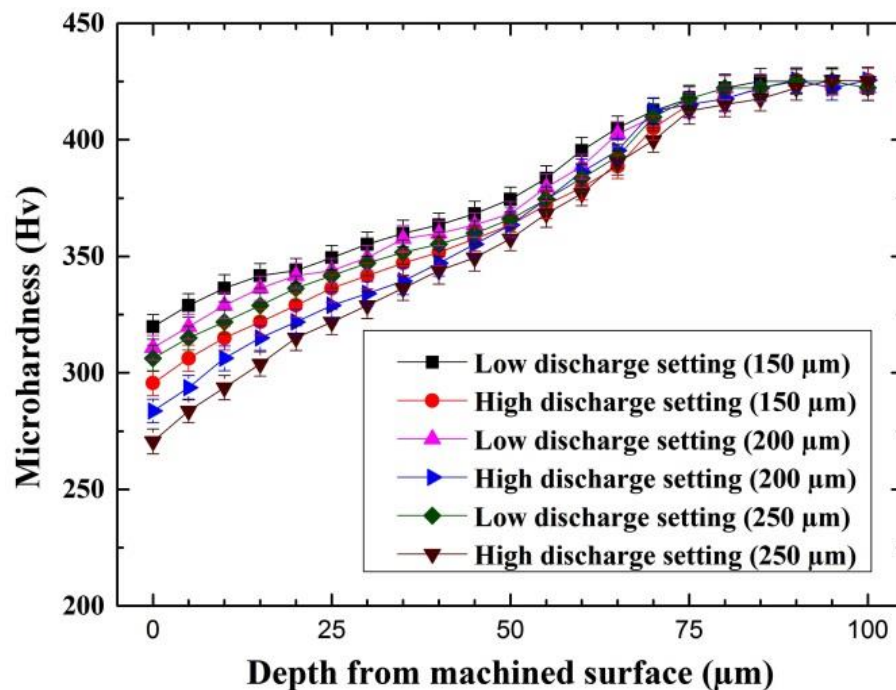
Figure 4.23 Subsurface microhardness of WED machined surface at low and high discharge energy followed by different diameter wires.

4.3.8 Recast layer formation on WED machined surface

The recast layer generally formed on the machined surface due to re-solidification of molten material followed by rapid heating and cooling during WEDM process. The SEM graph of the cross-section of WED machined surface revealed that there is a more tendency of recast layer formation at high discharge energy setting accompanied by inadequate flushing conditions. From the Figure 4.24(a–f), it was revealed that the recast layer thickness (RLT) is slightly higher with larger diameter wire and vice versa. Since, larger diameter wire offers slightly rough surface on the machined component and thus, offers relatively thick recast layer on the machined surface.

From the Figure 4.24(a), 4.24(c) and 4.24(e), it was observed that RLT has been reduced significantly due to low discharge energy of the spark. However, a thick recast layer has been detected under high discharge energy setting as shown in Figure 4.24(b), 4.24(d) and 4.24(f). This is because, under high discharge energy setting, workpiece material is subjected to high amount thermal energy which melts comparatively more volume of material from the machined surface. A part of this molten metal is flushed away by pressurized waves generated during WEDM process. When, remaining molten metal resolidify on the machined surface, then forms a thick recast layer on machined component.

Due to high temperature of electrical discharge, elemental changes may occur on the recast surface. Figure 4.25(a) shows the selected region of the recast surface for EDS analysis. The EDS analysis exposed the depletion of Ni, Fe and Cr, and the addition of Cu, Zn and O to the recast surface as shown in Figure 4.25(b). This, in turn, creates elemental changes on WED machined component. Owing to altered material properties, the microhardness of the recast surface has been reduced significantly. Almost similar results have also been reported by Li et al. (2013).
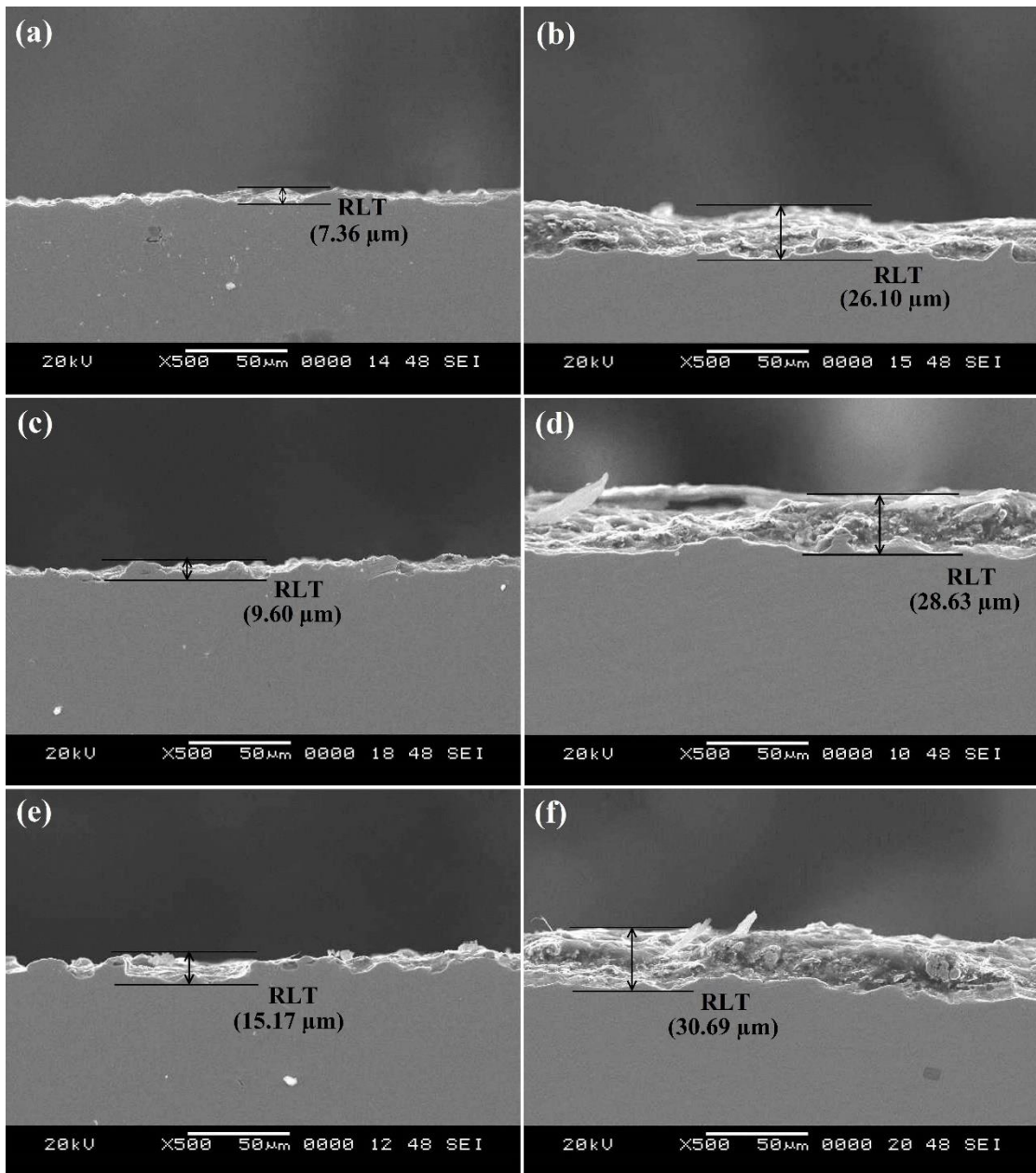
Figure 4.24 Recast surface of WED machined component of Inconel 706 at: (a) low discharge energy – 150 μm wire; (b) high discharge energy – 150 μm wire; (c) low discharge energy – 200 μm wire; (d); high discharge energy – 200 μm wire; (e) low discharge energy – 250 μm wire ; (f) high discharge energy – 250 μm wire.
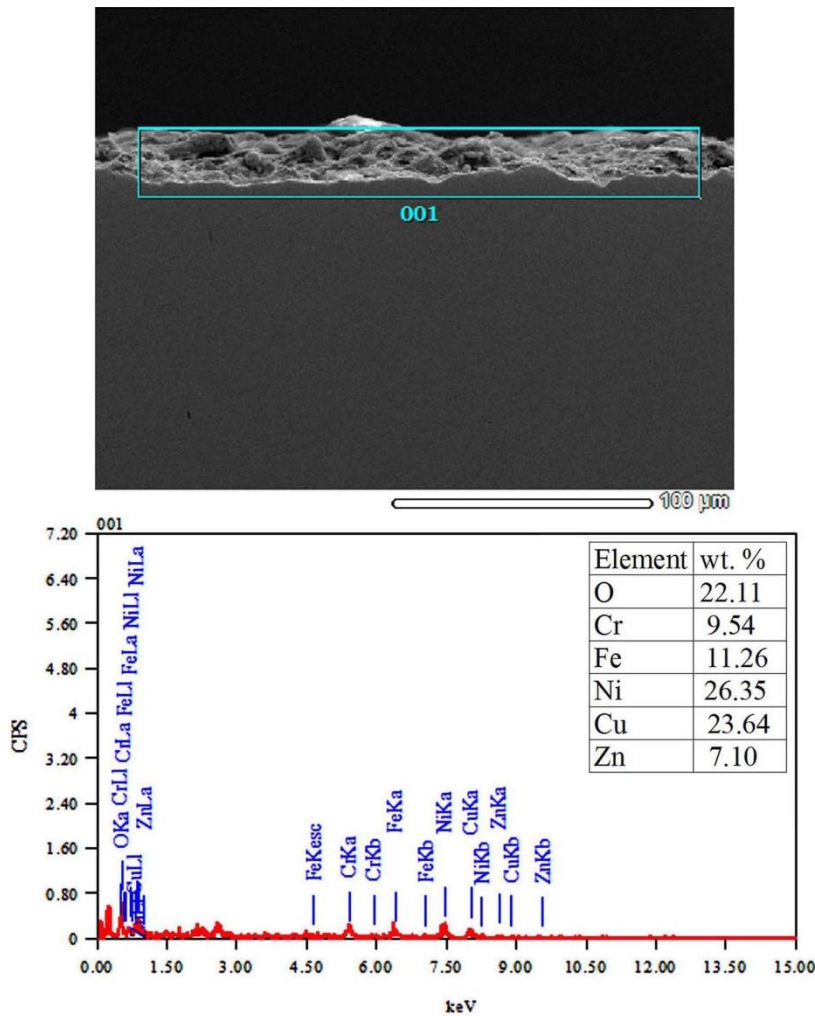
Figure 4.25 (a) Recast surface of Inconel 706; (b) EDS analysis of recast surface.

4.3.9 Summary based on effect of different diameter wires

In this section, the effect of wire diameter on WED machinability of Inconel 706 superalloy has been investigated. WEDM performance characteristics such as cutting speed, surface roughness, recast layer thickness, microstructure, wire topography, microhardness, WED machined surface topography and elemental changes have been evaluated. Based on the experimental investigation, the observations are noted as follows:

- The smaller diameter wire improves the cutting speed as well as surface finish of the machined component for the same setting of control parameters. This is because, with the smaller diameter wire, the relative wire transport speed is comparatively higher. This, in turn, increases the splashing of molten material

108

from the machining region leading to improved WEDM performance. With the use of smaller diameter wire, manufacturing time has been reduced to 30% compared to the larger diameter wire.

- Although, the smaller diameter wire performs better compared to larger diameter wire in terms of minimum corner radius, minimum production time, minimum amplitude of vibrations, minimum spark gap and improved surface quality of the machined parts. But, more frequent wire breakage was observed because of its lower tensile strength.

- Pulse on time and servo voltage were found to be major factors which influences the wire rupture. The EDS analysis exposed the presence of Ni, and Cr on the wire surface which has been migrated from workpiece materials and exhibits different wire properties leading to wire rupture.

- As a result of SEM analysis, micro voids, micro globules, craters and melted debris were observed on the machined surface, but no micro cracks were observed due to high toughness of Inconel 706. The formation of micro voids, craters and micro globules were considerably reduced at low discharge setting.

- The topography of machined surface revealed that with the usage of smaller diameter wire, finer and smoother surface can be obtained at low discharge energy setting. However, the topography of machined surface turns out to be rougher at high discharge energy setting.

- The microhardness of WED machined surface has been changed below the depth of 75 μm. Hard brass wire of 150 μm diameter has shown the minimum hardness alteration for WEDM processed Inconel 706. However, more reduction in microhardness was observed at high discharge energy setting.

- The recast layer thickness is comparatively lower with the smaller diameter wire and vice versa. But, there is a more tendency of recast layer formation at high discharge energy setting due to significant thermal degradation.

- The EDS analysis has exposed the addition of Cu, O and Zn, and depletion of Fe, Ni and Cr from the machined surface and thus exhibits different material properties leading to lower hardness of recast surface.

4.4 CONCLUSION

In this chapter, various WEDM performance characteristics such material removal rate, cutting speed, surface roughness, surface topography, recast layer thickness, residual stresses, microstructural and elemental changes have been evaluated. The WEDM performance characteristics have been categorized based on OFAT approach, different diameter wires and different wire materials and the following observations have been concluded based on the experimental results:

- Pulse on time, servo voltage and servo voltage are the major influencing factors which affecting the MRR and SR however wire feed of 6 m/min and flushing pressure of 1.96 bar has shown the improved MRR and SR.

- Hard brass has shown better surface integrity, such as lower residual stresses, lower surface roughness, smoother topography and less recast layer formation, however, zinc coated wire has shown improved productivity while cutting complex shape profile through Inconel 706.

- Hard brass wire of diameter 150 μm has shown improved productivity as well as better surface quality compared to the wires of 200 μm and 250 μm and suitable for manufacturing of gas turbine components.

CHAPTER 5

MANUFACTURING OF TURBINE DISC PROFILE SLOT AND ITS CHARACTERIZATION

5.1   INTRODUCTION

This chapter demonstrates the manufacturing of turbine disc profile slots using WEDM process as per standards of gas turbine industries. And it also discusses the evaluation of several WEDM performance characteristics of turbine disc profile slots such as cutting speed, surface roughness, microstructure, recast layer formation, subsurface microhardness, surface topography, residual stresses and profile accuracy. Moreover, the comparison of different WEDM mode has been presented, followed by different wire materials as well as different wire diameters. WED manufactured fir tree profile slots and turbine blade roots have been shown in Figure 5.1.
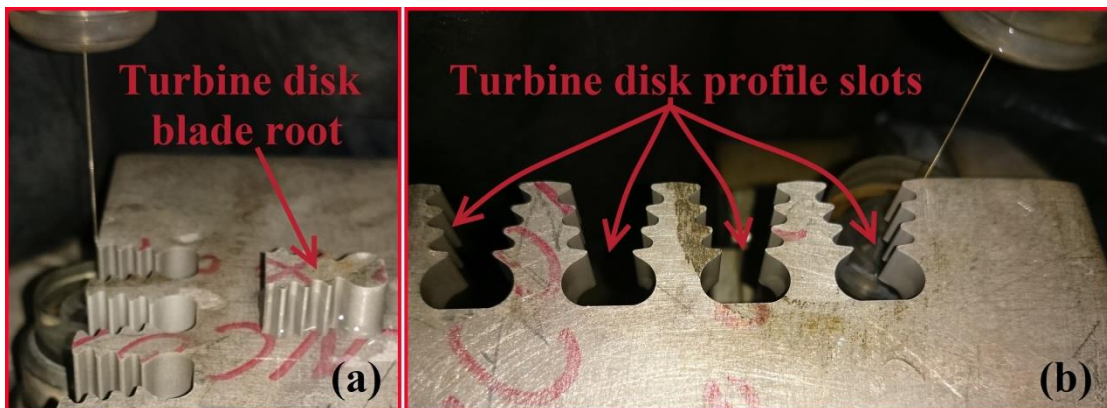
Figure 5.1 WED manufactured components: (a) Turbine disc blade root; (b) Turbine disc profile slots.

5.2   EXPERIMENTAL DETAILS

The experimental work was conducted on 'Electronica Eco cut' WED machine, followed by one rough cut and two trim cut. This machine can be operated in a rough cut mode as well as trim cut mode depending upon the requirement. In rough cut mode, high discharge pulse is used which forms larger craters on the machined

surface. Whereas, in trim cut mode, low discharge pulse is used which forms smaller craters leading to a smoother surface. In the current study, rough cut was used for basic cutting operation, whereas trim cut was used to improve the dimensional accuracy and surface finish. The experimental setup of WED machine has been shown in Figure 5.2.
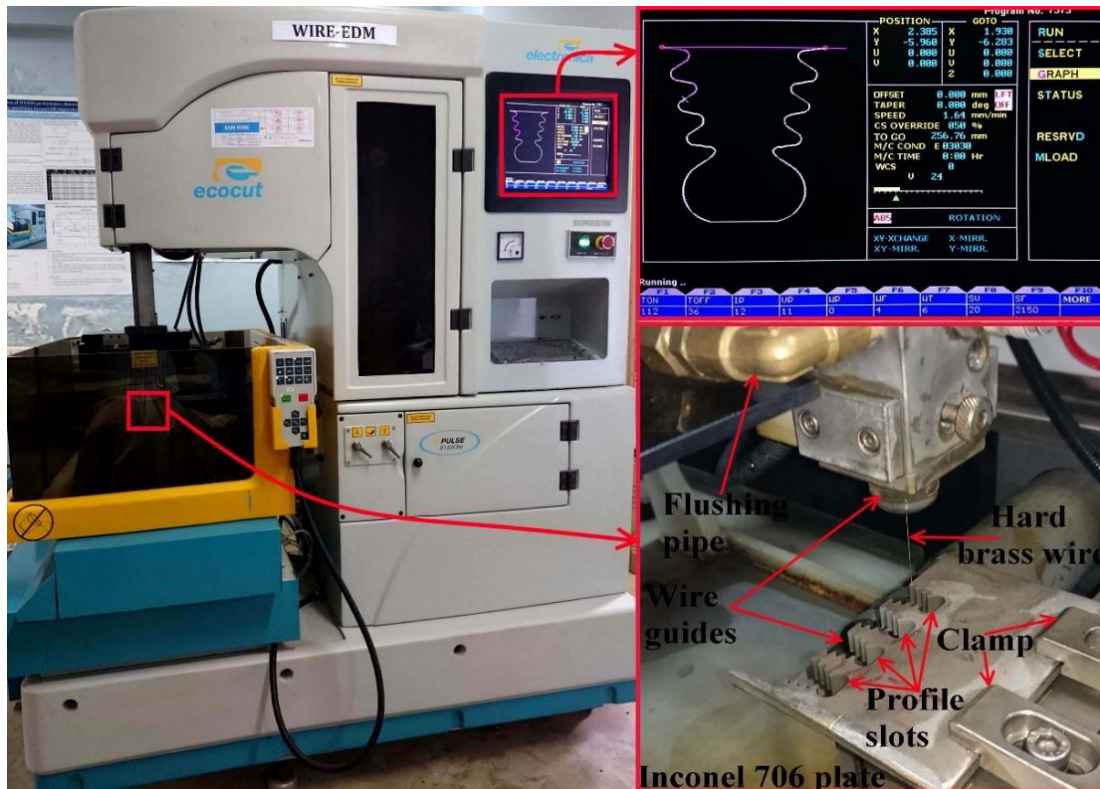
Figure 5.2 Experimental setup of WED machine for free tree sot production.

Based on the pilot experiments, six control parameters such as pulse current, pulse on time, pulse off time, servo voltage, servo feed and wire offset were selected. In the current investigation, WEDM performance characteristics have been investigated by considering the three different wire materials such as hard brass wire, diffused wire and zinc coated wire as well as different diameter wires such as 150 μm, 200 μm and 250 μm. Basically, current study employed six categories of wires such as B-150, B-200, B-250, D-250, Zn-200 and Zn-250 as these wires are commercially available. However, D-150, D-200 and Zn-150 wires are not available due to the difficulties occurred in the processing of smaller diameter coated wire and diffused wire. In the different category of wires, B denotes the hard brass wire; D denotes the diffused wire

112

and Zn denotes the zinc coated wire The experimental settings of control parameters were shown in Table 5.1 in which one rough cut and two different trim cuts were selected in such a way that there is no gap-short and wire rupture during WEDM process.

Table 5.1 Experimental setting of control parameters for different cutting mode.

WEDM Mode	Pulse current (A)	Pulse on Time (µs)	Pulse off Time (µs)	Servo Voltage (V)	Servo Feed (mu)	Wire offset (µm)
Rough cut	12	112	36	20	2150	0
Trim cut 1	2	105	20	10	200	50
Trim cut 2	1	105	20	10	100	60

Table 5.2 Constant process parameters used during the WEDM process.

Dielectric fluid	De-ionized water
Polarity	Positive
Discharge current	12 A
Discharge voltage	28 V
Wire feed	6 m/min
Flushing pressure	1.96 bar
Cutting speed over ride (%)	50
Dwell time	3 sec
Corner control factor	3

Some researchers (Aspinwall et al., 2008; Li et al., 2014) have used multiple trim cut strategy to minimize the recast layer thickness and improve the surface finish. However, in the present study, two trim cuts have been used. This is because, no significant change in surface roughness has been observed under second trim cut and third trim cut. Therefore, only two trim cuts have been selected to minimize the production time of the profile slots. Other control parameters, which are shown in Table 5.2, were kept constant throughout the experimentation. Based on the earlier investigations carried out in section 4.2 and 4.3, best diameter and best wire material was selected for manufacturing of fir tree slots through Inconel 706 superalloy.

5.3 EVALUATION OF CUTTING SPEED AND SURFACE ROUGHNESS

Usually, the productivity of WEDM process is measured in terms of cutting speed. The experimental data of cutting speed along with their standard error have been presented in Table 5.3. Figure 5.3 (a) shows the effect of wire diameter as well as effect of wire materials on cutting speed. The experimental investigation revealed that cutting speed slightly decreases with increase in wire diameter and increases with decrease in wire diameter, which is applicable when both hard brass and zinc coated wire are compared in their increasing order of diameter. The behaviour can be explained by the fact that the wire transport speed is comparatively lower with larger diameter wire which tends to slightly reduce the wire feed. The amount of molten metal to be splashed through sparking zone is relatively reduced and hence it will lead to slightly lower cutting speed.

Table 5.3 Experimental data of cutting speed correspond to different category of wires.

WEDM setting	Rough cut	Trim cut 1	Trim cut 2	Rough cut	Trim cut 1	Trim cut 2
	Average cutting speed (mm/min)			Cutting speed (Error in mm/min)		
B–150	1.69	7.16	4.45	0.011	0.235	0.303
B–200	1.60	7.04	4.21	0.021	0.050	0.189
B–250	1.56	6.78	4.04	0.016	0.031	0.142
D–250	1.64	8.21	4.43	0.021	0.255	0.083
Zn–250	1.89	9.09	5.02	0.019	0.112	0.299
Zn–200	1.95	9.87	5.28	0.017	0.027	0.232

On the other hand, within the same diameter range, zinc coated wire offers higher cutting speed over diffused wire and brass wire. This is because the zinc coating has a low melting point (419.5 °C) when it evaporates, it provides improved gap conductivity which leads to a better flushing during WEDM process. In addition, high intensity spark tends to blast off the zinc from wire core and it helps in cooling of wire core due to boiling of zinc particles and thus leading to higher cutting speed for

the same set of control parameters. A similar trend for the variation of cutting speed with wire materials has been reported in earlier literature (Garg et al., 2014).
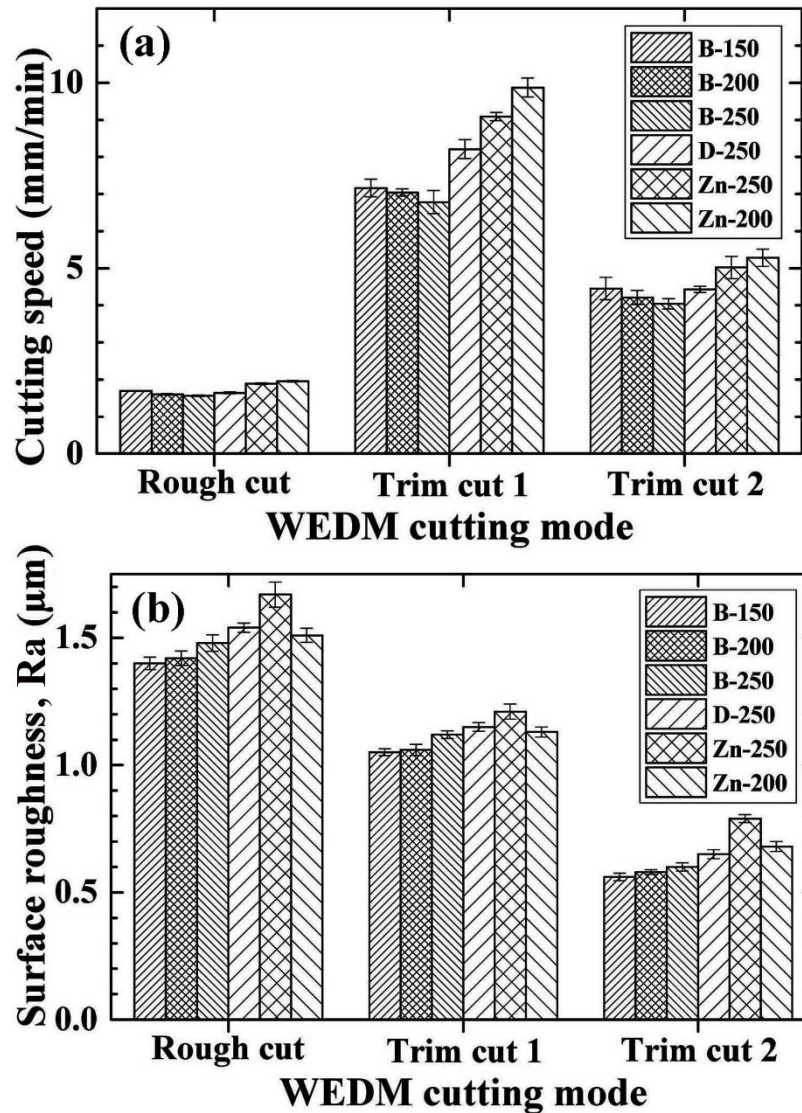
Figure 5.3 Effect of WEDM cutting mode on: (a) cutting speed; (b) surface roughness.

Figure 5.3(b) indicates the effect of wire materials and wire diameters on the surface roughness. The experimental data of surface roughness along with their standard error have been shown in Table 5.4. From the experimental investigation, it was observed that surface roughness is slightly decreases with the decrease in wire diameter and increases with the increase in wire diameter, which is applicable to both brass and zinc coated wire. This occurs due to the fact that the wire transport speed is relatively higher with smaller diameter which slightly improves the wire feed. This, in turn,

improves the splashing of molten metal through sparking zone and hence leading to lower surface roughness with smaller diameter wire. A similar trend between surface roughness and wire diameter has been described in previous literature (Newton, 2008). Additionally, the smaller diameter wire exhibits minimum corner radius, minimum spark gap and improved surface quality of machined parts which has been validated during experimentation. From Figure 5.3(a), it was also observed that surface roughness has been reduced significantly in second trim cut mode. More or less similar results have also been observed by Li et al. (2014). This is because, in trim cut mode, fine pulse are generated which helps to removes the existing recast layer from the machined surface and improves the surface quality of the machined components.

Table 5.4 Experimental data of surface roughness correspond to different category of wires.

WEDM setting	Rough cut	Trim cut 1	Trim cut 2	Rough cut	Trim cut 1	Trim cut 2
	Average surface roughness (µm)			Surface roughness (Error in µm)		
B–150	1.40	1.05	0.56	0.024	0.013	0.015
B–200	1.42	1.06	0.58	0.028	0.021	0.009
B–250	1.48	1.12	0.60	0.033	0.015	0.016
D–250	1.54	1.15	0.65	0.018	0.017	0.018
Zn–250	1.67	1.21	0.79	0.049	0.029	0.016
Zn–200	1.51	1.13	0.68	0.028	0.019	0.019

Moreover, within the similar diameter range (250 µm), hard brass wire has shown better surface finish when compared to zinc coated wire and diffused wire. This is because the hard brass wire helps to maintain a vertically straight cut due to its high tensile strength (1000 N/mm^2) and minimizes the wire vibration and wire deflection. Hence, it improves the shape accuracy as well as surface quality of the machined parts. Similar results for variation of surface quality with wire materials have been observed in the literature (Klocke et al., 2014). From Figure 5.3 (a–b), it can be concluded that Zn–200 wire is the most suited for higher production rates, whereas B–150 wire exhibits minimum surface roughness under the same setting of control

parameters. Fundamentally, higher cutting speed leads to lower manufacturing time. From Figure 5.4 it can be observed that with the use of zinc coated wire, manufacturing time has been reduced to around 20 % compared to the hard brass wire. The result is valid if both hard brass and zinc coated wire are compared within similar diameter range. The experimental results for the variation of manufacturing time with wire materials have already been stated in earlier literature (Klocke et al., 2014).
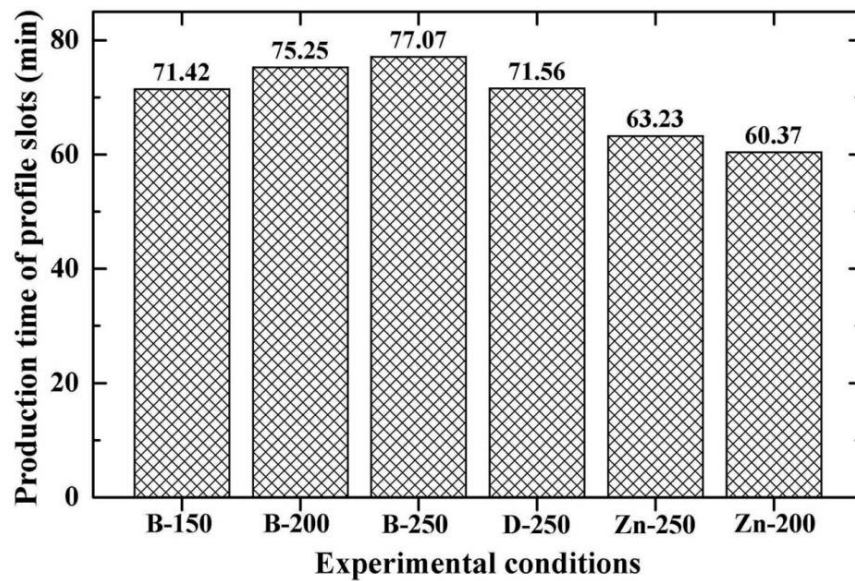
Figure 5.4 Effect of experimental conditions on production time of profile slots.

5.4   MICROSTRUCTURE STUDY OF WED MACHINED SURFACE

For assessment of surface characteristics of the WEDM machined components, microscopic images under rough cut mode and trim cut modes were compared. The SEM images of rough cut surfaces (Figure 5.5) have exhibited high density of micro globules, micro holes, craters and melted debris on WED machined surface without any micro cracks. The results are applicable to all categories of wires including B–150, B–200, B–250, D–250, Zn–250 and Zn–200. The behaviour can be explained by the fact that the rough cut mode in WEDM offers high discharge energy during cutting process which allows more amount of material to be melted. Within the discharge channel, pressure waves are generated due to the discontinuity of plasma. These pressure waves would splash most of the molten material from the machined surface. At the same time some gas bubbles get dissolved into molten material. When,

117

remaining molten material resolidify on machined surface, these gas bubbles would be trapped, resulting in formation of micro holes.

On the other hand, second trim cut surface exhibits no micro globules and no crater formation except few melted debris and few micro holes. The results are applicable to all categories of wires (i.e., B–150, B–200, B–250, D–250, Zn–250 and Zn–200). This is because, under trim cut mode, least amount of material is melted which can be easily flush away by pressurized waves and thus minimizes the formation of micro globules and craters leading to improved surface quality.
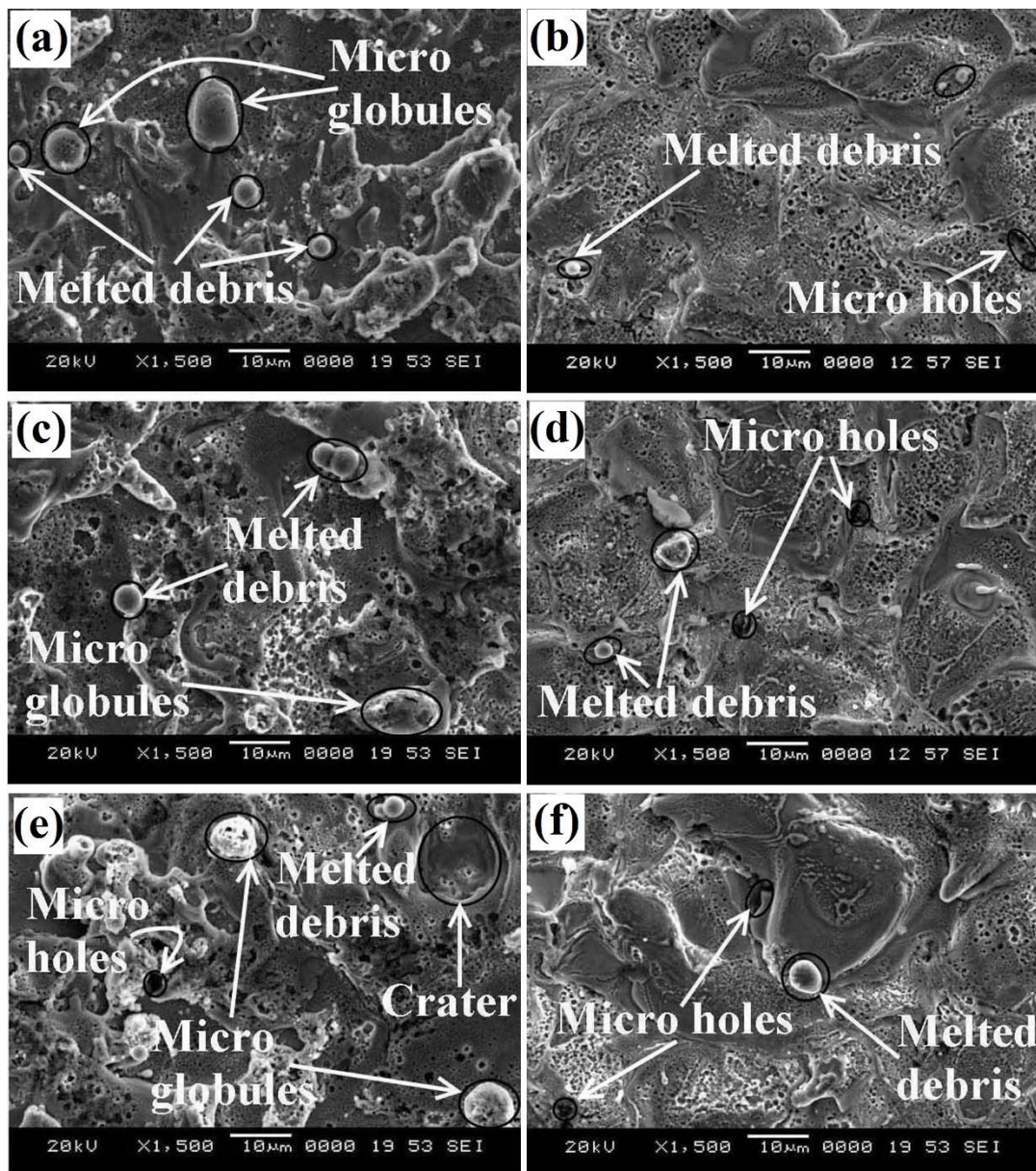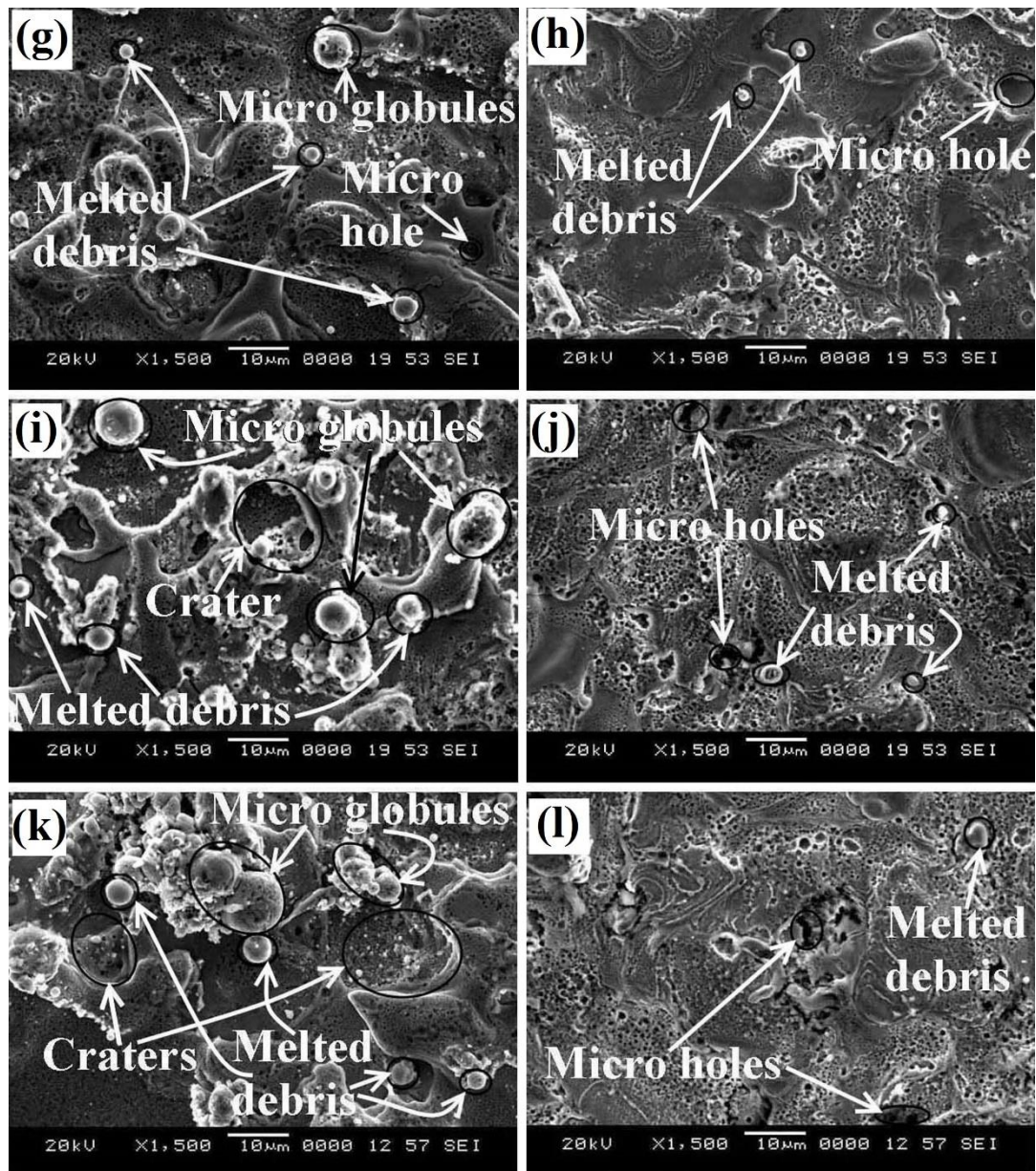
Figure 5.5 Microstructure graph of WED machined surface of Inconel 706 at:
(a) Rough cut (B–150); (b) Trim cut 2 (B–150); (c) Rough cut (B–200);
(d) Trim cut 2 (B–200); (e) Rough cut (B–250); (f) Trim cut 2 (B–250);
(g) Rough cut (D–250); (h) Trim cut 2 (D–250); (i) Rough cut (Zn–200);
(j) Trim cut 2 (Zn–200); (k) Rough cut (Zn–250); (l) Trim cut 2 (Zn–250).

Moreover, micro crack formation mainly depends on the thermal conductivity of the
material. A material with high thermal conductivity rapidly transfer the heat and thus
reduces the propensity of crack formation. On the contrary, material with low thermal
conductivity tends to form micro cracks. Although Inconel 706 has low thermal

119

conductivity, however, no micro cracks were found either in the rough cut mode or trim cut mode due to its high toughness. The experimental investigation revealed that second trim cut (B–150) shows better surface quality among all wire materials and wire diameters and best suited for WEDM process of Inconel 706 alloy. However, Zn–250 offers comparatively poor surface quality among all categories of wire under rough cut mode as shown in Figure 5.5(l).

5.5   SURFACE TOPOGRAPHY

The surface topography (Figure 5.6) of WED machined surface under rough cut mode as well as trim cut mode was captured at 2592X magnification. A scan area of 107 μm × 107 μm was selected for topographic investigation. The experimental results revealed that rough cut mode offers more surface irregularities and significantly increases the peak to valley height (Rz) leading to comparatively coarser surface on the machined components. This is because, under a rough cut mode, workpiece material is subjected to higher thermal energy which melts more amount of material from the workpiece. A part of melted material flush away by the pressurized waves when remaining molten material re-solidify it forms more irregular craters and micro globules leading to higher surface roughness (Rz).

On the other hand, under second trim cut mode, peak to valley height has been decreased to 8 μm and offers comparatively smoother surface on the machined components. This is because, under second trim cut mode, workpiece material is exposed to low thermal energy. Therefore, only a small amount of material is melted which can be easily flush away by pressurized waves and hence leading to lower surface roughness (Rz).

Further, experimental results revealed that under second trim cut modes, peak to valley height (Rz) is less than 10 μm which is applicable to B–150, B–200 and B–250. It means that Rz value lies within the range of ±5 μm and approves the quality check for turbine disc profile slots shown in Figure 5.10(b). Moreover, D–250, Zn–200 and Zn–250 were disqualified in quality check because of higher peak to valley height (Rz) of more than 10 μm.

120
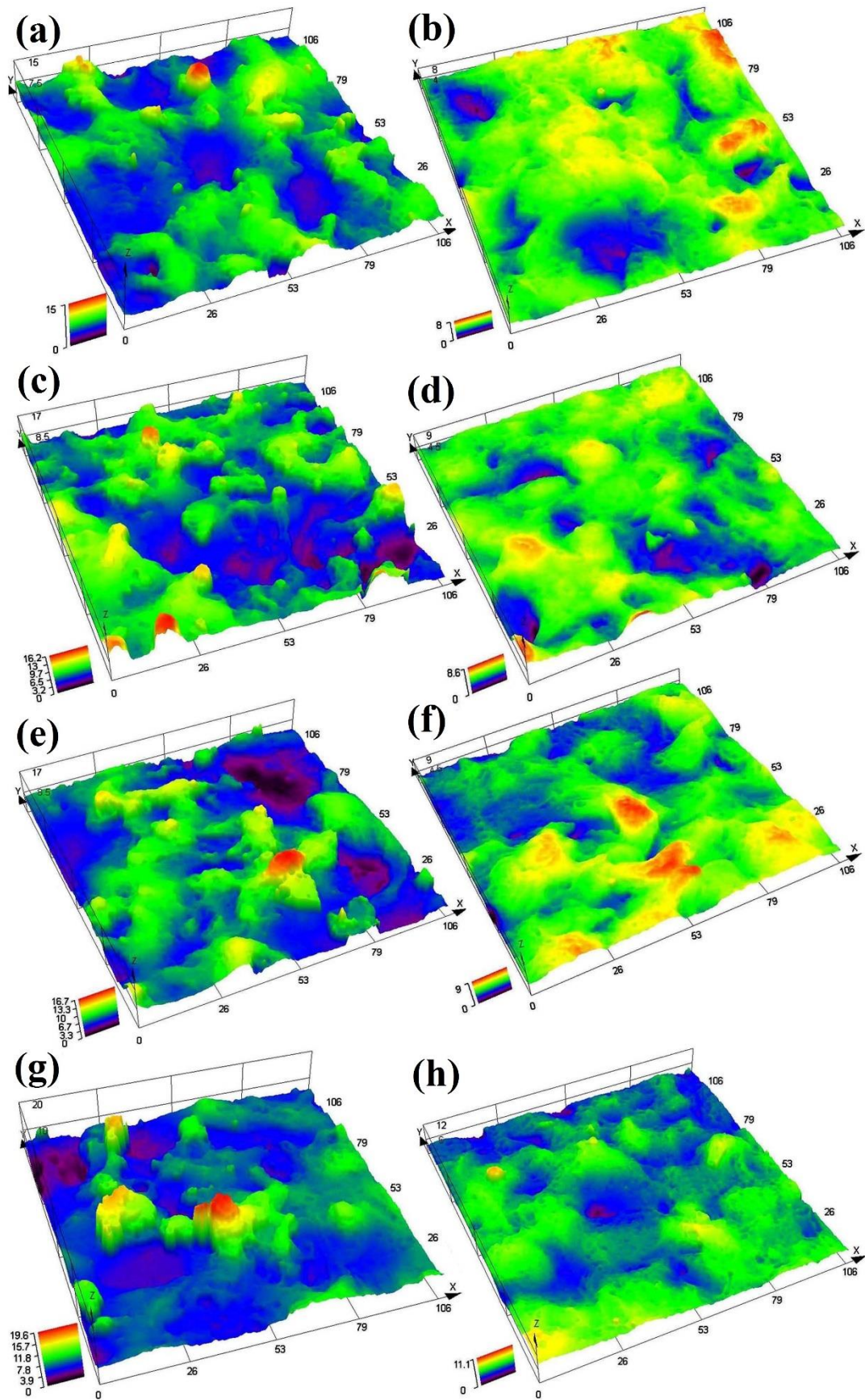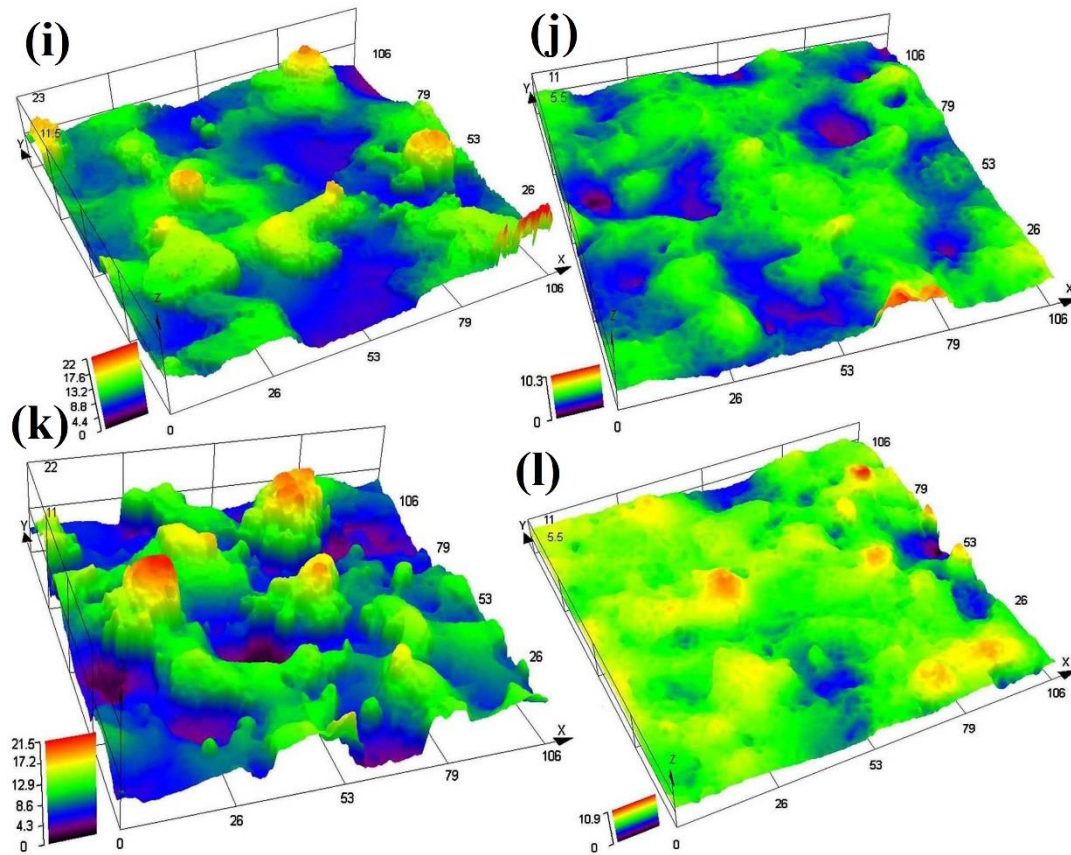
Figure 5.6 Topography of WED machined surface of Inconel 706 at:

(a) Rough cut (B–150); (b) Trim cut 2 (B–150); (c) Rough cut (B–200); (d) Trim cut 2 (B–200); (e) Rough cut (B–250); (f) Trim cut 2 (B–250); (g) Rough cut (D–250); (h) Trim cut 2 (D–250); (i) Rough cut (Zn–200); (j) Trim cut 2 (Zn–200); (k) Rough cut (Zn–250); (l) Trim cut 2 (Zn–250).

5.6   SUBSURFACE MICROSTRUCTURE

For microstructure evaluation of WED machined subsurface, the samples were cross–sectionally cold mounted, polished, cleaned and dried. The subsurface microstructure revealed the formation of a thick recast layer (20–30 µm) under rough cut mode, which is applicable to all categories of wire including B–150, B–200, B–250, D–250, Zn–250 and Zn–200 as shown in Figure 5.7. This behaviour can be explained by the fact that under rough cut mode, the material is subjected to high amount thermal energy which increases the depth of molten pools. Consequently, more amount of material will be melted. Some portion of this molten material was flushed away by pressurized waves and when remaining molten material re-solidify it forms a thick

recast layer. From the Figure 5.7 (a), 5.6 (c), 5.6 (e), 5.6 (g), 5.6 (i) and 5.6 (k) it was observed that there is no significant recast layer in trim cut mode. More or less similar results have also been observed by Antar et al. (2011). This is because, under a trim cut mode, only a small amount of material is melted due to the low thermal energy of the spark which can be easily flushed away from machined surface and hence leading to almost negligible recast layer on WED machined surface. The experimental results indicated that thermal damage of machined subsurface can be reduced or minimized by multiple trim cuts which is most desirable for aerospace application.

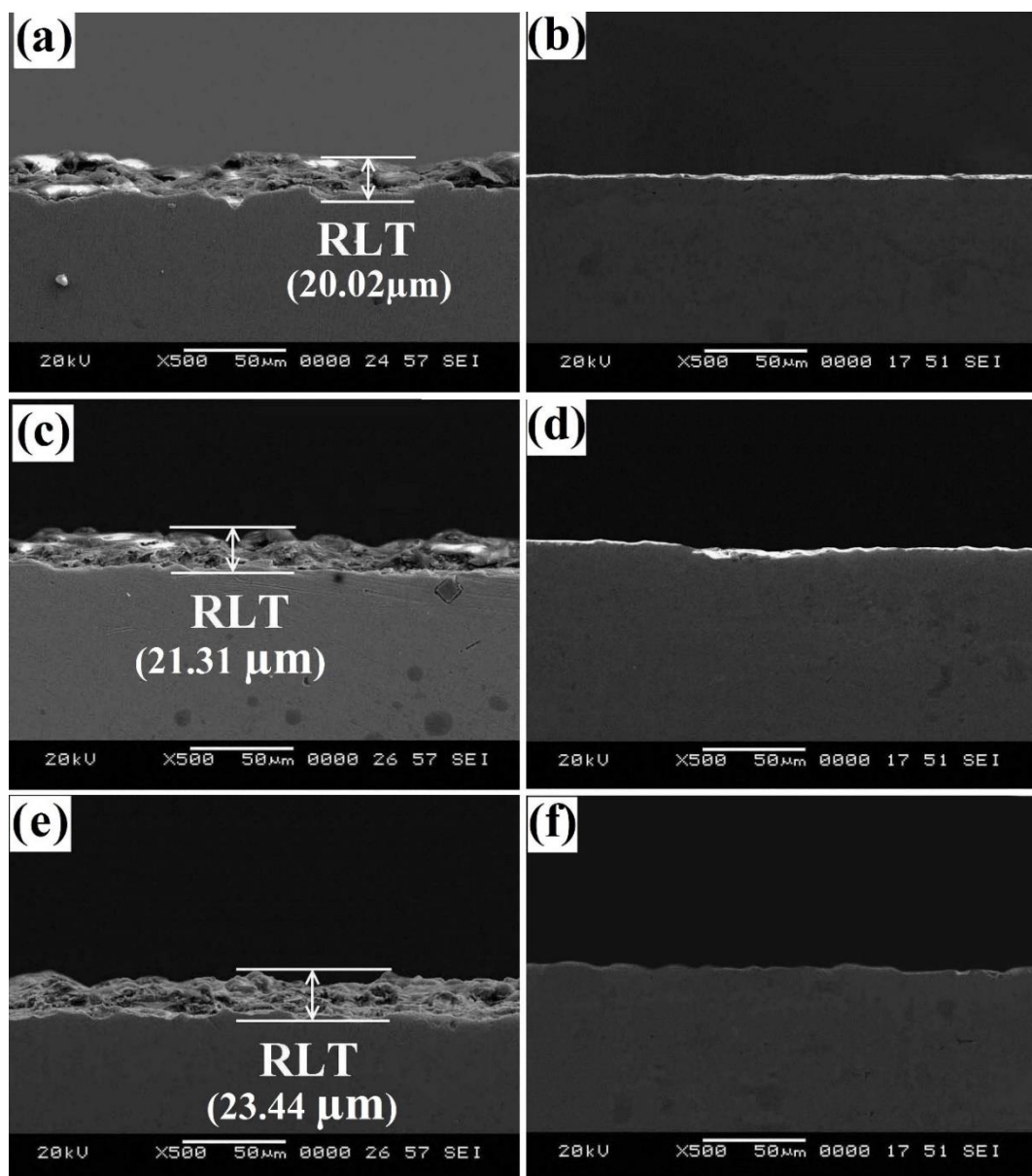**Figure 5.7** Recast layer formation on WED machined surface of Inconel 706 at: (a) Rough cut (B–150); (b) Trim cut 2 (B–150); (c) Rough cut (B–200); (d) Trim cut 2 (B–200); (e) Rough cut (B–250); (f) Trim cut 2 (B–250); (g) Rough cut (D–250); (h) Trim cut 2 (D–250); (i) Rough cut (Zn–200); (j) Trim cut 2 (Zn–200); (k) Rough cut (Zn–250); (l) Trim cut 2 (Zn–250).

5.7   SUBSURFACE MICROHARDNESS
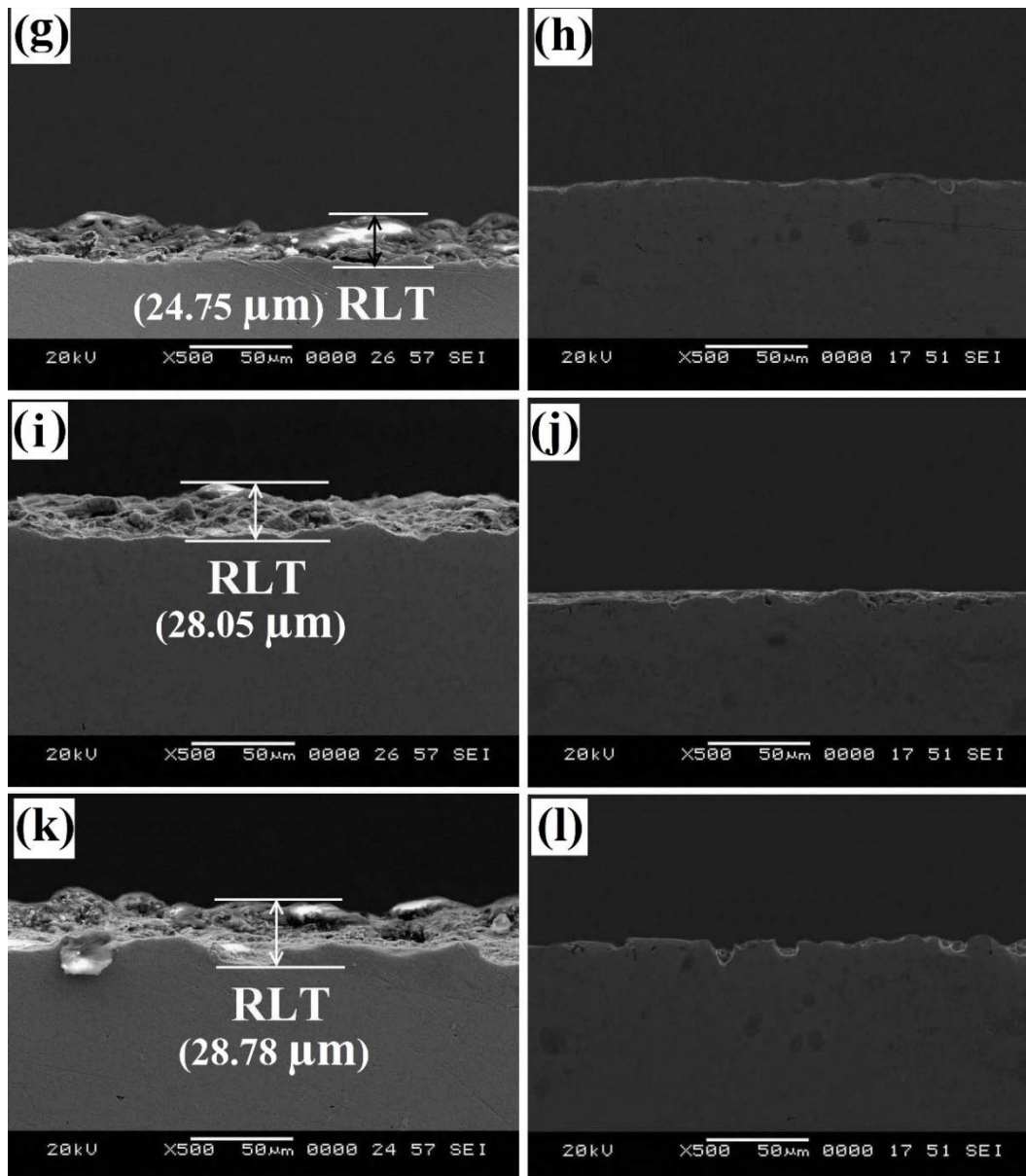
The subsurface microhardness of the profile slots formed under rough cut and second trim cut mode was shown in Figure 5.8 which exposed that the microhardness of WED machined profile slots has been significantly decreased below the depth of

70 μm under rough cut mode. This is because, under a rough cut mode, workpiece material will be subjected to higher elemental changes and form a thick recast layer, followed by sudden heating and cooling during WEDM process. Moreover, recast material exhibits altered material properties due to the addition of Cu and Zn content which has already been described in section 4.1.
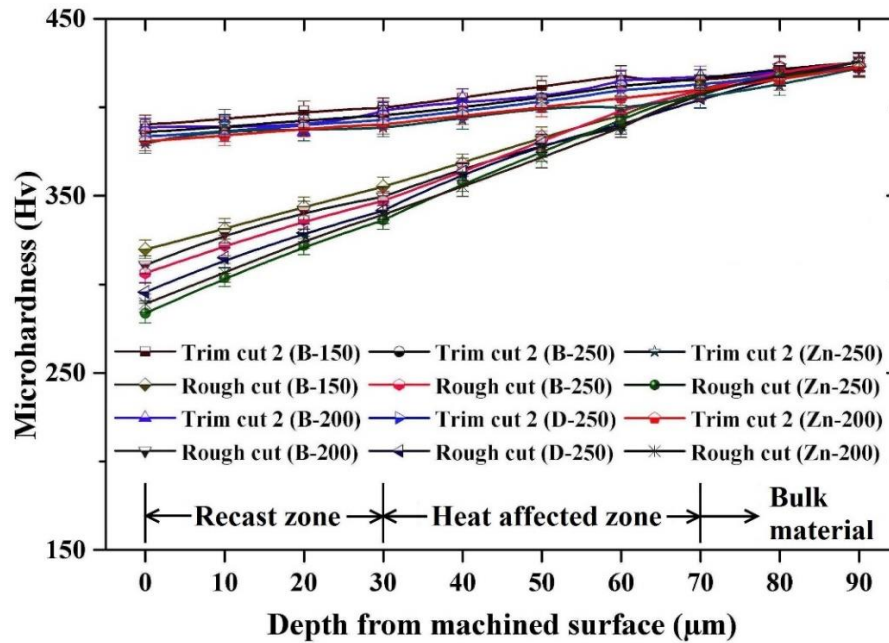
Figure 5.8 Subsurface microhardness of WED machined profile slots under rough cut mode as well as trim cut mode followed by different diameter wires and different wire materials.

But, under second trim cut modes, no more significant change in microhardness was observed as shown in Figure 5.8. More or less similar results have also been reported by Aspinwall et al. (2008). In trim cut mode, recast layer has been reduced significantly due to generation of finer pulse during WEDM process. Therefore, only few elemental changes were observed, which leads to minimum hardness alteration. The experimental investigation revealed that subsurface microhardness has been decreased to 283.62 Hv under rough cut mode (Zn–250) as that of bulk hardness of 425 Hv. Instead, B–150 has shown minimum hardness alteration among all categories of wire. Further investigation revealed that microhardeness has been reduced drastically under recast zone because of high thermal gradients which is acting on the machined component during WEDM process. However, in heat affected zone (HAZ),

changes in microhardness are limited to 70 μm due to low thermal conductivity of Inconel 706 superalloy.

5.8   EVALUATION OF RESIDUAL STRESSES

The residual stresses were measured using stress measuring system which is based on the principle of X-Ray diffraction technique. Due to rapid heating and cooling during WEDM process, workpiece material was subjected to high thermal gradients which produce residual stresses within machined surface. The nature of residual stresses can be explained by the fact that when the molten material re-solidifies, its temperature decreases equal to bulk material temperature and further its shrinkage is opposed by the bulk material. This, in turn, induces tensile residual stresses within WED machined surface, whereas bulk workpiece exhibits compressive residual stresses.
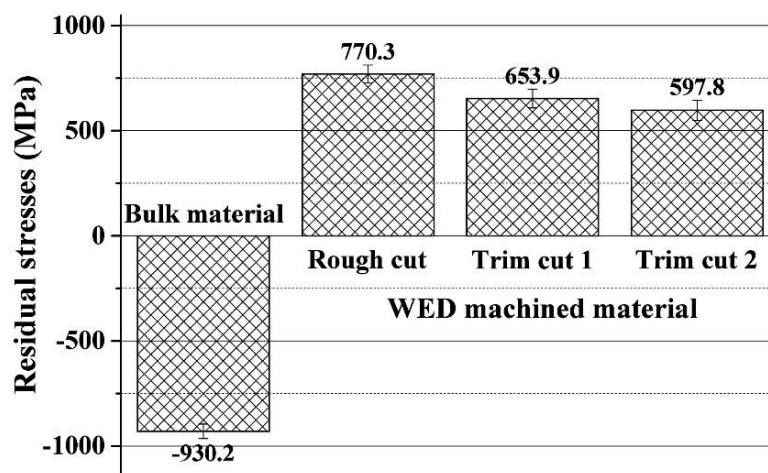
Figure 5.9 Residual stresses generated within bulk material and WED machined material.

To determine the fatigue life of the machined component, residual stress plays a major role. From Figure 5.9, it was detected that WEDM processed samples exhibit tensile residual stresses under rough cut mode as well as trim cut mode, whereas bulk material exhibits the higher amount of compressive residual stresses. However, under second trim cut (B–150), minimum tensile residual stresses of 597.8 MPa were observed, which helps to improve the fatigue life of turbine disc profile slots. Almost similar experimental results have been obtained by Antar et al. (2012) while comparing the residual stresses under WEDM rouging and WEDM finishing of Inconel 718. During operation, aircraft components such as turbine disc is subjected

to high amounts of centrifugal forces which may lead to cracking due to higher tensile residual stresses. It is essential to minimize the tensile residual stresses for aerospace application. This is because, high tensile residual stresses in WED machined surface leads to a shorter fatigue life of the component. As per the quality checklist of turbine disc profile slots as shown in Figure 5.10(b), tensile residual stresses should not exceed beyond 850 MPa which has already been achieved using appropriate trim cut strategy.

5.9 SURFACE PROFILE ANALYSIS OF TURBINE DISC SLOT

The typical geometry of turbine disc profile slots was shown in Figure 5.10(a). The geometrical data for fir tree profile slots was obtained from the literature (Klocke et al., 2014). The fir tree profile slot geometry was prepared in 'AutoCAD'. Afterwards, the geometry has been simulated in 'ELCAM' to generate the corresponding CNC program. WED machined surface profile of turbine disc slot has been analyzed under second trim cut mode as shown in Figure 5.11. The surface profile was measured at stylus speed of 0.25 mm/s for an evaluation length of 3 mm. From the surface profile analysis, it was perceived that the Rz value of all profile slots lies within the range of 10 μm. Therefore, it can be stated that accuracy of profile slots is within the tolerance of ±5 μm. The quality checklist of turbine disc profile slot was obtained from the literature (Klocke et al., 2012).
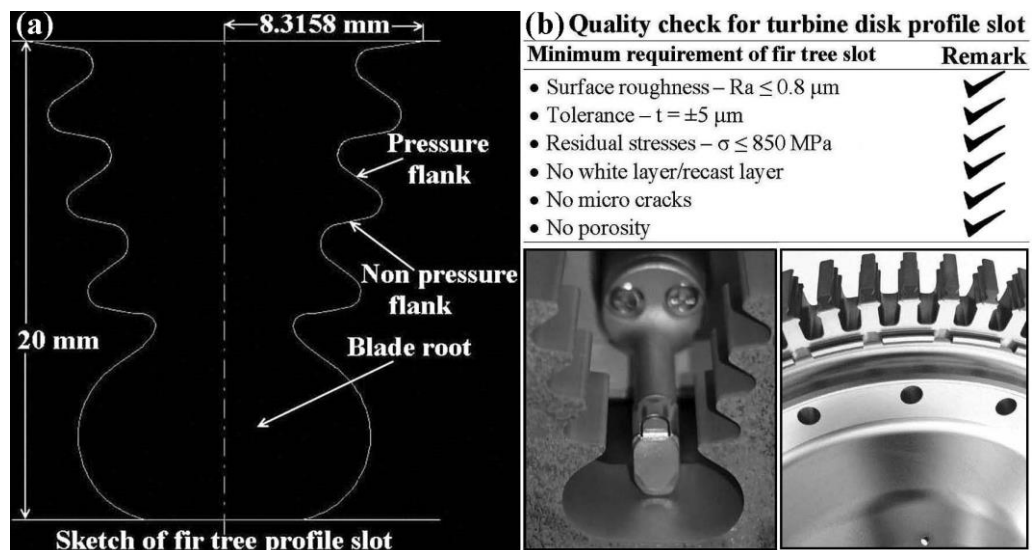
Figure 5.10 (a) Geometry of turbine disc profile slot; (b) Quality checklist for profile slot (Klocke et al., 2012).
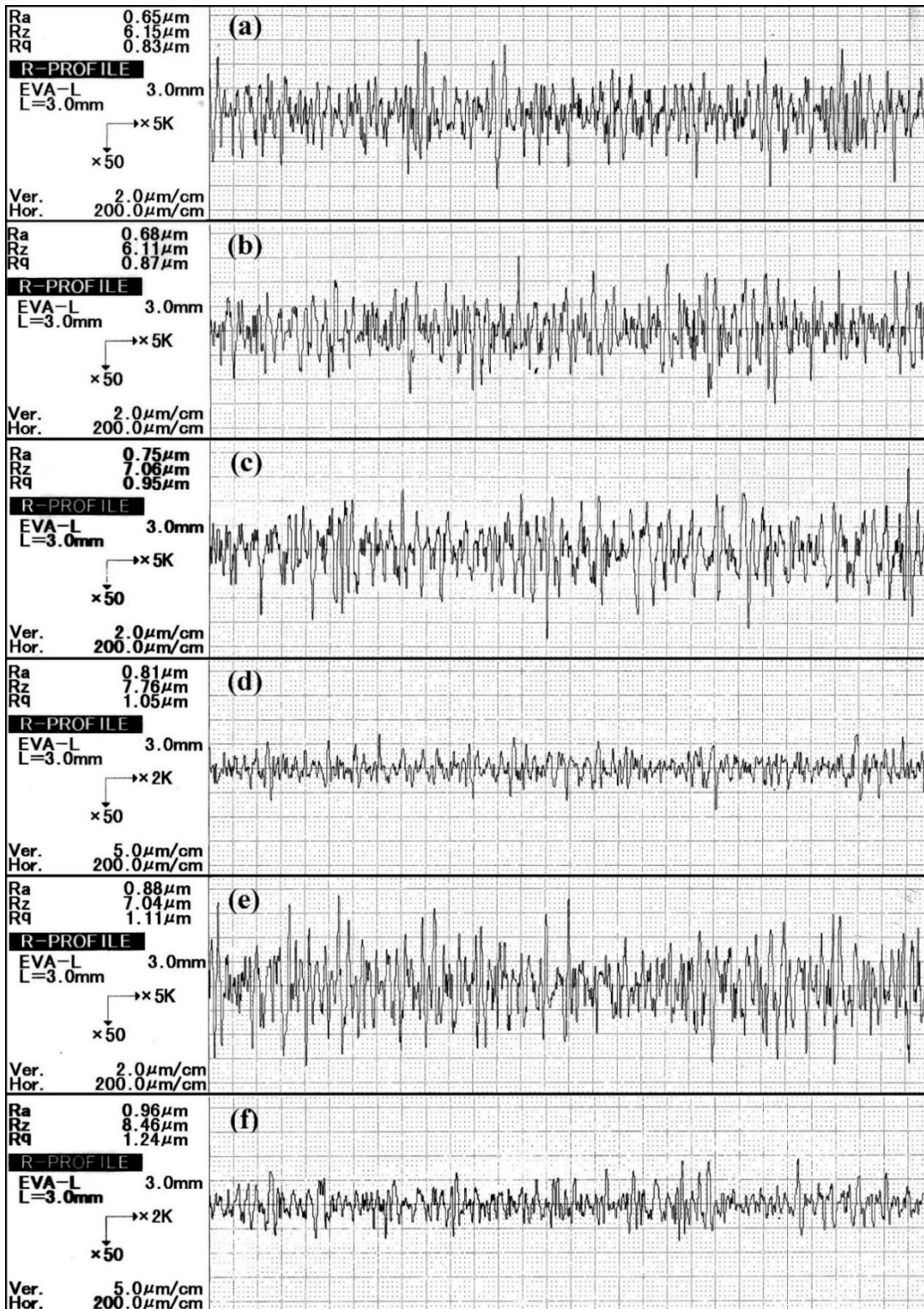
Figure 5.11 Surface profile analysis of turbine disc slots at: (a) Trim cut 2 (B–150); (b) Trim cut 2 (B–200); (c) Trim cut 2 (B–250); (d) Trim cut 2 (D–250); (e) Trim cut 2 (Zn–200); (f) Trim cut 2 (Zn–250).

128

Also, average surface roughness (Ra) of 0.65 μm (B–150), 0.68 μm (B–200) and 0.75 μm (B–250) have been achieved in second trim cut and fulfilled the minimum requirement of Ra less than 0.80 μm. Based on the surface profile analysis as shown in Figure 5.11, D–250, Zn–200 and Zn–250 were disqualified from quality check conducted under second trim cut mode.
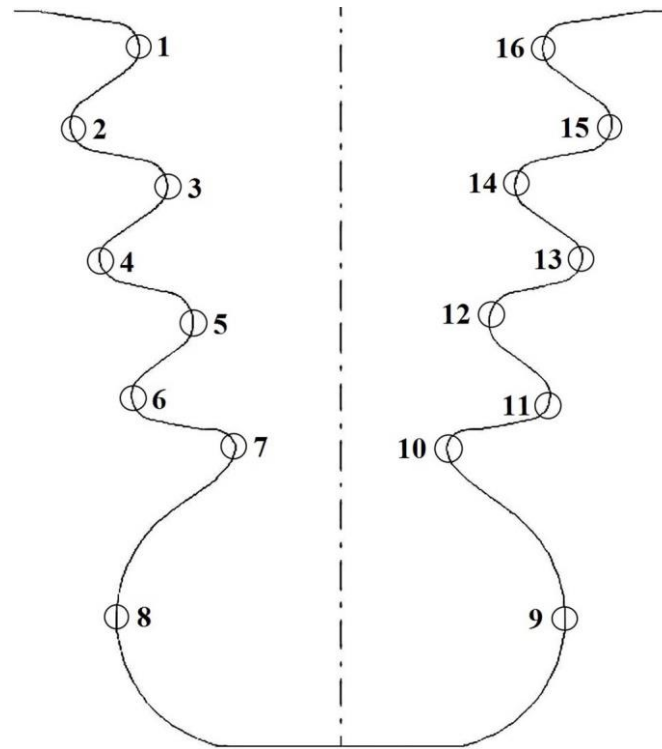
Figure 5.12 Location of CMM measured coordinates of turbine disc slot.

The profile accuracy was measured using a profile projector. The measured surface profile was matched to the nominal (actual) profile. A slight deviation from the nominal profile has been detected, but the measured profile lies within the tolerance band of ±5 μm. Further, profile accuracy of turbine disc profile slot, which has been manufactured under second trim cut (B–150), was confirmed using coordinate measuring machine (CMM). This can be achieved by comparing the coordinates of nominal profiles and CMM measured profiles. The coordinates of peak and valley of turbine disc slot, which have been obtained with the help of CMM, were indicated in Figure 5.12. The offset value has been incorporated into measured coordinates to determine the exact coordinates of the profile slot. However, the actual coordinates of the profile were calculated using 'ELCAM' software. The comparison of coordinates

of measured profile and actual profile has been shown in Table 5.5 which exhibits that the deviation in coordinates of the profile slots are within the range of 5 to 19 µm. The geometrical inaccuracy may occur due to wire vibration and wire deflection occurred during WEDM process. However, most of the coordinates are deviated by less than 10 µm which indicates the suitability of WEDM process for free tree slot production.

Table 5.5 Comparison of measured and actual coordinates of profile slot (B–150).

SL.	Measured coordinates of profile slot (mm)		Total offset (µm)	Actual coordinates of profile slot (mm)		Deviation in (µm)	
	X	Y		X	Y	X	Y
1.	2.742	–0.959	60	2.810	–0.968	8	9
2.	0.855	–3.006	60	0.926	–3.012	11	6
3.	3.483	–4.697	60	3.557	–4.709	14	12
4.	1.670	–6.744	60	1.738	–6.752	8	8
5.	4.195	–8.466	60	4.272	–8.473	17	7
6.	2.514	–10.508	60	2.583	–10.525	9	17
7.	5.343	–11.838	60	5.409	–11.847	6	9
8.	2.116	–16.547	60	2.181	–16.553	5	6
9.	13.689	–0.959	120	13.820	–0.968	11	9
10.	15.577	–3.006	120	15.705	–3.016	8	10
11.	12.917	–4.697	120	13.042	–4.706	5	9
12.	14.766	–6.744	120	14.893	–6.759	7	15
13.	12.227	–8.466	120	12.360	–8.473	13	7
14.	13.920	–10.508	120	14.049	–10.520	9	12
15.	11.762	–11.838	120	11.901	–11.843	19	5
16.	14.306	–16.547	120	14.433	–16.561	7	14

5.10   SUMMARY

In this chapter, fir tree profile slots have been manufactured successfully through advanced turbine disc alloy (Inconel 706) to fulfil their requirement of average surface roughness less than 0.8 µm and profile accuracy within the range of ±5 µm.

The manufactured profile slots have exhibited low levels of tensile residual stresses (less than 850 MPa), almost negligible recast layer, minimum hardness alteration, no micro cracks and minimum thermal modifications while using second trim cut (B–150). Further, WEDM performance characteristics have been investigated using best diameter wire as well as best wire material. Based on experimental results, the following observations are précised as follows:

- Zn–200 has shown higher productivity, whereas B–150 has exhibited the best surface quality of the machined components under similar experimental conditions. The production time of profile slots has been reduced to around 20% using zinc coated wire when compared with hard brass wire within similar diameter range. Moreover, B–150, B–200 and B–250 have confirmed all the safety requirements of turbine disc slots and found to be positive under all quality checks.

- The microstructure analysis revealed the formation of craters, micro globules, micro holes and melted debris under rough cut mode, but no craters and micro globules were detected on the machined surface under trim cut mode except few melted debris and micro holes.

- The surface topography analysis revealed that trim cut mode offers comparatively smoother surface on machined components and significantly reduces the peak to valley height up to 8 μm whereas more surface irregularities were detected under rough cut mode due to high discharge energy which leads to higher Rz.

- The subsurface microhardness of profile slot has been decreased to 70 μm under rough cut mode, whereas no significant change in subsurface microhardness was detected under second trim cut mode due to minimum surface damage induced by fine pulse. Due to higher elemental changes under rough cut mode, subsurface microhardness has been decreased to 283.62 Hv as that of bulk hardness of 425 Hv.

- The recast layer analysis exposed the thick recast layer (20–30 μm) on the machined surface of profile slots under rough cut mode due to high thermal damage induced by power pulse while no significant recast layer was detected under second trim cut mode.

- Residual stress analysis revealed the presence of tensile residual stresses within WED machined surface under rough cut mode as well as trim cut mode whereas bulk material exhibited the compressive residual stresses. Moreover, tensile residual stresses are less than 850 MPa under rough cut mode as well as trim cut mode, which approves the quality checklist of the turbine disc profile slot.

- CMM analysis of profile slot revealed that dimensional accuracy lies within the tolerance of ±5 µm under second trim cut mode (B–150). Moreover, B–200 and B–250 have also been passed the quality check whereas D–250, Zn–200 and Zn–250 has been disqualified due to their higher surface roughness (more than 0.8 µm).

CHAPTER 6

MODELING AND OPTIMIZATION OF WEDM PERFORMANCE CHARACTERISTICS

6.1   INTRODUCTION

This chapter outlines the modeling of WEDM performance characteristics using response surface methodology followed by backward elimination approach. Analysis of variance and response graph were obtained to study the WEDM performance characteristics. The individual and multi-objective optimization of WEDM control parameters were obtained using TLBO algorithm. Moreover, Pareto optimal solutions have been presented to attain the common control parameter settings which satisfy both the objectives.

6.2   EXPERIMENTAL DETAILS

'Electronica Ecocut' WED machine was used to perform experiments followed by rough cut strategy. Based on the earlier investigation carried out in section 4.1, four control parameters were selected for the current study as shown in Table 6.1. The levels of control parameter were selected in such a manner that there is no gap short and wire rupture during WEDM process. All the control parameters were examined at different levels to understand their effect on WEDM performance characteristics. Based on the investigation carried out in section 4.2 and section 4.3, a hard brass wire of diameter 150 μm was selected as a tool electrode. This is because, brass wire offers the best surface integrity on the machined components (Klocke et al., 2014). During experimentation, some control parameters were kept constant and are shown in Table 6.2.

The response surface methodology (RSM) was adopted to develop the predictive mathematical models for MRR and SR. Generally, RSM combines the experimental and regression analysis which not only reduces the cost and time, but also provides information about the interaction effects with the least number of trials. The experimental plan was based on the central composite design as shown in Table 6.3.

Table 6.1 WEDM control parameters and their levels.

SL No.	Control parameters	Level–1	Level–2	Level–3
1.	Pulse on time – T_{on}, (µs)	105	110	115
2.	Pulse off time – T_{off}, (µs)	33	44	55
3.	Servo voltage – SV, (V)	20	40	60
4.	Wire feed – WF, (m/min)	3	6	9

Table 6.2 Constant process parameters used during the WEDM process.

Wire material	Hard brass
Wire diameter	150 µm
Dielectric fluid	De-ionized water
Polarity	Positive
Discharge current	12 A
Discharge voltage	28 V
Servo feed	15 mm/min
Flushing pressure	1.96 bar
Cutting speed over ride (%)	50
Dwell time	3 µs
Corner control factor	3

6.3   MODELING OF WEDM RESPONSES USING RESPONSE SURFACE METHODOLOGY

Due to the complexity of WEDM operation, it is very difficult to predict the performance characteristics exactly by mathematical equations. Therefore, RSM-based backward elimination method has been used to identify useful predictors and to find the best regression models that correspond to MRR and SR. The steps involved in proposed methodology were shown in Figure 6.1. RSM is a systematic collection of statistical tools and techniques which is useful for modeling of problems where output response is influenced by various control factors (Montgomery, 2013). Moreover, RSM is also helpful for optimizing the output responses. As discussed

134

earlier in section 3.7, WEDM involves a complex interrelationship among control parameters and performance characteristics. Therefore, the second order model has been adopted for the current study. In the second order model, central composite design (CCD) is most popular in various modules of RSM which is proposed by Box and Hunter (1957). The CCD design provides the estimation of quadratic as well as interaction effects.
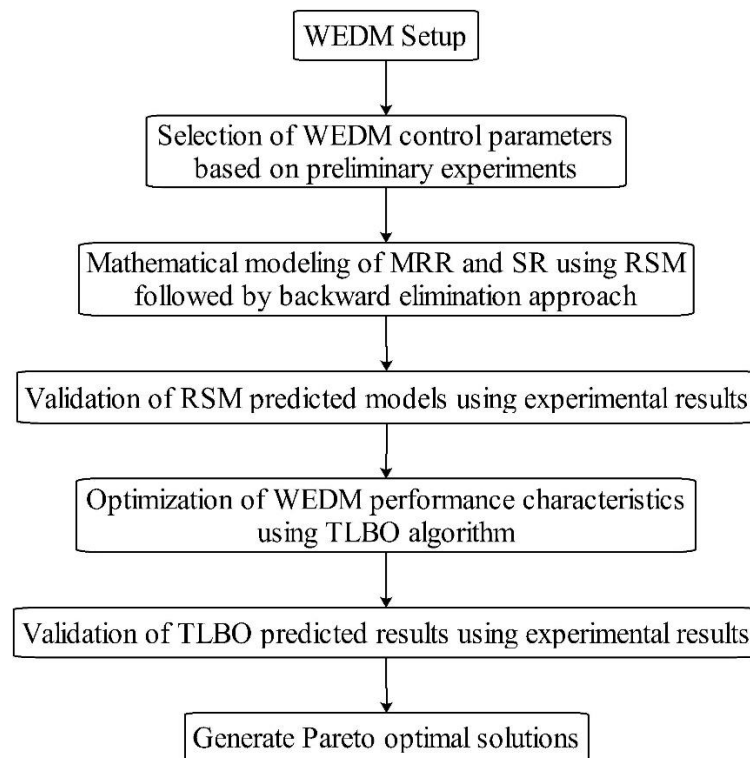
Figure 6.1 Steps involved in adopted methodology.

According to Khuri (2006), CCD is one of the most widely used RSM designs for fitting the second order surface models. The CCD composed of a full factorial design with all combinations of factors at high and low levels, eight star points and six center points. The center points are midst between low and high levels where as star points are the face of the cube which corresponds to α. The value of α indicates the design reason of interest. In a CCD, factorial points are basically employed to fit all linear and interaction terms, whereas axial points (star points) are used for the estimation of quadratic terms. In the special case of CCD, design regions allow the factors within a coded value of -1 to +1 and is known as face central cubic design (FCCD). FCCD involves a default value of design region (α=1) and also require 3 levels of each

135

control factor. The value of α is only significant when number of control parameters are more than five (Anderson and Whitcomb, 2005). In the current study, experimental plan was based on 3 center point blocked FCCD. A total of 27 experiments were conducted, including 3 center points, 8 axial points and 16 cube points. Each experiment has been repeated thrice under similar condition. The experimental design was obtained using Minitab 17 statistical software.

Due to complex mechanism of material removal and stochastic behaviour of WEDM process, it is tough to obtain statistical model based on electro-discharge principle. Therefore, second-order polynomial regression models (quadratic model) have been developed to determine the mathematical relation between WEDM control parameters and performance characteristics such as MRR and SR. The quadratic response model y_i for k control parameters can be represented by Eq. (6.1).

$$y_i = c_0 + \sum_{i=1}^{k} c_i x_i + \sum_{i=1}^{k} c_{ii} x_i^2 + \sum\sum_{i<j}^{k} c_{ij} x_i x_j \pm \varepsilon \qquad (6.1)$$

Where c_0 is a constant and c_i, c_{ii} and c_{ij} represent the coefficient of linear, quadratic and interaction terms, respectively (Montgomery, 2013). The variable x_i represents control parameters under study, whereas y_i resembles to the response surface which may include linear, squared and interaction terms. During experimental work, some unusual observations have been recorded. These observations have been repeated again to increase the model accuracy. Moreover, repeatability of WEDM process has been confirmed by performing the experiments at 3 center points of control parameters. The percentage error has been calculated using Eq. (6.2) which shows the inconsistency of WEDM performance characteristics with reference to their average value. The experimental observation as shown in Table 6.3 revealed that the MRR and SR are reproduced within the acceptable range of ±5% (Montgomery, 2013).

$$\text{Percentage error (\% error)} = \left(\frac{\text{Average data} - \text{Experimental data}}{\text{Average data}} \right) \times 100 \qquad (6.2)$$

The empirical relationship between response characteristics and control parameters can be expressed by Eq. (6.3) and Eq. (6.4) which is based on the actual experimental factors. Based on 95% confidence level, the insignificant terms have been removed from the model using the backward elimination method. To check the fitness of the

models, the determination coefficient (R^2) has been calculated which measures the degree of fit of the model. R^2, adjusted R^2 and predicted R^2 value of the model for MRR were found to be 97.27%, 96.26% and 95.16% respectively. Similarly, R^2, adjusted R^2 and predicted R^2 value of the model for SR were found to be 98.58%, 96.92% and 93.50% respectively. On the basis of the high value of R^2, it can be stated that the proposed quadratic models are adequate in representing the MRR and SR.

$$MRR = -18.39 + 0.2291\,A - 0.07238\,B + 0.2852\,C - 0.3705\,D + 0.03177\,D^2 - 0.003229\,AC + 0.000811\,BC$$

$$(6.3)$$

$$SR = 44.7 - 0.932\,A - 0.00657\,B + 0.1608\,C + 0.00499\,A^2 + 0.000387\,C^2 - 0.001844\,AC$$

$$(6.4)$$

Where, A=pulse on time, B=pulse off time, C=servo voltage and D=wire feed. The value of R-squared and adjusted R-squared shows adequacy of developed statistical models. The normal probability graph for MRR and SR has been shown in Figure 6.2, in which residuals are falling along a straight line indicating that the errors are normally spread. Moreover, a check on the normal probability plot revealed that more than 97% of residuals are within three sigma limits.

Analysis of variance (ANOVA) was performed on experimental data to statistically examine the developed mathematical model. The significant control parameters and interaction terms have been identified. A control factor is considered as significant if its measured F value is greater than the tabulated F value at similar confidence level. For the current study, the 95% confidence level has been selected. If, probability (P) value of the model is smaller than 0.05, then control factors have a significant effect on the response at 95% confidence level (Montgomery, 2013).

Besides, the effects of control parameters on MRR and SR have been studied with the help of 3D surface plot. The experimental results shown in Table 6.3 have been analyzed using Minitab 17 statistical software. In WEDM process, MRR and SR were considered as a key performance characteristics because of their vital effect on productivity and surface integrity. Further, multi-objective optimization has been performed using TLBO algorithm followed by Pareto optimal solutions.

Table 6.3 Experimental design based on FCCD and corresponding WEDM performance characteristics.

SL No.	Pulse on time (μs)	Pulse off time (μs)	Servo voltage (V)	Wire Feed (m/min)	MRR (mm³/min)	SR (μm)
1.	105	33	20	3	1.8258	1.05
2.	115	33	20	3	3.7242	2.43
3.	105	55	20	3	0.8172	0.97
4.	115	55	20	3	2.2548	2.23
5.	105	33	60	3	0.834	0.97
6.	115	33	60	3	1.2462	1.58
7.	105	55	60	3	0.2886	0.91
8.	115	55	60	3	0.672	1.45
9.	105	33	20	9	1.9224	1.07
10.	115	33	20	9	3.8592	2.46
11.	105	55	20	9	0.8358	1.01
12.	115	55	20	9	2.3874	2.26
13.	105	33	60	9	0.8214	0.98
14.	115	33	60	9	1.266	1.63
15.	105	55	60	9	0.3036	0.95
16.	115	55	60	9	0.7218	1.48
17.	105	44	40	6	0.9552	0.96
18.	115	44	40	6	1.4676	1.59
19.	110	33	40	6	1.4832	1.42
20.	110	55	40	6	0.7926	1.03
21.	110	44	20	6	1.4868	1.53
22.	110	44	60	6	0.6222	1.08
23.	110	44	40	3	1.2174	1.18
24.	110	44	40	9	1.3446	1.21
25.	110	44	40	6	1.2546	1.14
26.	110	44	40	6	1.3044	1.16
27.	110	44	40	6	1.2312	1.19
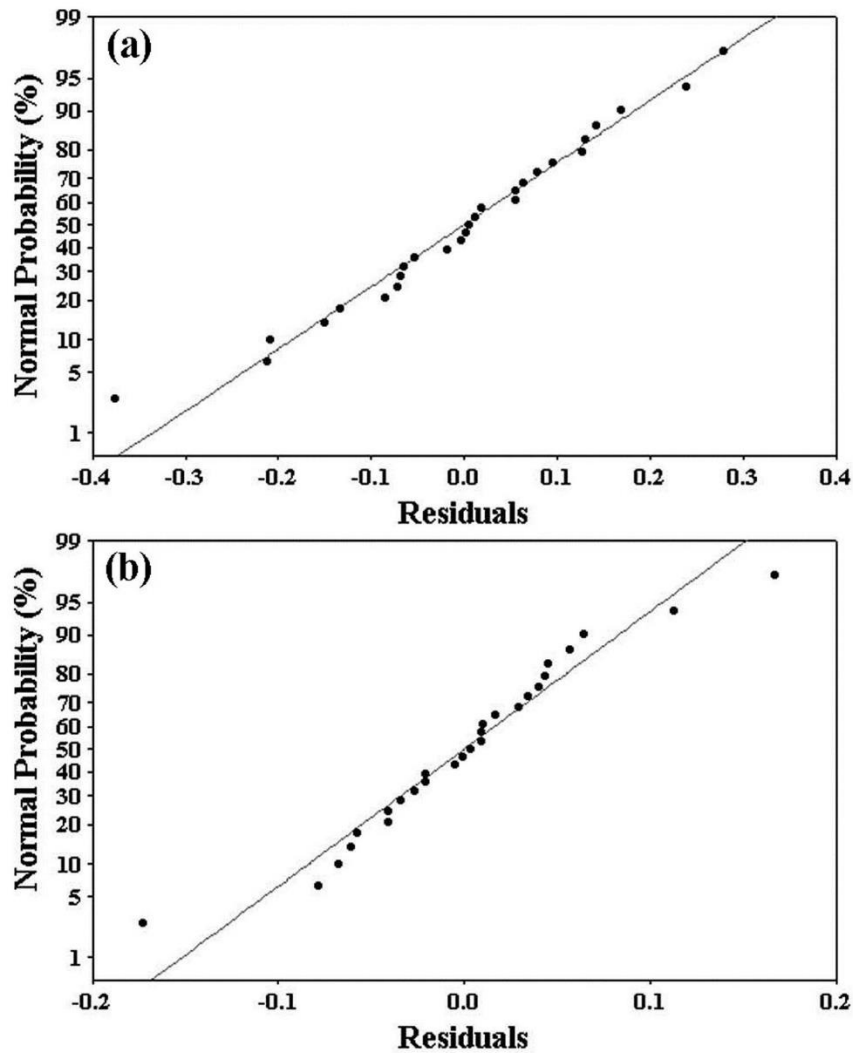
Figure 6.2 Normal probability plots of residuals: (a) MRR; (b) SR.

From the ANOVA results of MRR, it can be perceived that pulse on time, pulse off time, servo voltage and interaction terms (pulse on time – servo voltage and pulse off time – servo voltage) are statistically significant as shown in Table 6.4. However, servo voltage is found to be the most significant factor affecting the cutting speed. The interaction effects of control parameters on MRR have been shown in Figure 6.3. From Figure 6.3(a), it was observed MRR is higher at high pulse on time and low servo voltage whereas MRR is lower at low pulse on time and high servo voltage. The behaviour can be explained by the fact that at high pulse on time, number of electrical sparks per unit time will increase, whereas at low servo voltage, spark intensity increases due to reduced spark gap. This contributes to the increased thermal energy during WEDM process leading to higher cutting speed. Instead, at low pulse on time,

number of electrical discharge will reduce whereas at high servo voltage, spark intensity reduces due to increased spark gap which provides better flushing. This, in turn, decreases the cutting speed due to the low thermal energy of the spark.
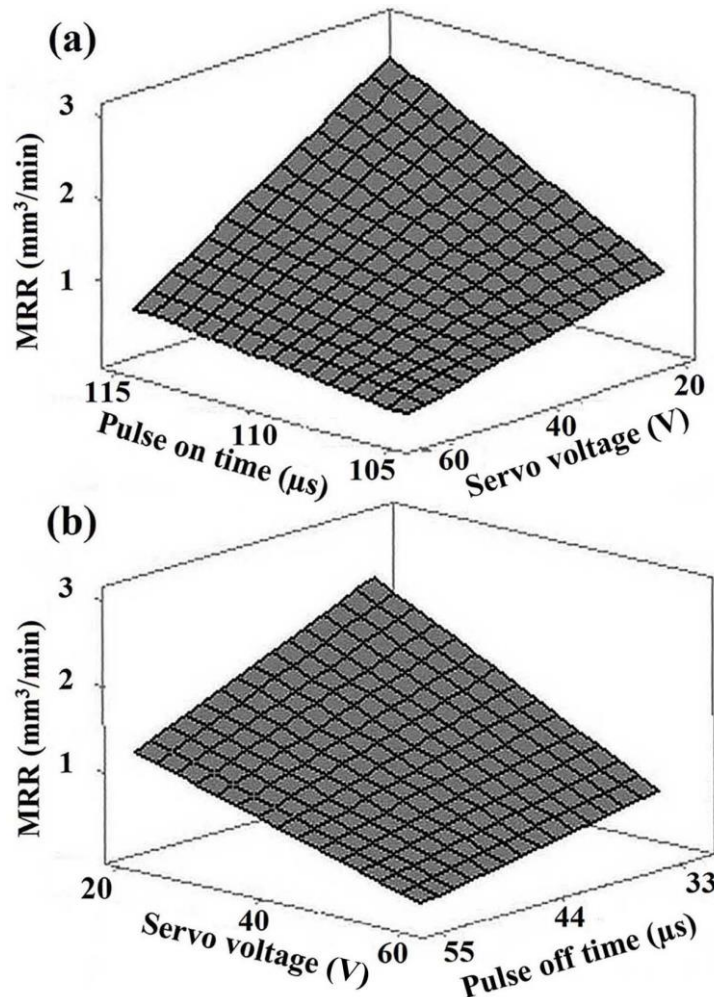
Figure 6.3 Response surface plots: (a) Interactive effect of pulse on time and servo voltage on MRR at pulse off time of 44 μs and wire feed of 6 m/min; (b) Interactive effect of servo voltage and pulse off time on MRR at pulse on time of 115 μs and wire feed of 6 m/min.

Figure 6.3(b) shows that MRR increases with decrease in servo voltage and pulse off time and vice versa. The behaviour can be explained by the fact that low servo voltage tends to increase the spark intensity due to reduced spark gap whereas low pulse off time tends to increase the number of electrical sparks per unit time This, in turn, increases the thermal energy during WEDM process. Therefore, consequently, more amount of material will be melted which lead to higher MR. On the other hand, high

servo voltage tends to reduce the spark intensity due to increased spark gap and high pulse off time tends to the reduce the number of electrical sparks per unit time. This, in turn, reduces the amount of thermal energy transferred to material leading to lower MRR. The comparison of experimental results and RSM predicted results of MRR has been shown in Figure 6.4 which indicates that deviations between experimental results and RSM predicted results are marginal. Therefore, it can be state that RSM predicted MRR has good agreement with the experimental MRR.

Table 6.4 Pooled ANOVA results for MRR after backward elimination.

Source	DOF	SS	MS	F–ratio	P–value	Percentage contribution
Model	7	19.1134	2.7304	96.69	<0.0001	97.26
A–T_{on}	1	4.4952	4.4952	159.18	<0.0001	22.88
B–T_{off}	1	3.4748	3.4748	123.05	<0.0001	17.68
C–SV	1	8.4567	8.4567	299.47	<0.0001	43.04
D–WF	1	0.0188	0.0188	0.67	0.474	0.09
D^2	1	0.4905	0.4905	17.37	0.001	2.50
AC	1	1.6680	1.6680	59.07	<0.0001	8.49
BC	1	0.5094	0.5094	18.04	<0.0001	2.59
Residual Error	19	0.5365	0.0282	–	–	–
Total	26	19.65	–	–	–	–
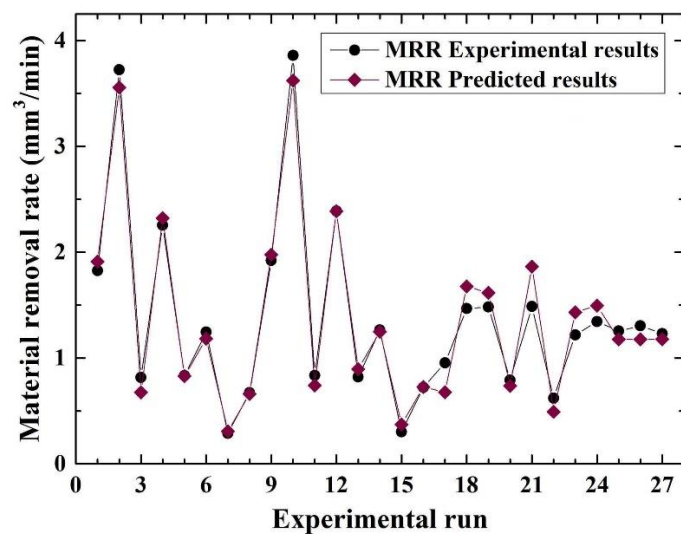
Figure 6.4 Comparison of experimental and RSM predicted value of MRR.

From the ANOVA results of SR, it was observed that pulse on time, servo voltage and pulse off time linearly affecting the SR. Besides, the interaction term (pulse on time – servo voltage) and square terms (servo voltage – servo voltage) also have a significant effect on SR as shown in Table 6.5. The interaction effect of control parameters on SR has been shown in Figure 6.5. From the Figure 6.5, it can be observed that surface roughness increases with increase in pulse on time and decrease in servo voltage. This behaviour can be explained by the fact that at high pulse on time, number of electrical sparks per unit time increases and at low servo voltage, spark intensity will increase due to reduced spark gap. Therefore, more amount of thermal energy transferred to the material which melts comparatively more amount of material from the workpiece. A part of molten metal is flushed away by pressurized waves which are generated during WEDM process in the absence of plasma channel. When, remaining molten metal resolidify, some gas bubbles get trapped into molten material. During this process, few gas bubbles collapse and, forms crater and micro holes on the machined surface leading to higher surface roughness.
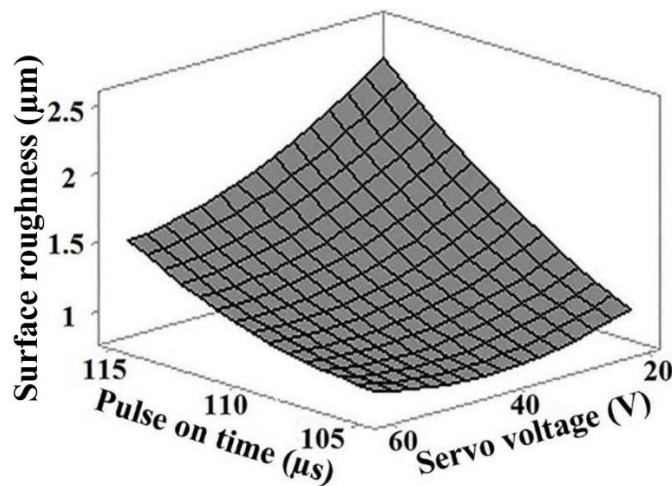
Figure 6.5 Response surface plot of pulse on time and servo voltage on SR at pulse off time of 44 μs and wire feed of 6 m/min.

However, at low pulse on time, number of electrical sparks per unit time decreases whereas at high servo voltage, spark intensity gets reduced due to increased spark gap. Therefore, low amount of thermal energy transferred to the material which melts comparatively less material from the workpiece which can be easily flushed away by

pressurized waves. It will reduce the formation of craters and micro holes due to low thermal damage leading to lower surface roughness of the machined components. The comparison of experimental results and RSM predicted results of SR has been shown in Figure 6.6 which indicates that there is a minimal difference between experimental results and RSM predicted results. Hence, it can be stated that RSM predicted SR is in good agreement with the experimental SR.

Table 6.5 Pooled ANOVA results for SR after backward elimination.

Source	DOF	SS	MS	F–ratio	P–value	Percentage contribution
Model	6	5.6809	0.9468	172.19	<0.0001	98.10
A–T_{on}	1	3.7721	3.7721	685.98	<0.0001	65.14
B–T_{off}	1	0.0939	0.0939	17.07	0.001	1.62
C–SV	1	0.8800	0.8800	160.04	<0.0001	15.20
A^2	1	0.0518	0.0518	9.42	0.006	0.89
C^2	1	0.0797	0.0797	14.50	0.001	1.38
AC	1	0.5439	0.5439	98.91	<0.0001	9.39
Residual Error	20	0.10998	0.0055	–	–	–
Total	26	5.79092	–	–	–	–
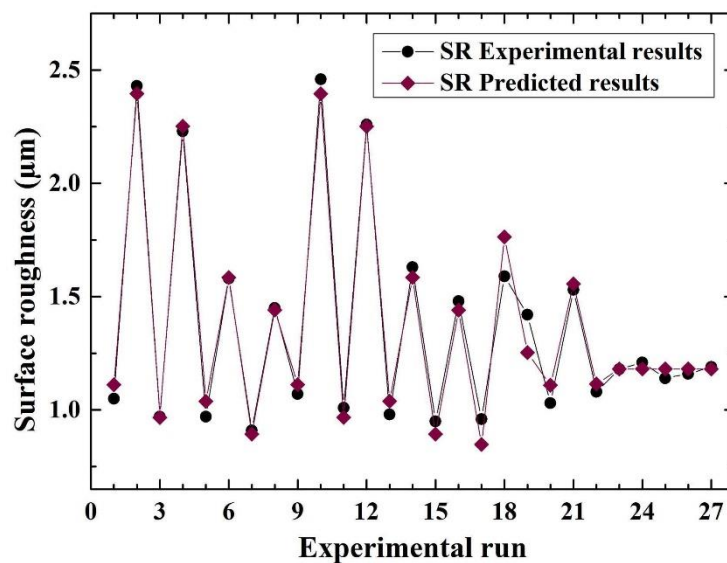
Figure 6.6 Comparison of experimental and RSM predicted value of SR.

6.4   OPTIMIZATION OF WEDM RESPONSES USING TEACHING LEARNING BASED OPTIMIZATION

In the current study, TLBO algorithm has been used which is a newly developed population-based evolutionary algorithm, inspired by sharing knowledge within a teaching space, where students first obtain knowledge from a teacher and then from colleagues. TLBO algorithm hunts for a best solution among students to attain the knowledge of the teacher, who is treated as the most educated person in the society, thus achieving best solutions. TLBO was formerly developed by Rao et al. (2011). In many aspects, TLBO look like Evolutionary Algorithms (EAs). Rao et al. (2014) have shown the importance of TLBO algorithm for optimization of process parameters of selected casting process. However, in the current study, the author has used the TLBO algorithm for individual and multiple performance optimization of WEDM process and also efforts have made to generate the Pareto optimal solutions. The flow chart of TLBO algorithm has been shown in Figure 6.7. The working principle of TLBO was subdivided into two phases, first is "teacher phase" and the second is "student phase".

6.4.1   Teacher phase

In this phase, the algorithm model produces a number of arbitrary points called students within the population. Then, these points were updated as a teacher who shares his knowledge with students. In the first part of TLBO algorithm, the mean of the class increases from M_i to M_{new} depending upon the best teacher. Rao et al. (2011) has assumed that a best teacher is one who can bring his/her students up to his/her level in terms of knowledge. But, practically, it is impossible. A student can only move the mean of a class up to a certain extent depending on the teaching factor (T_F). Let T_i is the teacher and M_i be the mean at any iteration i. Then, T_i will try to move the mean M_i up to its own level, therefore new mean will be T_i which is designated as M_{new}. Based on the difference between the existing and new mean, the solution was upgraded according to Eq. (6.5) proposed by Rao et al. (2011).

$$Difference\_Mean_i = r_i(M_{new} - T_F M_i) \qquad (6.5)$$

Where, T_F decides the value of the mean to be improved and r_i is a random variable within the range of 0 to 1.

The value of T_F may be either 1 or 2, which is again a heuristic step. T_F is calculated arbitrarily with equal probability using Eq. (6.6).

$$T_F = round[1 + rand(0,1)\{2-1\}]$$ (6.6)

Then, the existing solution was modified using Eq. (6.7).

$$X_{new,i} = X_{old,i} + Difference\_Mean_i$$ (6.7)
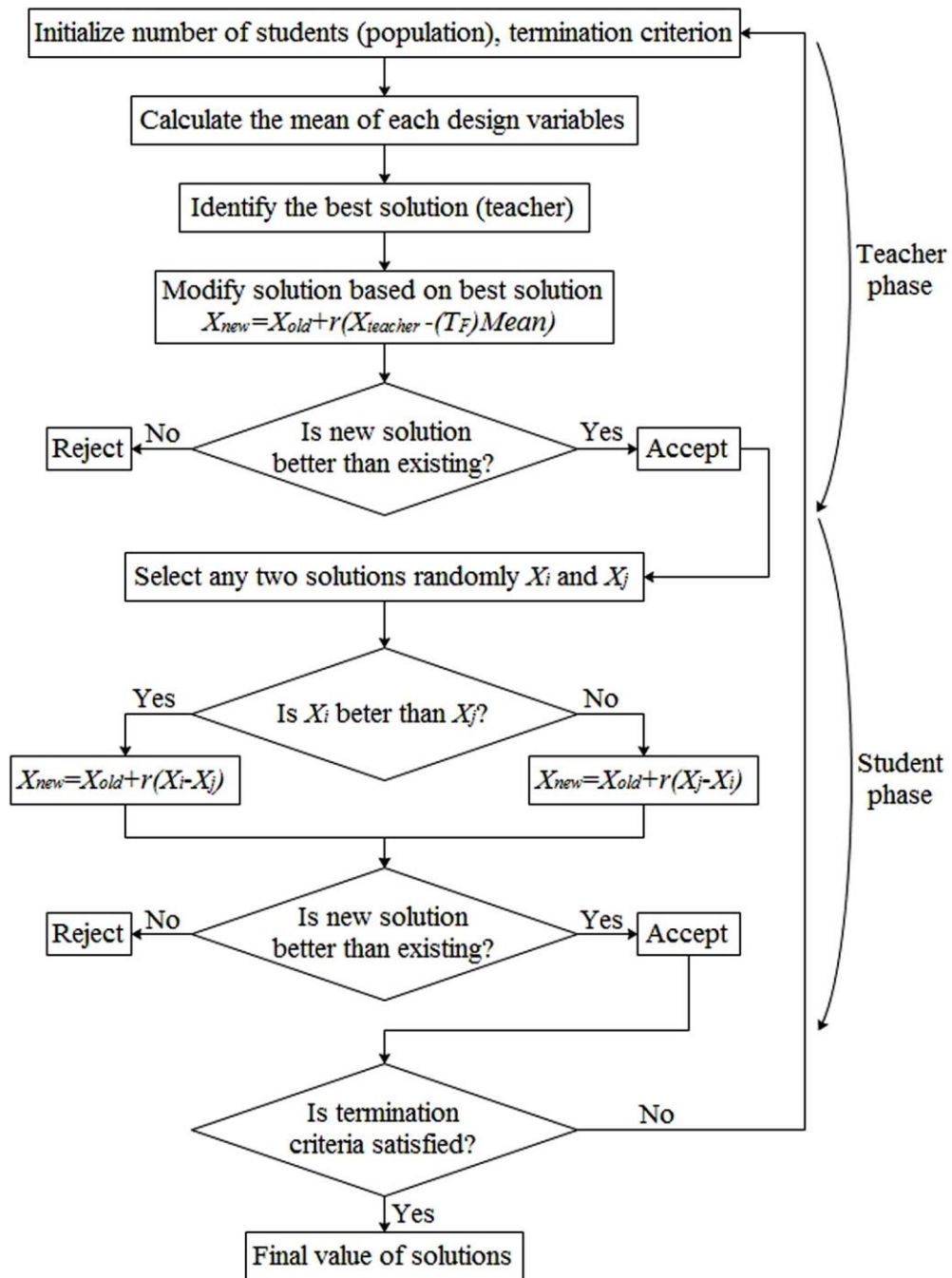
Figure 6.7 Flow chart of TLBO algorithm.

145

6.4.2   Student phase

In this phase, students upgrade their knowledge by interacting among colleagues. Therefore, a solution is arbitrarily interacted to obtain something new from other solutions in the population. The solution will acquire new information if the other solutions have more knowledge than him/her. Statistically, this teaching learning phenomenon can be expressed by Eq. (6.8) and Eq. (6.9).

$$X_{new,i} = X_{old,i} + r_i(X_i - X_j), \text{ if } f(X_i) < f(X_j) \tag{6.8}$$

$$X_{new,i} = X_{old,i} + r_i(X_j - X_i), \text{ if } f(X_j) < f(X_i) \tag{6.9}$$

Considering two different students X_i and X_j at any iteration i, where $i \neq j$. If it gives better function value, then X_{new} is accepted. After a number of progressive teaching-learning rounds, the randomness of points within the population becomes lower. It means that knowledge level of class has been improved and the algorithm converges towards a best solution. Based on the maximum number of iterations, termination criteria can be predetermined.

The regression equations, shown in Eq. (6.3) and Eq. (6.4), were used as fitness function in TLBO algorithm. The minimum and maximum range of control parameters was obtained from the FCCD design as shown in Table 6.3. The maximum and minimum range has been defined as a constraint limit of WEDM control parameters in TLBO algorithm.

Pulse on time = 105–115 (µs)
Pulse off time = 33–55 (µs)
Servo voltage = 20–60 (V)
Wire feed = 3–9 (m/min).

In the first step, the process parameters optimization has been carried out to achieve the optimum setting for individual performance characteristics. In the second step, simultaneous optimization has been achieved by combining the individual objective functions. Then, the multi-objective function was treated as an individual objective function to obtain the common settings of MRR and SR.

6.4.3 Pareto optimal solution

During WEDM process, it was observed that productivity and surface quality are conflicting in nature. There are well known facts that MRR increases with an increase in surface roughness and hence it is essential to cultivate a methodical tactic to formulate an acceptable adjustment between these two output responses (Sarkar et al., 2010). Such type of multiple objective optimization problems can be solved either by formulating a constrained optimization algorithm or generating Pareto optimal solutions (Deb, 2012). However, for the current study, Pareto optimal solutions have been derived to achieve the feasibility in manufacturing of gas turbine components. In Pareto optimal front, there may be a number of optimal solutions. However, suitability of the solution mainly depends upon the user's requirement.

Table 6.6 Results obtained by TLBO algorithm for MRR.

Control parameters	TLBO results for MRR (mm^3/min)		
	Best	Average	Std. deviation
Pulse on time – T_{on} (µs)	114.99		
Pulse off time – T_{off} (µs)	33.08		
Servo voltage – SV (V)	20.04		
Wire feed – WF (m/min)	8.98		
Output response – MRR	3.62	3.27	0.18

Table 6.7 Results obtained by TLBO algorithm for SR.

Control parameters	TLBO results for SR (µm)		
	Best	Average	Std. deviation
Pulse on time – T_{on} (µs)	105.17		
Pulse off time – T_{off} (µs)	49.64		
Servo voltage – SV (V)	44.18		
Wire feed – WF (m/min)	5.69		
Output response – SR	0.84	0.85	0.02

6.4.4 Individual performance optimization

For individual response optimization, number of generations and the population size have been defined based on the number of trials. Finally, a number of generation of 20 and a population size of 100 were used for running the TLBO algorithm for optimization of a single response. The optimum results achieved using a TLBO algorithm for MRR and SR has been presented in Table 6.6 and Table 6.7 respectively. The convergences of MRR and SR with respect to generations were shown in Figure 6.8.
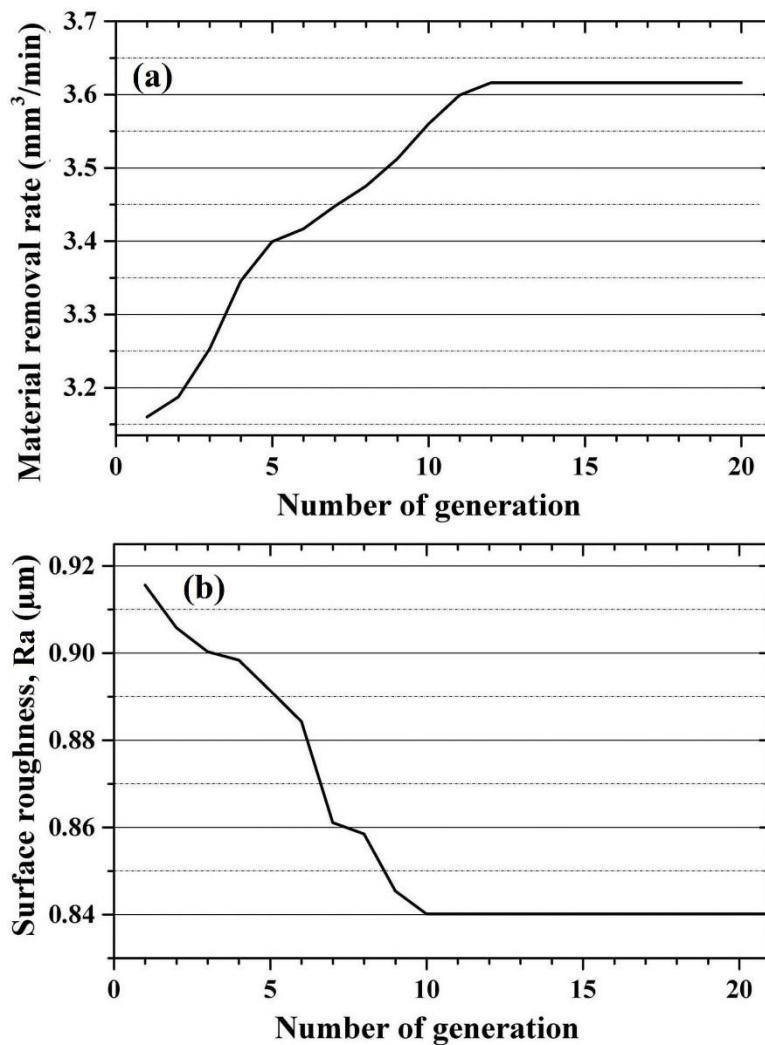
Figure 6.8 Convergence graphs of TLBO algorithm for: (a) MRR; (b) SR.

In order to examine the stability of the results, the algorithm has been run for 20 times. The average results and standard deviation have been noted. In case of MRR,

the average result of 20 runs was found to be 3.27 mm³/min whereas standard deviation of 0.18 is noted. Similarly, in case of SR, the average results and the standard deviation of 20 runs recorded are 0.85 μm and 0.02 respectively. In both the cases, average results of 20 runs are almost nearer to best results. Moreover, standard deviation observed is comparatively small.

6.4.5 Multiple performance optimization

In the current study, efforts have been made to achieve the common factor setting which satisfies both the objectives and provides enhanced WEDM performance. For this aim, a combined objective function has been developed by normalizing the MRR and SR and assigning some weightage to them. Basically, normalization transforms the data in the range of 0 to 1. The combined objective function was given in Eq. (6.10).

$$Max(z) = w_1 \times \left(\frac{MRR - MRR_{min}}{MRR_{max} - MRR_{min}} \right) + w_2 \times \left(\frac{SR_{max} - SR}{SR_{max} - SR_{min}} \right); \qquad w_1 + w_2 = 1 \qquad (6.10)$$

Where, MRR_{max}, MRR_{min}, SR_{max} and SR_{min} are maximum and minimum values of MRR and SR respectively, which can be achieved by attempting an individual objective function for maximization and minimization respectively. In the present study, w_1 is the weight assigned to the MRR and w_2 is the weight assigned to the SR.
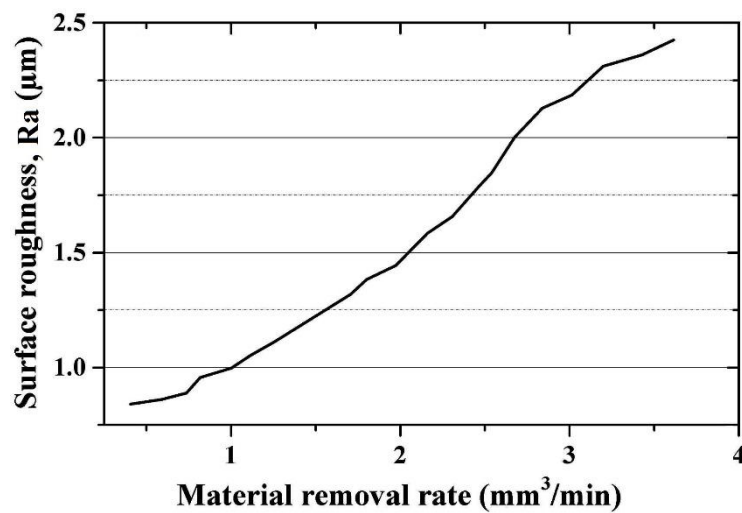
Figure 6.9 Pareto optimal curve for multiple objective optimization of WED machined Inconel 706.

Table 6.8 Pareto optimal solutions for WED machined Inconel 706 at different weightage.

w_1 (MRR)	w_2 (SR)	MRR (mm^3/min)	SR (μm)	T_{on} (μs)	T_{off} (μs)	SV (V)	WF (m/min)
0.00	1.00	0.4076	0.8401	105.17	49.64	44.18	5.69
0.05	0.95	0.5918	0.8602	106.26	53.37	44.79	8.56
0.10	0.90	0.7376	0.8883	105.40	52.24	31.22	8.58
0.15	0.85	0.8192	0.9561	106.77	46.24	38.46	6.70
0.20	0.80	1.0023	0.9962	107.57	51.27	36.23	8.82
0.25	0.75	1.1165	1.0518	108.29	40.57	46.60	8.24
0.30	0.70	1.2575	1.1112	108.49	41.09	38.66	4.29
0.35	0.65	1.4711	1.2093	107.42	45.03	23.36	8.19
0.40	0.60	1.7074	1.3175	110.37	42.93	35.03	8.76
0.45	0.55	1.8024	1.3824	109.70	38.09	28.96	6.05
0.50	0.50	1.9748	1.4438	109.23	39.29	23.11	1.97
0.55	0.45	2.1613	1.5835	110.63	41.49	23.83	3.30
0.60	0.40	2.3080	1.6561	111.52	40.31	25.88	8.57
0.65	0.35	2.4638	1.7864	112.80	34.51	29.26	4.22
0.70	0.30	2.5408	1.8466	112.15	35.52	23.19	5.46
0.75	0.25	2.6777	2.0020	113.60	39.71	24.43	3.30
0.80	0.20	2.8407	2.1279	114.86	37.01	27.57	8.40
0.85	0.15	3.0151	2.1852	114.28	36.95	22.63	6.32
0.90	0.10	3.2001	2.3104	114.99	33.04	23.27	7.59
0.95	0.05	3.4294	2.3597	114.70	33.05	20.36	8.35
1.00	0.00	3.6160	2.4248	114.99	33.08	20.36	8.98

To obtain the Pareto optimal points, the weightage is varied in the steps of 0.05. For combined objective function, TLBO algorithm has been run for a population size 100 and 20 generations and a number of Pareto optimal solutions have been obtained which have been presented in Figure 6.9. Moreover, common parameters setting corresponding to each Pareto optimal points were presented in Table 6.8. These solutions are also called as final set of solutions that corresponds to different

weightage. However, the section of any one solution depends upon the requirement of the manufacturer.

6.4.6   Comparison of experimental results with TLBO predicted results

The effectiveness of TLBO algorithm was validated against 5 trials of experimental data set as shown in Table 6.9 and Table 6.10. The deviations between TLBO predicted results and experimental results are marginal. An experimental error of 4.63% and 3.45 % were observed for MRR and SR respectively. However, the experimental error is quite considerable and lies within the acceptable range of $\pm$ 5 %. Moreover, the comparative results presented in Table 6.9 and Table 6.10 has indicated that TLBO predicted values have good agreement with the experimental results.

Table 6.9 Comparison of experimental MRR with TLBO predicted MRR.

Control parameters	Comparative results for MRR (mm³/min)		
	TLBO Best	**Experimental Results**	**Error (%)**
Pulse on time – T_{on} (µs)	114.99	115	
Pulse off time – T_{off} (µs)	33.08	33	
Servo voltage – SV (V)	20.04	20	
Wire feed – WF (m/min)	8.98	9	
Output response – MRR	**3.62**	**3.79**	**+ 4.63**

Table 6.10 Comparison of experimental SR with TLBO predicted SR.

Control parameters	Comparative results for SR (µm)		
	TLBO Best	**Experimental Results**	**Error (%)**
Pulse on time – T_{on} (µs)	105.17	105	
Pulse off time – T_{off} (µs)	49.64	50	
Servo voltage – SV (V)	44.18	44	
Wire feed – WF (m/min)	5.69	6	
Output response – SR	**0.84**	**0.87**	**+ 3.45**

6.5 SUMMARY

In this chapter, RSM-based TLBO algorithm has been adopted in which RSM has been used for mathematical modeling of MRR and SR, whereas TLBO has been used to predict the individual as well as multiple performance characteristics more accurately. Moreover, Pareto optimal solutions have been presented which helps the manufacturer to select the WEDM control parameters setting for improved productivity as well as better surface quality. Based on the experimental studies carried out in Chapter 6, the following observations are found:

- The mathematical models developed at the 95% confidence level are more reliable representation of experimental observations with prediction errors less than ±5%. Moreover, 97% residuals are falling within three sigma limits which represent the adequacy of developed statistical model.

- ANOVA results revealed that servo voltage (43.04 %) is the most influencing factor for MRR whereas pulse on time (65.14 %) most significantly affects the SR. However, the wire feed was found to be an insignificant factor for MRR and SR.

- The response surface analysis revealed that the interaction of pulse on time and servo voltage is statistically significant for both the responses. This interaction term exhibits a percentage contribution of 8.49 % and 9.39 % to affect the MRR and SR respectively.

- The mathematical models developed by RSM were used as a fitness function in TLBO algorithm. The effectiveness of TLBO algorithm for individual response optimization of WEDM process has been verified using a convergence plot of MRR and SR. Multi-objective mathematical model developed by normalizing the MRR and SR are attempted as a single objective function using a TLBO algorithm to predict the multiple performance characteristics.

- Pareto optimal points obtained at different weightage describe common parameter settings for simultaneous optimization of MRR and SR which may help the manufacturing industries to select the WEDM control parameters for high productivity and improved surface quality of machined parts. Moreover, the best

operating control parameters recommended for WEDM process of Inconel 706 have been presented in Table 6.11.

Table 6.11 Operating parameters recommended for WEDM process of Inconel 706.

Best operating parameters	Specifications
Control parameters	Pulse on time (112 μs)
	Pulse off time (36 μs)
	Servo voltage (23 V)
	Wire feed (5 m/min)
	Servo feed (15 mm/min)
	Flushing pressure (1.96 bar)
Wire material	Hard brass wire
Wire diameter	150 μm

CHAPTER 7

CONCLUSION AND SCOPE FOR FUTURE WORK

7.1   CONCLUSION

In the present work, wire electrical discharge machining (WEDM) of Inconel 706 has been carried out to achieve the feasibility in manufacturing of turbine disc profile slots as per the standard of gas turbine industries. To attain this, the effect of different wire diameter as well as different wire materials on WEDM performance characteristics has been evaluated by considering the different discharge energy mode. Further, WEDM technology has been developed to manufacture the turbine disc profile slots using optimum wire diameter as well as optimum wire materials. Finally, Modeling and optimization of WEDM performance characteristics have been carried out and Pareto optimal solutions were obtained which might be beneficial to gas turbine industries. Based on the experimental investigation and optimization, the following conclusion have been derived:

- Pulse on time, pulse off time and servo voltage are the major factors influencing the MRR as well as the SR of the machined components whereas wire feed of 6 m/min and flushing pressure of 1.96 bar have shown the improved MRR as well as SR with the usage of hard brass wire.
- Zinc coated wire improves the productivity, however hard brass wire was found to be optimum in terms of in terms of better surface integrity such as low surface roughness, smooth topography, low recast layer formation, low hardness alterations, lower residual stresses and suitable for manufacturing of aero engine components.
- The hard brass wire of diameter 150 μm has shown improved productivity and better surface quality compared to the hard brass wire of diameter 200 μm and 250 μm and most suited for WED machining of Inconel 706 superalloy.
- The turbine disc profile slots have been manufactured successfully as per the standard of gas turbine industries. The manufactured fir tree profile slots have

shown minimum hardness alteration, almost negligible recast layer, surface roughness less than 0.8 μm, residual stress less than 850 MPa and profile accuracy within the range of ±5 μm while using hard brass wire of diameter 150 μm.

- The empirical models were developed successfully for material removal rate and surface roughness using RSM followed by backward elimination approach. These developed models are used as a fitness function for TLBO algorithm. TLBO predicted results have been obtained for individual as well as multiple performance optimization.

- Pareto optimal solutions have been obtained at different weightage which is believed to be global optimal solutions and might be beneficial to gas turbine industries.

7.2 SCOPE FOR FUTURE WORK

Although the WED machining of advanced turbine disc alloy (Inconel 706) has been studied in detail. Still, there is a scope for further investigation. The current research work has implied the future scope for the development of smaller diameter coated wire to get the further improvement in the WEDM process in terms of improved tensile strength of wire, minimum wire breakage, higher cutting speed, minimum corner radius, the minimum amplitude of vibrations, minimum spark gap and improved surface quality of machined parts while cutting the complex shape with high precision for the specific application.

Nevertheless, in the current study, turbine disc profile slots have been manufactured successfully as per the requirement of gas turbine industries. Further, vibration analysis needs to be carried out in order to minimize the wire vibration and wire deflection, and to improve the geometrical inaccuracy of machined parts. Moreover, Non-destructive testing (NDT) can also be conducted on WEDM manufactured fir tree profile slots and blade roots to examine the components before being used in aircraft engines.

APPENDIX I

CNC PROGRAM FOR FIR TREE PROFILE SLOT

To produce fir tree profile slot, the manufacturer has to select the correct offset value to minimize the profile inaccuracy.

```
;Turbine disc profile slot
G71
G9
G27
G40
G47
G50
G90
G75
; Wire Compensation Definitions
D0=0
D1=0
;#1.0  Cavity=1 RoughCut
G0 X0 Y0 U0 V0
M21
G41 D0 ;D0=0
G3 X2.196538 Y-0.323107 I5.540741 J30.039109
G41 D1 ;D1=0
G2 X2.473132 Y-1.605798 I-0.075725 J-0.687497
G2 X1.340778 Y-2.4117 I-9.218654 J11.754464
G3 X1.633168 Y-3.801895 I0.324343 J-0.657629
G1 X3.005584 Y-4.075013
G2 X3.275222 Y-5.325448 I-0.124779 J-0.681196
G1 X1.930124 Y-6.283521
G1 X1.813253 Y-6.434032
```

G1 X1.742582 Y-6.608659

G1 X1.734324 Y-6.788479

G1 X1.771577 Y-6.917281

G1 X1.840042 Y-7.036834

G1 X1.930124 Y-7.146832

G1 X2.161395 Y-7.346923

G1 X3.479571 Y-7.6382

G2 X3.835708 Y-9.200442 I-0.020516 J-0.826392

G2 X2.917386 Y-9.903985 I-1275.01888 J1663.306718

G1 X2.778224 Y-10.021768

G1 X2.709365 Y-10.102914

G1 X2.632227 Y-10.241725

G1 X2.591725 Y-10.451279

G1 X2.626985 Y-10.667946

G1 X2.730345 Y-10.86071

G1 X2.879611 Y-11.004035

G1 X2.996977 Y-11.074463

G1 X3.176958 Y-11.141966

G3 X4.578281 Y-11.368299 I3.71756 J18.565728

G1 X4.693178 Y-11.369696

G1 X4.861521 Y-11.386172

G1 X4.9883 Y-11.415319

G1 X5.112265 Y-11.463401

G1 X5.224055 Y-11.529588

G1 X5.319834 Y-11.614144

G1 X5.381842 Y-11.697425

G1 X5.422273 Y-11.789177

G1 X5.439245 Y-11.915814

G1 X5.417982 Y-12.046397

G1 X5.3203 Y-12.254675

G1 X5.21017 Y-12.408161

G1 X5.018175 Y-12.620397

G1 X4.875771 Y-12.747894

G2 X3.696687 Y-13.613042 I-29.151745 J38.493957

G3 X5.040008 Y-19.999997 I2.067422 J-2.899917

G1 X11.591698 Y-19.999997

G3 X12.935019 Y-13.613042 I-0.7241 J3.487038

G2 X11.755935 Y-12.747894 I27.972662 J39.359106

G1 X11.613531 Y-12.620397

G1 X11.421537 Y-12.408161

G1 X11.311406 Y-12.254675

G1 X11.213724 Y-12.046397

G1 X11.192461 Y-11.915814

G1 X11.209433 Y-11.789177

G1 X11.249864 Y-11.697425

G1 X11.311872 Y-11.614144

G1 X11.407651 Y-11.529588

G1 X11.519441 Y-11.463401

G1 X11.643406 Y-11.415319

G1 X11.770185 Y-11.386172

G1 X11.938528 Y-11.369696

G1 X12.053425 Y-11.368299

G3 X13.454748 Y-11.141966 I-2.316237 J18.792061

G1 X13.634729 Y-11.074463

G1 X13.752095 Y-11.004035

G1 X13.901361 Y-10.86071

G1 X14.004721 Y-10.667946

G1 X14.039981 Y-10.451279

G1 X13.999479 Y-10.241725

G1 X13.922341 Y-10.102914

G1 X13.853482 Y-10.021768

G1 X13.71432 Y-9.903985

G2 X12.795998 Y-9.200442 I1274.100565 J1664.010262

G2 X13.152136 Y-7.6382 I0.376653 J0.735851

G1 X14.470311 Y-7.346923

G1 X14.701582 Y-7.146832

G1 X14.791664 Y-7.036834

G1 X14.860129 Y-6.917281

G1 X14.897382 Y-6.788479

G1 X14.889124 Y-6.608659

G1 X14.818453 Y-6.434032

G1 X14.701582 Y-6.283521

G1 X13.356484 Y-5.325448

G2 X13.626123 Y-4.075013 I0.394418 J0.569239

G1 X14.998538 Y-3.801895

G3 X15.290929 Y-2.4117 I-0.031953 J0.732566

G2 X14.158574 Y-1.605798 I8.086299 J12.560365

G2 X14.435168 Y-0.323107 I0.35232 J0.595195

G3 X16.631707 Y0 I-3.344203 J30.362216

M0

G41 D0 ;D0=0

G1 X0 Y0

G40

M0

Sketch of fir tree profile slot

159
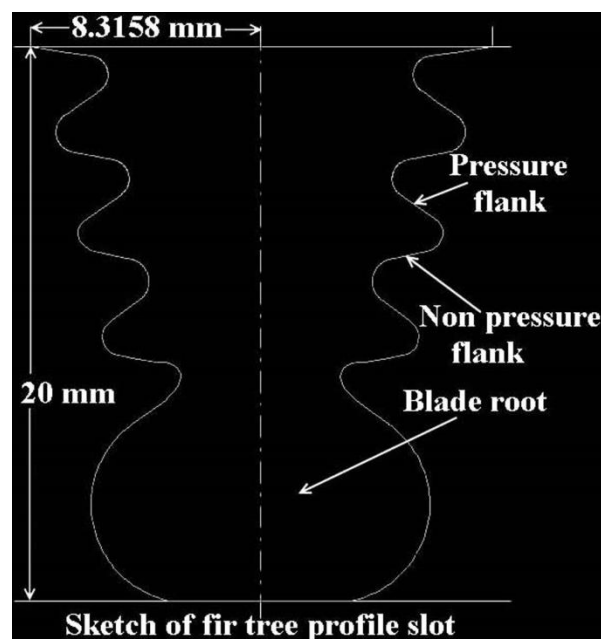
APPENDIX II

MATLAB CODE OF TLBO ALGORITHM

The user has to create separate MATLAB files for each function (i.e., main, mainline, tlbo and fun) to run TLBO code and then main.m file in need to be executed.

%%%%%%%%%%%%%%%% Code for MRR %%%%%%%%%%%%%%%%
%%%%%%%%%%%%%%%%%%%%% main %%%%%%%%%%%%%%%%%%%%%

```
clear all
clc
no_of_run = 20;
no_of_student = 100; %specify population size
no_of_iteration = 20; %specify number of iterations
materialremovalrate = [];
mrr = 0;
for k = 1:20
tf = 1;
for i = 1:no_of_run
[bvf bvx]=mainline(no_of_student, no_of_iteration, tf);
bvf1(i,:)=bvf;
bvx1(i,:)=bvx;
end
bvf = bvf1(:,1);
[bvfmin,k0]=max(bvf)
bvxmin = bvx1(k0,:)
bvfmin = bvf1(k0,:)
materialremovalrate(k) = bvfmin;
mrr(k) = bvxmin(2);
end
```

%%%%%%%%%%%%%%%% main line %%%%%%%%%%%%%%%%

```matlab
function [bvf bvx]= mainline(no_of_student, no_of_iteration, tf)
no_of_variable = 4;
% specify number of variables
% specify the lower bound
% specify the upper bound
lowerlimitofa = 105;
upperlimitofa = 115;
lowerlimitofb = 33;
upperlimitofb = 55;
lowerlimitofc = 20;
upperlimitofc = 60;
lowerlimitofd = 3;
upperlimitofd = 9;
for i = 1:no_of_student
% initialization of the variables
a = lowerlimitofa + rand*(upperlimitofa-lowerlimitofa);
b = lowerlimitofb + rand*(upperlimitofb-lowerlimitofb);
c = lowerlimitofc + rand*(upperlimitofc-lowerlimitofc);
d = lowerlimitofd + rand*(upperlimitofd-lowerlimitofd);
x(i,:)=[a b c d];
end
% limit array
limit=[lowerlimitofa;
upperlimitofa;
lowerlimitofb;
upperlimitofb;
lowerlimitofc;
upperlimitofc;
lowerlimitofd;
upperlimitofd ];
parameter=[no_of_student;
no_of_iteration;
```

```
tf;
no_of_variable];
[bvf,bvx]=tlbo(limit,x,parameter);

%%%%%%%%%%%%%%%% tlbo %%%%%%%%%%%%%%%%%

function [bvf,bvx]=tlbo(limit,x,parameter)
no_of_student = parameter(1);
no_of_iteration = parameter(2);
tf = parameter(3);
no_of_variable = parameter(4);
for i = 1:no_of_student
variable = x(i,:);
[funxz]= fun(variable);
fxx(i,1)=funxz;
end
for ng1 = 1:no_of_iteration;
m = mean(x);
[sfx,k0]=max(fxx);
bt = x(k0,:);
for i = 1:no_of_student
k = 1;
for j = 1:no_of_variable
xs(i,j)=x(i,j)+rand*(bt(1,j)-tf*m(1,j));
if xs(i,j)<limit(k) || xs(i,j)>limit(k + 1)
x1(i,j)=x(i,j);
else
x1(i,j)=xs(i,j);
end
k = j + 2;
end
variable = x1(i,:);
end
```

```
for i = 1:no_of_student
variable = x1(i,:);
[funxz]=fun(variable);
fxx1(i,1)=funxz;
end
for i = 1:no_of_student
if fxx1(i,1)<fxx(i,1)
fxx1(i,:)=fxx(i,:);
x1(i,:)=x(i,:);
end
end
[sfx1,k1]=max(fxx1);
bs = x1(k1,:);
for i = 1:no_of_student
k = 1;
for j = 1:no_of_variable
xs(i,j)=x1(i,j)+rand*(bs(1,j)-x1(i,j));
if xs(i,j)<limit(k) || xs(i,j)>limit(k + 1)
x(i,j)=x1(i,j);
else
x(i,j)=xs(i,j);
end
k = j + 2;
end
variable = x(i,:);
end
for i = 1:no_of_student
variable = x(i,:);
[funxz]=fun(variable);
fxx(i,1)=funxz;
end
for i = 1:no_of_student
```

```
if fxx(i,1)<fxx1(i,1)
fxx(i,:)=fxx1(i,:);
x(i,:)=x1(i,:);
end
end
end
[bvff,k2]=max(fxx);
bvf(1,:)=fxx(k2,:);
bvx = x(k2,:);

%%%%%%%%%%%%%%%% fun % %%%%%%%%%%%%%%%%

function funxz = fun(variable)
no_of_variable = 4;
funxz = -18.39+0.2291*variable(1)-0.07238*variable(2)+0.2852*variable(3)-
0.3705*variable(4)+0.03177*variable(4)*variable(4)-
0.003229*variable(1)*variable(3)+0.000811*variable(2)*variable(3);
end
```

%%%%%%%%%%%%% Code for SR %%%%%%%%%%%%%
The MATLAB code for SR is almost similar to MRR problem. However, some appropriate changes need to be done in MATLAB files to solve the problem for minimization of SR.

%%%%%%%%% Code for combined objective function %%%%%%%%%
The MATLAB code for combined objective function is almost similar to MRR problem. However, some appropriate changes need to be done in MATLAB files to replace the single objective function by combined objective function.

REFERENCES

Aggarwal, V., Khangura, S. S., and Garg, R. K. (2015). "Parametric modeling and optimization for wire electrical discharge machining of Inconel 718 using response surface methodology." *Int. J. Adv. Manuf. Tech.*, 79(1–4), 31–47.

Anderson, M.J., and Whitcomb, P.J. (2004). "RSM simplified: optimizing processes using response surface methods for design of experiments." Productivity Press, New York

Antar, M. T., Soo, S. L., Aspinwall, D. K., Jones, D., and Perez, R. (2011). "Productivity and workpiece surface integrity when WEDM aerospace alloys using coated wires." *Procedia Eng.*, 19, 3–8.

Antar, M. T., Soo, S. L., Aspinwall, D. K., Sage, C., Cuttell, M., Perez, R., and Winn, A. J. (2012). "Fatigue response of Udimet 720 following minimum damage wire electrical discharge machining." *Mater. Design*, 42, 295–300.

Arunachalam, R., and Mannan, M. A. (2000). "Machinability of nickel-based high temperature alloys."*Mach. Sci. Technol.*, 4(1), 127–168.

Aspinwall, D. K., Soo, S. L., Berrisford, A. E., and Walder, G. (2008). "Workpiece surface roughness and integrity after WEDM of Ti–6Al–4V and Inconel 718 using minimum damage generator technology." *CIRP Ann. Manuf. Technol*., 57(1), 187–190.

Atzeni, E., Bassoli, E., Gatto, A., Iuliano, L., Minetola, P., and Salmi, A. (2014). "Surface and Sub Surface evaluation in Coated-Wire Electrical Discharge Machining (WEDM) of INCONEL® alloy 718." *Procedia CIRP*, 33, 389–394.

Ayesta, I., Izquierdo, B., Sánchez, J. a., Ramos, J. M., Plaza, S., Pombo, I., and Zamakona, I. (2013). "Influence of EDM Parameters on Slot Machining in C1023 Aeronautical Alloy." *Procedia CIRP*, 6, 129–134.

Bedder, J., & Baylis, R. (2013, February 28). "Into the melting pot: The superalloy market and its impact on minor metals." Retrieved from https://roskill.com/wp/wp-content/uploads/2014/11/download-roskills-paper-on-the-superalloy-and-minor-metal-markets.attachment1.pdf (July 12, 2016).

Bez'yazychnyi, V. F., Volkov, S. A., and Fomenko, R. N. (2008). "Selecting the machining processes for slot arrays in gas-turbine disks." *Russ. Eng. Res.*, 28(5), 503–507.

Box, G. E., and Hunter, J. S. (1957). "Multi-factor experimental designs for exploring response surfaces." *Ann. Math. Stat.*, 195–241.

Campbell, F.C. (2006). "Manufacturing technology for aerospace structural materials." First Edition, Elsevier, New York.

Caron, P., and Khan, T. (1999). "Evolution of Ni-based superalloys for single crystal gas turbine blade applications." *Aerosp. Sci. Technol.*, 3(8), 513–523.

Choudhury, I. A., and El-Baradie, M. A. (1998). "Machinability of nickel-base super alloys: a general review." *J. Mater. Process. Tech.*, 77(1), 278–284.

Curtis, D. T., Soo, S. L., Aspinwall, D. K., Huber, C., Fuhlendorf, J., and Grimm, A. (2008). "Production of complex blade mounting slots in turbine disks using novel machining techniques." *3rd CIRP HPC Conference,* 1, 219–228.

Dabade, U. A., and Karidkar, S. S. (2016). "Analysis of Response Variables in WEDM of Inconel 718 Using Taguchi Technique." *Procedia CIRP*, *41*, 886–891.

Deb, K. (2012). "Optimization for engineering design: Algorithms and examples." second ed., PHI Learning Private Limited, New Delhi.

Deng, J. L. (1989). "Introduction to grey system theory." *J. Grey Syst.*, 1(1), 1–24.

Dhanabalan, S., Sivakumar, K., and Narayanan, C. S. (2013). "Optimization of machining parameters of EDM while machining Inconel 718 for form tolerance and orientation tolerance." *Indian J. Eng. Mater. S.*, 20(5), 391–397.

El-Hofy, H. (2005). "Advanced machining processes: nontraditional and hybrid machining processes". McGraw Hill, New York.

Ezugwu, E. O., Wang, Z. M., and Machado, A. R. (1998). "The machinability of nickel-based alloys: a review." *J. Mater. Process. Tech.*, 86(1), 1–16.

Garg, R. K., Aggarwal, V., and Singh, S. (2014). "Effect of wire materials on cutting performance of WEDM for machining of Inconel superalloy."*Appl. Mech. Mater.*, 624, 124–128.

Geddes, B., Leon, H., and Huang, X. (2010). "Superalloys: alloying and performance." ASM International, Materials Park, Ohio, USA.

Gostimirovic, M., Kovac, P., Sekulic, M., and Skoric, B. (2012). "Influence of discharge energy on machining characteristics in EDM." *J. Mech. Sci. Technol.*, 26(1), 173–179.

Goswami, A., and Kumar, J. (2014). "Study of machining characteristics of Nimonic 80A using wire-cut EDM." *Int. J. Adv. Eng. Appl.*, 7(1), 73–81.

Hewidy, M. S., El-Taweel, T. A., and El-Safty, M. F. (2005). "Modelling the machining parameters of wire electrical discharge machining of Inconel 601 using RSM." *J. Mater. Process. Tech.*, 169(2), 328–336.

Izquierdo, B., Plaza, S., Sánchez, J. A., Pombo, I., and Ortega, N. (2012). "Numerical prediction of heat affected layer in the EDM of aeronautical alloys." *Appl. Surf. Sci.*, 259, 780–790.

Jakhar, B., Katyal, P., and Gulati, V. (2015). "Investigating the Process Parameters for optimization on Inconel 600 using wire cut EDM." *Int. J. Adv. Innov. Res.*, 3(3), 508–513.

Karidkar, S. S., and Dabade, U. A. (2016). "Experimental Investigation and Optimization of Response Variables in WEDM of Inconel-718." *Iop Conf. Ser. Mater. Sci. Eng.*, 114(1), 012121.

Khuri, A. I. (2006). "Response Surface Methodology and Related Topics." World Scientific Publishing Co. Pte. Ltd., Hackensack.

Klocke, F., Welling, D., Dieckmann, J., Veselovac, D., and Perez, R. (2012). "Developments in Wire-EDM for the manufacturing of fir tree slots in turbine discs made of Inconel 718." *Key Eng. Mat*., 504, 1177–1182.

Klocke, F., Welling, D., Klink, A., and Perez, R. (2014 a). "Quality Assessment through In-process Monitoring of Wire-EDM for Fir Tree Slot Production". *Procedia CIRP*, 24, 97–102.

Klocke, F., Welling, D., Klink, A., Veselovac, D., Nöthe, T., and Perez, R. (2014). "Evaluation of Advanced Wire-EDM Capabilities for the Manufacture of Fir Tree Slots in Inconel 718." *Procedia CIRP*, 14, 430–435.

Kumar, V., Jangra, K., and Kumar, V. (2016). "An experimental study on trim cutting operation using metal powder mixed dielectric in WEDM of Nimonic-90." *Int. J. Ind. Eng. Comput.*, 7(1), 133–146.

Kumar, V., Jangra, K., Kumar, V., and Sharma, N. (2016 a). "WEDM of nickel based aerospace alloy: optimization of process parameters and modelling." Int. J. Interact. Des. Manuf., 1–13. Doi: 10.1007/s12008-016-0298-3.

Li, L., Guo, Y. B., Wei, X. T., and Li, W. (2013). "Surface integrity characteristics in wire-EDM of Inconel 718 at different discharge energy." *Procedia CIRP*, 6, 220–225.

Li, L., Wei, X. T., and Li, Z. Y. (2014). "Surface integrity evolution and machining efficiency analysis of W-EDM of nickel-based alloy." *Appl. Surf. Sci*., 313, 138–143.

Lin, M. Y., Tsao, C. C., Hsu, C. Y., Chiou, A. H., Huang, P. C., and Lin, Y. C. (2013). "Optimization of micro milling electrical discharge machining of Inconel 718 by Grey-Taguchi method." *Trans. Nonferrous Met. Soc. China.*, 23(3), 661–666.

Locq, D., and Caron, P. (2011). "On some advanced nickel-based superalloys for disk applications." *J. Aerosp. Lab*., 3, 1–9.

Maher, I., Sarhan, A. A., and Hamdi, M. (2014). "Review of improvements in wire electrode properties for longer working time and utilization in wire EDM machining." *Int. J. Adv. Manuf. Tech.*, 76(1–4), 329–351.

Mandal, A., Dixit, A. R., Das, A. K., and Mandal, N. (2016). "Modeling and Optimization of Machining Nimonic C-263 Superalloy using Multicut Strategy in WEDM." *Mater. Manuf. Process*, 31, 860–868.

Manjaiah, M., Laubscher, R. F., Narendranath, S., Basavarajappa, S., and Gaitonde, V. N. (2016). "Evaluation of wire electro discharge machining characteristics of Ti 50 Ni 50− x Cu x shape memory alloys." *J. Mater. Res.*, *31*(12), 1801–1808.

Manjaiah, M., Narendranath, S., and Basavarajappa, S. (2016a). "Wire Electro Discharge Machining Performance of TiNiCu Shape Memory Alloy." *Silicon*, *8*(3), 467-475.

Manjaiah, M., Narendranath, S., Basavarajappa, S., and Gaitonde, V. N. (2015). "Effect of electrode material in wire electro discharge machining characteristics of Ti 50 Ni 50− x Cu x shape memory alloy." *Precis. Eng.*, *41*, 68–77.

Montgomery, D. C. (1997). "Design and analysis of experiments." fourth ed., John Wiley & Sons Inc., New York, USA.

Montgomery, D. C. (2013). "Design and analysis of experiments." eight ed., John Wiley & Sons, New York, USA.

Muktinutalapati, N. R. (2011). "Materials for Gas Turbines–An Overview." Adv. Gas Turbine Technol., InTech 293–314.

Muthu, K.V., Suresh, B.A., Venkatasamy, R., and Raajenthiren, M. (2010). "Optimization of the WEDM parameters on machining Incoloy800 super alloy with multiple quality characteristics." *Optimization*, 2(6), 1538–1547.

Myers, R. H., Montgomery, D. C., and Anderson-Cook, C. M. (2003). "Response surface methodology: process and product optimization using designed experiments." John Wiley & Sons Inc., New York, USA.

Narendranath, S., Manjaiah, M., Basavarajappa, S., and Gaitonde, V. N. (2013). "Experimental investigations on performance characteristics in wire electro discharge machining of Ti50Ni42.4Cu7.6 shape memory alloy." *P. I. Mech. Eng. B-J Eng.*, 227(8), 1180–1187.

Newton, T. R. (2008). "Investigation of the effect of process parameters on the formation of recast layer in wire-EDM of Inconel 718." MTech thesis, Georgia Institute of Technology, Atlanta, Georgia.

Newton, T. R., Melkote, S. N., Watkins, T. R., Trejo, R. M., and Reister, L. (2009). "Investigation of the effect of process parameters on the formation and characteristics of recast layer in wire-EDM of Inconel 718." *Mater. Sci. Eng*., 513, 208–215.

Okada, A., Konishi, T., Okamoto, Y., and Kurihara, H. (2015). "Wire breakage and deflection caused by nozzle jet flushing in wire EDM." *CIRP Ann. Manuf. Technol.*, 64(1), 233–236.

Pollock, T. M., and Tin, S. (2006). "Nickel-based superalloys for advanced turbine engines: chemistry, microstructure and properties." *J. Propul. Power*., 22(2), 361–374.

Rajyalakshmi, G., and Ramaiah, P. V. (2013). "Multiple process parameter optimization of wire electrical discharge machining on Inconel 825 using Taguchi grey relational analysis." *Int. J. Adv. Manuf. Tech.*, 69(5–8), 1249–1262.

Rajyalakshmi, G., and Ramaiah, P. V. (2015). "Application of Taguchi, Fuzzy-Grey Relational Analysis for Process Parameters Optimization of WEDM on Inconel-825." *Indian J. Sci. Technol.*, *8*(35) 1–12.

Ramakrishnan, R., and Karunamoorthy, L. (2008). "Modeling and multi-response optimization of Inconel 718 on machining of CNC WEDM process." *J. Mater. Process. Tech.*, 207(1), 343–349.

Rao, M. S., and Venkaiah, N. (2015). "Parametric Optimization in Machining of Nimonic-263 Alloy using RSM and Particle Swarm Optimization." *Procedia Materials Science*, 10, 70–79.

Rao, R. V., and Kalyankar, V. D. (2013). "Parameter optimization of modern machining processes using teaching-learning-based optimization algorithm." *Eng. Appl. Artif. Intel.*, 26(1), 524–531.

Rao, R. V., Kalyankar, V. D., & Waghmare, G. (2014). Parameters optimization of selected casting processes using teaching–learning-based optimization algorithm. Appl. Math. Model., 38(23), 5592–5608.

Rao, R. V., Kalyankar, V. D., and Waghmare, G. (2014). "Parameters optimization of selected casting processes using teaching–learning-based optimization algorithm." *Appl. Math. Model.*, 38(23), 5592–5608.

Rao, R. V., Savsani, V. J., and Vakharia, D. P. (2011). "Teaching–learning-based optimization: a novel method for constrained mechanical design optimization problems." *Comput. Aided Des.*, 43(3), 303–315.

Rao, S., and Venkaiah, N. (2016). "Modeling of circularity error while machining Inconel-690 using WEDM." *IJAER*, 11(6), 3999–4006.

Rasheed, M. S. (2013). "Comparison of micro-holes produced by micro-EDM with laser machining." *Int. J. Sci. Mod. Eng.*, 1(3) 14–18.

Reed, R. C. (2006). "The superalloys: Fundamentals and applications." Cambridge, Cambridge University Press, UK.

Rolls Royce. (2015). "The jet engine." John Wiley & Sons Inc., New York, USA.

Sarkar, S., Ghosh, K., Mitra, S., and Bhattacharyya, B. (2010). "An integrated approach to optimization of WEDM combining single-pass and multipass cutting operation. *Mater. Manuf. Process*," 25(8), 799–807.

Sarkar, S., Sekh, M., Mitra, S., and Bhattacharyya, B. (2011). "A novel method of determination of wire lag for enhanced profile accuracy in WEDM." *Precis. Eng.*, *35*(2), 339–347.

Satapathy, S., and Naik, A. (2013). "Improved teaching learning based optimization for global function optimization." *Decision Science Letters*, 2(1), 23–34.

Schafrik, R., and Sprague, R. (2004). "Saga of Gas Turbine Materials: Part III." *Adv. Mater. Processes.*, 162, 33–35.

Schilke, P. W., Foster, A. D., and Pepe, J. J. (2004). "Advanced gas turbine materials and coatings." General Electric Company, New York.

Schilke, P. W., Pepe, J. J., and Schwant, R. C. (1994). "Alloy 706 metallurgy and turbine wheel application." *Superalloys*. 718 (625,706), 1.

Schwade, M. (2014). "Fundamental Analysis of High Frequent Electrical Process Signals for Advanced Technology Developments in W-EDM." *Procedia CIRP*, 14, 436–441.

Sharma, P., Chakradhar, D., and Narendranath, S. (2014). "Multi-Response Optimization of WEDM Process Using Hybrid Approach while Machining Inconel 625 Superalloy." *Journal of Machining and Forming Technologies*, 6 (3-4), 107-116.

Sharma, P., Chakradhar, D., and Narendranath, S. (2015). "Evaluation of WEDM performance characteristics of Inconel 706 for turbine disk application." *Mater. Design*, 88, 558–566.

Sharma, P., Chakradhar, D., and Narendranath, S. (2017). "Analysis and optimization of WEDM performance characteristics of Inconel 706 for aerospace application." *Silicon*, DOI: 10.1007/s12633-017-9549-6.

Sims. C.T., Stoloff. N.S. and Hagel. W.C., (1987). "Superalloys II- High Temperature Materials for Aerospace and Industrial Power." John Wiley & Sons Inc., New York, USA.

Sines, G., and Carlson, R. (1952). "Hardness measurements for determination of residual stresses." ASTM Bull, 180, 357.

Singh, J., and Jain, S. C. (1995). "Mechanical issues in laser and abrasive water jet cutting." *Jom-J. Min. Met. Mat. S.*, 47(1), 28–30.

Technical bulletin: Inconel alloy 706 (Publication number SMC–091), Special Metals Corporation. Retrieved from

http://www.specialmetals.com/assets/documents/alloys/inconel/inconel-alloy-706.pdf (July 12, 2016)

Uhlmann, E., and Domingos, D. C. (2013). "Development and Optimization of the Die-Sinking EDM-Technology for Machining the Nickel-based Alloy MAR-M247 for Turbine Components." *Procedia CIRP*, 6, 180–185.

Wang, F., Liu, Y., Shen, Y., Ji, R., Tang, Z., and Zhang, Y. (2013). "Machining performance of Inconel 718 using high current density electrical discharge milling." *Mater. Manuf. Processes.*, 28(10), 1147–1152.

WEDM Technology Manual, Electronica Machine Tools. Retrieved from http://www.electronicagroup.com/download/ecocut.pdf (July 12, 2016).

Welling, D. (2014). "Results of Surface Integrity and Fatigue Study of Wire-EDM Compared to Broaching and Grinding for Demanding Jet Engine Components Made of Inconel 718." *Procedia CIRP*, 13, 339–344.

Xu, C. S. (2012). "Working Principle and Performance of Wire Electrical Discharge Machining." *In Adv. Mat. Res.*, 507, 180–183.

Yeh, C. C., Wu, K. L., Lee, J. W., and Yan, B. H. (2013). "Study on surface characteristics using phosphorous dielectric on wire electrical discharge machining of polycrystalline silicon." Int. J. Adv. Manuf. Tech., 69(1–4), 71–80.

Zhang, S., and Zhao, D. (2012). "Aerospace Materials Handbook." CRC Press, Boca Raton.

Zhang, Z., Huang, H., Ming, W., Xu, Z., Huang, Y., and Zhang, G. (2016). "Study on machining characteristics of WEDM with ultrasonic vibration and magnetic field assisted techniques." *J. Mater. Process. Tech.*, *234*, 342–352.

Zhong, M., Sun, H., Liu, W., Zhu, X., and He, J. (2005). "Boundary liquation and interface cracking characterization in laser deposition of Inconel 738 on directionally solidified Ni-based superalloy." *Scripta materialia*, 53(2), 159–164.

LIST OF PUBLICATIONS BASED ON PHD RESEARCH WORK

SL No.	Title of the Paper	Authors	Name of the Journal / Conference / Symposium, Vol., No., Pages	Month & Year of Publication	Category *
1	Analysis and optimization of WEDM performance characteristics of Inconel 706 for aerospace application	Priyaranjan Sharma, D. Chakradhar, Narendranath S.	Silicon (DOI: 10.1007/s12633-017-9549-6)	January, 2017	1
2	Effect of wire diameter on surface integrity of wire electrical discharge machined Inconel 706 for gas turbine application	Priyaranjan Sharma, D. Chakradhar, Narendranath S.	Journal of Manufacturing Processes, 24, 170-178. (DOI-10.1016/j.jmapro.2016.09.001)	September, 2016	1
3	Effect of wire material on productivity and surface integrity of WEDM processed Inconel 706 for aircraft application	Priyaranjan Sharma, D. Chakradhar, Narendranath S.	Journal of Materials Engineering and Performance, 25(9), 3672-3681. (DOI:10.1007/s11665-016-2216-z)	July, 2016	1
4	Evaluation of WEDM performance characteristics of Inconel 706 for turbine disk application	Priyaranjan Sharma, D. Chakradhar, Narendranath S.	Materials and Design, 88, 558-566. (DOI:10.1016/j.matdes.2015.09.036)	September, 2015	1
5	Multi-response optimization of WEDM process using Hybrid approach while machining Inconel 625	Priyaranjan Sharma, D. Chakradhar, Narendranath S.	Journal of Machining and Forming Technologies, 6 (3-4), 107-116. (ISSN: 1947-4369)	November, 2014	1
6	An examination of surface and subsurface characteristics of turbine disk profile slots manufactured by WEDM process	Priyaranjan Sharma, D. Chakradhar, Narendranath S.	Journal of Materials Processing Technology	(Under Review)	1
7	Modeling and optimization of WEDM performance characteristics of advanced turbine disk alloy using RSM-based TLBO algorithm	Priyaranjan Sharma, D. Chakradhar, Narendranath S.	Machining Science and Technology	(Under Review)	1

8	Modeling and Optimization of WEDM performance attributes of Inconel 706 superalloy using RSM-based PSO approach	Priyaranjan Sharma, D. Chakradhar, Narendranath S.	The Ninth International Conference on Materials Technologies and Modeling (MMT-2016), Ariel University, Ariel 40700, Israel.	July, 2016	3
9	Optimization of WEDM performance characteristics while machining Inconel 600 Superalloy	Priyaranjan Sharma, D. Chakradhar, Narendranath S.	Conf. on Advances in Light metals and its Composites (CALM-2014), SRM University, Chennai, India.	December, 2014	4
10	Multi-response optimization of WEDM process using Hybrid approach while machining Inconel 625	Priyaranjan Sharma, D. Chakradhar, Narendranath S.	Int. Conf. on Industrial, Mechanical and Production Engineering: Advancements and Current Trends (ICIMPACT-2014), MANIT, Bhopal, India.	November, 2014	3

* Category: 1 : Journal paper, full paper reviewed   2 : Journal paper, Abstract reviewed
                  3 : Conference/Symposium paper, full paper reviewed   4 : Conference/Symposium paper, abstract reviewed
                  5 : others (including papers in Workshops, NITK Research Bulletins, Short notes etc.)

Priyaranjan Sharma   **Dr. D. Chakradhar**   **Prof. Narendranath S.**
(Research Scholar)   (Research Guide)   (Research Guide)

BIODATA

1. **Name:**   Priyaranjan Sharma

2. **Father's Name:**   Jamuna Lal Sharma

3. **Date of Birth:**   03/12/1989

4. **Nationality:**   Indian

5. **Address:**

Permanent Address	**Present Address**
S/o. Jamuna Lal Sharma,	Department of Mechanical Engineering,
Vard No. 12/ House No. 85,	National Institute of Technology Karnataka,
Anand Colony, Jhareda Road	Surathkal-575025, Srinivasanagar,
Hindaun City - 322230, Karauli (Dist),	Dhakshina Kannada (Dist),
Rajasthan, India.	Karnataka, India.

6. **Mobile Number:**   +91-7415750299/9916809016.

7. **E-mail id.:**   priya333ranjan@gmail.com/priya333ranjan@hotmail.com

8. **Educational Qualification:**

Qualification	College/school	University/Board	Year of Passing	Percentage / CGPA
Ph.D. in Mechanical Engineering	National Institute of Technology Karnataka	National Institute of Technology Karnataka	2017	8.5
M. Tech in Manufacturing Technology	Jaypee University of Engg. & Technology, Guna (M.P.)	Jaypee University of Engg. & Technology, Guna (M.P.)	2013	8.9
B. Tech in Mechanical Engineering	Gyan Vihar School of Engg. & Technology, Jaipur (Rajasthan)	Rajasthan Technical University	2010	65.48 %
Senior Secondary Examination (12th)	Govt. Sr. Sec. School, Rawatbhata, Kota	Rajasthan board of SecondaryEducation (Ajmer)	2006	61.69 %
Secondary School Examination (10th)	Bal Mandir Secondary School, Rawatbhata, Kota	Rajasthan Board of SecondaryEducation (Ajmer)	2004	79.17 %

I declare that the above information is true and correct to best of my knowledge.

(Priyaranjan Sharma)